

NUMERICAL ANALYSIS OF TURBULENT FLOW THROUGH A SHELL AND TUBE HEAT EXCHANGER USING KAYS- CRAWFORD MODEL

by

ShamimaAirinSweety
Student No. **1018092517F**
Session: **October, 2018**

**MASTER OF SCIENCE
IN
MATHEMATICS**




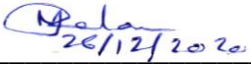
Department of MATHEMATICS
BANGLADESH UNIVERSITY OF ENGINEERING AND TECNOLOGY, DHAKA
November, 2020


References

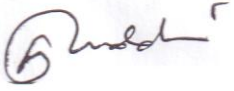
The thesis entitled “**NUMERICAL ANALYSIS OF TURBULENT FLOW THROUGH A SHELL AND TUBE HEAT EXCHANGER USING KAYS-CRAWFORD MODEL**”, submitted by **Shamima Airin Sweety**, Roll no: **1018092517F**, Registration No. **1018092517F**, Session: **October-2018** has been accepted as satisfactory in partial fulfillment of the requirement for the degree of Master of Science in Mathematics on **22 November, 2020**.

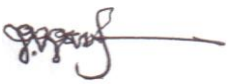
Board of Examiners

1. 

Dr. Rehana Nasrin
Professor
Department of Mathematics
BUET, Dhaka-1000
**Chairman
(Supervisor)**
2. 

Head
Department of Mathematics
BUET, Dhaka-1000
**Member
(Ex-Officio)**
3. 

Dr. Md. Mustafizur Rahman
Professor
Department of Mathematics
BUET, Dhaka-1000
Member
4. 

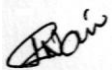
Dr. Mohammed Forhad Uddin
Professor
Department of Mathematics
BUET, Dhaka-1000
Member
5. 

Dr. Md. Habibur Rahman
Professor
Department of Mathematics
KUET, Khulna-9203
**Member
(External)**

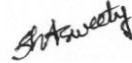
References

Certificate of Research

This is to certify that the work presented in this thesis has been carried out by the author under the supervision of **Dr. Rehena Nasrin**, Professor, Department of Mathematics, Bangladesh University of Engineering and Technology, Dhaka-1000.



Dr. Rehena Nasrin
Professor
Dept. of Mathematics
BUET, Dhaka-1000



Shamima Airin Sweety

References

Candidate's Declaration

It is hereby declared that this thesis or any part of it has not been submitted elsewhere for the award of any degree or diploma.



Shamima Airin Sweety

[1] .

This work is dedicated
To the
Researchers of My Country

Acknowledgement

I would like to affirm the continual mercy, help and blessing showered by the Almighty without which it would have been impossible to accomplish the arduous job I was assigned to.

With my great pleasure I would like to express my deep and sincere gratitude to my respected supervisor Dr. Rehana Nasrin, Professor, Department of Mathematics, Bangladesh University of Engineering and Technology, Dhaka-1000 for her expert guidance and valuable suggestions throughout this work. Her priceless suggestions made this work interesting and learning to me. It would not have been possible to carry out this study successfully without the continuous inspiration and encouragement from supervisor.

I owe a favor to the Head, Department of Mathematics, BUET, for his support in allowing me to use the departmental facilities in various stages of my work. I also thank the staffs of the Department of Mathematics, BUET for being so helpful.

I would like to thank and express profound respect to Dr. Md. Mustafizur Rahman, Professor, Department of Mathematics, BUET for his constant support, intuitive, suggestions and continuous guidance throughout my thesis.

I would like to offer my humble gratitude and profound respect to Dr. Mohammed Forhad Uddin, Professor, Department of Mathematics, BUET for his comments and constructive concept which helped me for better understanding the issues of this thesis.

Furthermore, I would like to express my gratitude to my excellent external member of the Board of Examiners for sharing his encouraging expertise generously. I am fortunate to get his valuable suggestions throughout my research.

Abstract

Shell and tube heat exchangers are considered as the most effective type of heat exchangers. These are used in various industrial process applications for performing tasks such as removal of process heat and feed water preheating, cooling of hydraulic and lube oil, cooling of turbine, compressor and engine, condensing process vapor or steam and evaporating process liquid or steam. In this research, a numerical analysis of turbulent flow has been carried out in a shell and tube heat exchanger using Kays-Crawford model to investigate the heat transfer performance of water and different concentrated water-MWCNT (Multi Walled Carbon Nanotube) nanofluids. A two-dimensional model of a part of shell and tube heat exchanger has been used which consists of a bundle of tubes through which the cooling fluid will flow in abundant supply entering from one side and maintaining a constant temperature. Hot fluid will enter from above the tubes and the tubes will be assumed to be made of stainless steel. The Reynold-Averaged Navier-Stokes (RANS) equations and heat transport equations with appropriate boundary conditions have been solved using finite element method. The implications of solid concentration, velocity and temperature of water- MWCNT nanofluid on the flow structure and heat transfer characteristics have been investigated in details. In addition, the present numerical result has been compared with that of Yang and Liu [44]. The numerical results indicate that the occurring solid volume fraction of nanoparticles, inflow velocity variation and inlet temperature variation characteristic significant changes in the flow and heat transfer performance. Moreover, it is noticed that using 3% concentrated water-MWCNT nanofluid, higher rate of heat transfer (12.24%) is achieved compared that of water (base fluid) and therefore to enhance the efficiency of shell and tube heat exchanger.

Contents

Abstract.....	vii
List of Tables	xii
List of Figures.....	xiii
Chapter 1.....	1
Introduction	1
1.1 Introduction	1
1.2 Literature Review	17
1.3 Objectives.....	19
1.4 Outline of the Thesis	20
Chapter 2.....	21
Numerical Analysis	21
2.1 Introduction	21
2.2 Finite Element Method	21
2.3 Problem Formulation	23
2.4 Mathematical Modeling.....	27
2.5 Computational Procedure	32
Chapter 3.....	36
Results and Discussions	36
3.1 Introduction	36
3.2 Effect of Solid Concentration.....	36
3.3 Effect of velocity	56
3.4 Effect of temperature.....	71

3.5 Heat Transfer Rate	86
3.6 Comparison.....	87
Chapter 4.....	89
Conclusions and Recommendations	89
4.1 Conclusions	89
4.2 Recommendations	90
References	91

Nomenclature

C_p → Specific heat at constant pressure ($\text{Jkg}^{-1}\text{K}^{-1}$)

k → Thermal conductivity ($\text{Wm}^{-1}\text{K}^{-1}$)

L → Pipe radius (m)

m → Mass (kg)

Nu → Nusselt number

P → Pressure (kgms^{-2})

Pr → Prandtl number

Re → Reynolds number

T → Dimensional temperature (K)

u, v → Dimensional x and y components of velocity (ms^{-1})

x, y → Cartesian coordinates (m)

Greek Symbols

α → Thermal diffusivity (m^2s^{-1})

ϵ → Turbulent energy dissipation/(J/kg. s)

κ → Turbulent kinematic energy (J/kg)

μ → Dynamic viscosity (Nsm^{-2})

ν → Kinematic viscosity (m^2/s)

ρ → Density (kgm^{-3})

ϕ → Weight fraction (%)

Subscripts

f → Fluid

in → inlet

nf → nanofluid

T → Turbulent

w → wall

Abbreviation

CAD → Computer aided design

FEA → Finite element analysis

FEM → Finite element method

HTF → Heat transferring fluid

MWCNT → Multi walled carbon nanotube

RANS → Reynolds Averaged Navier Stokes

SEM → Scanning Electron Microscope

TEM → Transmission Electron Microscopy

List of Tables

Items	Table Caption	Page
Table 2.1	Different constants values	32
Table 2.2	Thermo- physical properties of base fluid, nanoparticle and pipe material	32
Table 2.3	Grid sensitivity check at $\phi = 0.01$, $v_{in} = 1.5$ m/s, $T_{in} = 323$ K	35
Table 3.1	Heat Transfer rate at different concentration of water-MWCNT nanofluid	87
Table 3.2	Comparison of Nusselt number between present numerical results and results of Yang and Liu [44] against Reynolds number	88

List of Figures

Items	Figure Caption	Page
Figure 1.1	Working methodology of heat exchanger	2
Figure 1.2	Configuration of shell and tube heat exchanger	3
Figure 1.3(a)	1-pass straight-tube heat exchangers	4
Figure 1.3(b)	2-pass straight-tube heat exchanger	4
Figure 1.4	Difference in dye trace of laminar and turbulent flow	6
Figure 1.5	Heat transfer system	8
Figure 1.6	Forced convection in terms of heating/cooling a room using a fan	9
Figure 1.7	Forced convection by a fan in a snow machine	10
Figure 1.8	Thermal conductivity in terms of heat flow	11
Figure 1.9	Relation between flow velocity and local shear velocity	12
Figure 1.10	SEM image of MWCNT	13
Figure 1.11	TEM image of MWCNT	14
Figure 1.12	Single-walled carbon nanotube	14
Figure 1.13:	Multi-walled carbon nanotube	15
Figure 2.1	FEM mesh	23
Figure 2.2	A tube bundle from a shell and tube heat exchanger	24
Figure 2.3	The model region	24
Figure 2.4	The modeled 2D region	25
Figure 2.5	Close view of the modeled 2D region	26
Figure 2.6	Loaded CAD model in COMSOL Multiphysics geometry	27
Figure 2.7	Modeled 2D geometry with boundary condition	30
Figure 2.8	FEM mesh generation (a) normal and (b) fine mesh type	34
Figure 3.1	(a) Streamlines, (b) isothermal lines and (c) surface plot for velocity field for velocity magnitude of tabular heat exchanger using water	37
Figure 3.2	Velocity contours using (a) 0.1, (b) 1, (c) 2 and (d) 3% concentrated water-MWCNT nanofluid	38

Figure 3.3	Temperature contours using (a) 0.1, (b) 1, (c) 2 and (d) 3% concentrated water-MWCNT nanofluid	40
Figure 3.4(a)	Velocity field of y-component at y = 400, 500, 600 and 700 mm for water	41
Figure 3.4(b)	Velocity field of y-component at y = 400, 500, 600 and 700 mm for 0.1% concentrated water-MWCNT nanofluid	42
Figure 3.4(c)	Velocity field of y-component at y = 400, 500, 600 and 700 mm for 1% concentrated water-MWCNT nanofluid	43
Figure 3.4(d)	Velocity field of y-component at y = 400, 500, 600 and 700 mm for 2% concentrated water-MWCNT nanofluid	44
Figure 3.4(e)	Velocity field of y-component at y = 400, 500, 600 and 700 mm for 3% concentrated water-MWCNT nanofluid	45
Figure 3.5(a)	Pressure at y = 400, 500, 600 and 700 mm for water	46
Figure 3.5(b)	Pressure at y=400,500,600 and 700 mm for 0.1% concentrated water-MWCNT nanofluid	47
Figure 3.5(c)	Pressure at y = 400, 500, 600 and 700 mm for 1% concentrated water-MWCNT nanofluid	48
Figure 3.5(d)	Pressure at y = 400, 500, 600 and 700 mm for 2% concentrated water-MWCNT nanofluid	49
Figure 3.5(e)	Pressure at y = 400, 500, 600 and 700 mm for 3% concentrated water-MWCNT nanofluid	50
Figure 3.6(a)	Temperature at y = 400, 500, 600 and 700 mm for water	51
Figure 3.6(b)	Temperature at y = 400, 500, 600 and 700 mm for 0.1% concentrated water-MWCNT nanofluid	52
Figure 3.6(c)	Temperature at y = 400, 500, 600 and 700 mm for 1% concentrated water-MWCNT nanofluid	53
Figure 3.6(d)	Temperature at y = 400, 500, 600 and 700 mm for 2% concentrated water-MWCNT nanofluid	54
Figure 3.6(e)	Temperature at y = 400, 500, 600 and 700 mm for 3% concentrated water-MWCNT nanofluid	55
Figure 3.7	Velocity contours using v_{in} (a) - 0.1, (b) - 0.5, (c) - 1 and (d) - 1.5 m/s	57

Figure 3.8	Temperature contours using v_{in} (a) - 0.1, (b) - 0.5, (c) - 1 and (d) - 1.5 m/s	58
Figure 3.9(a)	Velocity field of y-component at $y = 400, 500, 600$ and 700 mm using $v_{in} = - 0.1$ m/s	59
Figure 3.9(b)	Velocity field of y-component at $y = 400, 500, 600$ and 700 mm using $v_{in} = - 0.5$ m/s	60
Figure 3.9(c)	Velocity field of y-component at $y = 400, 500, 600$ and 700 mm using $v_{in} = - 1$ m/s	61
Figure 3.9(d)	Velocity field of y-component at $y = 400, 500, 600$ and 700 mm using $v_{in} = - 1.5$ m/s	62
Figure 3.10(a)	Pressure at $y = 400, 500, 600$ and 700 mm using $v_{in} = - 0.1$ m/s	63
Figure 3.10(b)	Pressure at $y = 400, 500, 600$ and 700 mm using $v_{in} = - 0.5$ m/s	64
Figure 3.10(c)	Pressure at $y = 400, 500, 600$ and 700 mm using $v_{in} = - 1$ m/s	65
Figure 3.10(d)	Pressure at $y = 400, 500, 600$ and 700 mm using $v_{in} = - 1.5$ m/s	66
Figure 3.11(a)	Temperature at $y = 400, 500, 600$ and 700 mm using $v_{in} = - 0.1$ m/s	67
Figure 3.11(b)	Temperature at $y = 400, 500, 600$ and 700 mm using $v_{in} = - 0.5$ m/s	68
Figure 3.11(c)	Temperature at $y = 400, 500, 600$ and 700 mm using $v_{in} = - 1$ m/s	69
Figure 3.11(d)	Temperature at $y = 400, 500, 600$ and 700 mm using $v_{in} = - 1.5$ m/s	70
Figure 3.12	Velocity contours using T_{in} (a) 323, (b) 318, (c) 313 and (d) 308 K	72
Figure 3.13	Temperature contours using T_{in} (a) 323, (b) 318, (c) 313 and (d) 308 K	73
Figure 3.14(a)	Velocity of y-component at $y = 400, 500, 600$ and 700 mm using $T_{in} = 323$ K	74
Figure 3.14(b)	Velocity of y-component at $y = 400, 500, 600$ and 700 mm using $T_{in} = 318$ K	75
Figure 3.14(c)	Velocity of y-component at $y = 400, 500, 600$ and 700 mm using inlet temperature 313 K	76
Figure 3.14(d)	Velocity of y-component at $y = 400, 500, 600$ and 700 mm using $T_{in} = 308$ K	77
Figure 3.15(a)	Pressure at $y = 400, 500, 600$ and 700 mm using $T_{in} = 323$ K	78
Figure 3.15(b)	Pressure at $y = 400, 500, 600$ and 700 mm using $T_{in} = 318$ K	79
Figure 3.15(c)	Pressure at $y = 400, 500, 600$ and 700 mm using $T_{in} = 313$ K	80

Figure 3.15(d)	Pressure at $y = 400, 500, 600$ and 700 mm using $T_{in} = 308$ K	81
Figure 3.16(a)	Temperature at $y = 400, 500, 600$ and 700 mm using $T_{in} = 323$ K	82
Figure 3.16(b)	Temperature at $y = 400, 500, 600$ and 700 mm using $T_{in} = 318$ K	83
Figure 3.16(c)	Temperature at $y = 400, 500, 600$ and 700 mm using $T_{in} = 313$ K	84
Figure 3.16(d)	Temperature at $y = 400, 500, 600$ and 700 mm using $T_{in} = 308$ K	85
Figure 3.17	Average Nusselt number against solid concentration of water-MWCNT nanofluid	86
Figure 3.18	Comparison for Nu between Yang and Liu [44] (blue color) and present research (red color)	88

Chapter 1

Introduction

1.1 Introduction

Nanotechnology has added innovative potential to improve industrial productivity and performance. Increasing thermal properties to improve heat transfer performance using nanofluids is one of the promising applications of this technology. In this respect, nanofluids are largely used to enhance the efficiency of heat exchangers.

Shell and tube heat exchangers are the most common type of heat exchanger and are suitable for higher pressure applications. These are commonly used in water cooling applications in combination with a cooling tower in industrial processes and HVAC (Heating, Ventilating, Air Conditioning) systems. The simple design of a shell and tube heat exchanger makes it an ideal cooling solution for a wide variety of applications. They are less sensitive for dirty water from the open evaporative water cooling tower than plate heat exchangers and therefore more popular. One of the big advantages of using a shell and tube heat exchanger is that they are often easy to service particularly with models where a floating tube bundle (where the tube plates are not welded to the outer shell) is available. Different types of nanofluids are being applied by the researchers to check the improvement in the heat transfer performance to enhance the efficiency of shell and tube heat exchangers and these researches are being played a fruitful role in practical use. Research by applying MWCNT nanofluid in turbulent flow through a shell and tube heat exchanger using Kays-Crawford model can provide a helpful basis in designing more efficient shell and tube heat exchanger for enhancing the turbulent flow heat transfer rate and reducing wastage of heat energy.

1.1.1 Heat exchanger

A heat exchanger is a device that transfers heat from one fluid (a liquid or gas) to another fluid (another liquid or gas) without having mixed or come into direct contact. These are widely used in space heating, refrigeration, air conditioning, power stations, chemical plants, petrochemical plants, petroleum refineries, natural-gas processing and sewage treatment. The classic example

of a heat exchanger is found in an internal combustion engine in which a circulating fluid known as engine coolant flows through radiator coils and air flows past the coils, which cools the coolant and heats the incoming air. Another example is a heat sink, which is a passive heat exchanger that transfers the heat generated by an electronic or a mechanical device to a fluid medium, often air or a liquid coolant. The following figure is representing the working methodology of heat exchanger (Figure 1.1).

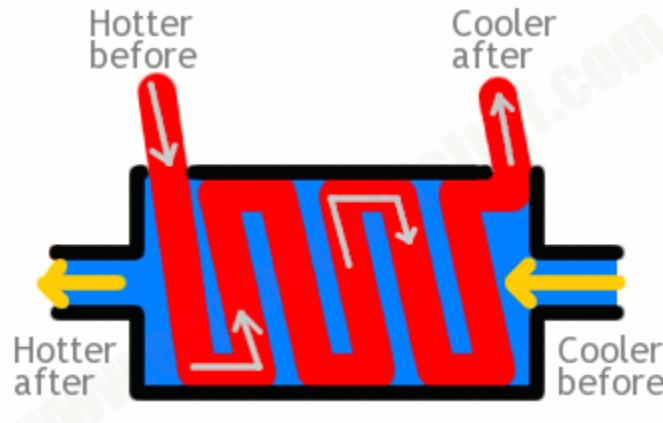


Figure 1.1: Working methodology of heat exchanger

Heat exchangers usually act as medium for heating or cooling or helping engines and machines to work more efficiently. For example, refrigerators and air conditioners use heat exchangers to remove heat from a compartment or room to cool it. In this case, heat exchangers pump heat away in a fluid and dump out it to some other place. In power plants or engines, exhaust gases often contain heat that's heading uselessly away into the open air and it causes wastage of energy. To solve this problem heat exchangers are positioned inside the exhaust tail pipes or smokestacks. As the hot exhaust gases drift upward, they brush past copper fins with water flowing through them so that the water can carry the heat away and back into the plant. There it may be used to warm the cold gases that feed into the engine or furnace, saving the energy that would otherwise be needed to heat them up or to some other good use, for example, heating an office near the smokestack.

1.1.2 Shell and tube heat exchanger

Shell and tube heat exchanger consists of an enclosed cylindrical area called the shell and a bundle of tubes is looped through the shell. It performs its task by circulating a hot liquid around tubes that contain a cooler liquid. Hot liquid in the shell warms the cooler liquid in the tubes, while the cooler liquid in the tubes cools the warm liquid in the shell. The tubes may be permanently positioned inside the shell (fixed tube-sheet exchanger) or may be removable for ease of cleaning and replacement (floating-head or U-tube exchanger). Figure 1.2 is showing configuration of a shell and tube heat exchanger.

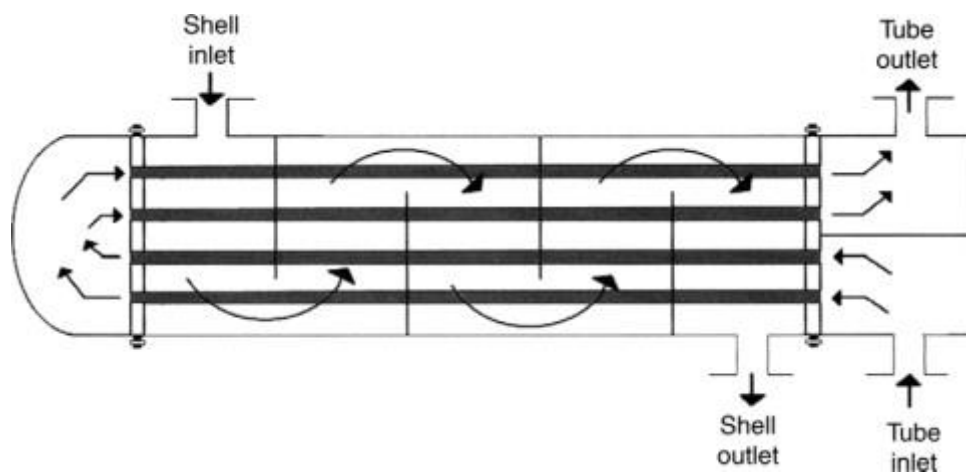


Figure 1.2: Configuration of shell and tube heat exchanger

In nuclear power plants, large two phase shell and tube heat exchangers called steam generators which typically have U-tubes are used to boil water recycled from a surface condenser into steam to drive a turbine to produce power. Most shell-and-tube heat exchangers are either 1, 2, or 4 pass designs on the tube side which refers to the number of times the fluid in the tubes passes through the fluid in the shell. The fluid goes in one end of each tube and out the other in a single pass heat exchanger.

Surface condensers in power plants are often 1-pass straight-tube heat exchangers as shown in figure 1.3(a). Two and four pass designs are common as the fluid can enter and exit on the same side which makes construction much simpler. Figure 1.3(b) is representing a 2-pass straight-tube heat exchanger.

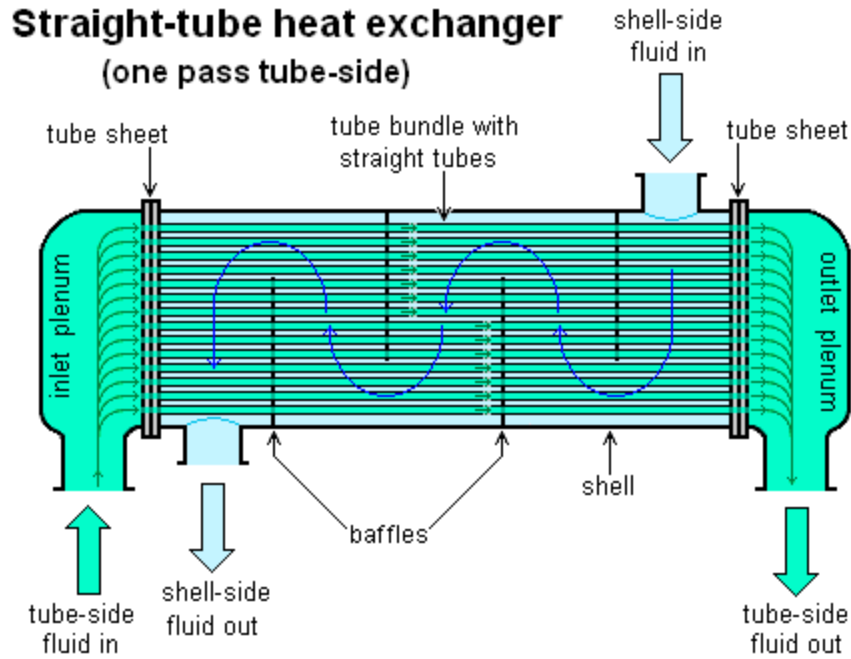


Figure 1.3(a): 1-pass straight-tube heat exchangers

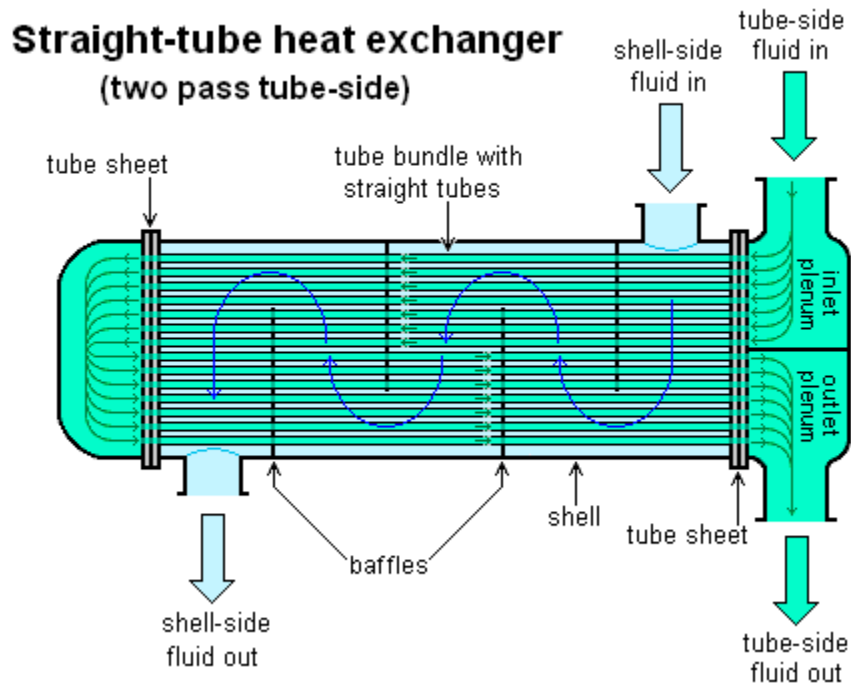


Figure 1.3(b): 2-pass straight-tube heat exchanger

Baffles are often used in directing flow through the shell side so that the fluid does not take a short cut through the shell side leaving ineffective low flow volumes. Generally, these baffles are attached to the tube bundle rather than the shell in order that the bundle is still removable for maintenance.

A shell and tube heat exchanger is an ideal cooling solution for a wide variety of applications for its simple design. Among them, one of the most common applications is the cooling of hydraulic fluid and oil in engines, transmissions and hydraulic power packs. They can also be used to cool or heat other mediums, such as swimming pool water or charge air with the right choice of materials. They are often easy to service, particularly with models where a floating tube bundle (where the tube plates are not welded to the outer shell) is available and it is a big advantage of using shell and tube heat exchangers.

1.1.3 Turbulent flow

In fluid dynamics, turbulent flow is characterized by the irregular movement of particles (one can say chaotic) of the fluid. In other words, it is a type of fluid (gas or liquid) flow in which the fluid undergoes irregular fluctuations, or mixing, in contrast to laminar flow, in which the fluid moves in smooth paths or layers. That is, in contrast to laminar flow, the fluid does not flow in parallel layers, the lateral mixing is very high and there is a disruption between the layers. In turbulent flow, the speed of the fluid at a point is continuously undergoing changes in both magnitude and direction. For example, the flow of wind and river is generally turbulent in this sense, even if the currents are gentle as the air or water swirls and eddies while its overall bulk moves along a specific direction.

Behavior of turbulent flow regime is very important in engineering, because most industrial flows, especially those in nuclear engineering are turbulent. But unfortunately, turbulence complicates all analysis for its highly intermittent and irregular character and therefore turbulence is often said to be the “last unsolved problem in classical mathematical physics”. The main tool available for their analysis is CFD (Computational Fluid Dynamics) analysis which uses numerical analysis and algorithms to solve and analyze problems that involve turbulent fluid flow. The difference in dye trace between laminar and turbulent flow has represented in following figure (Figure 1.4).

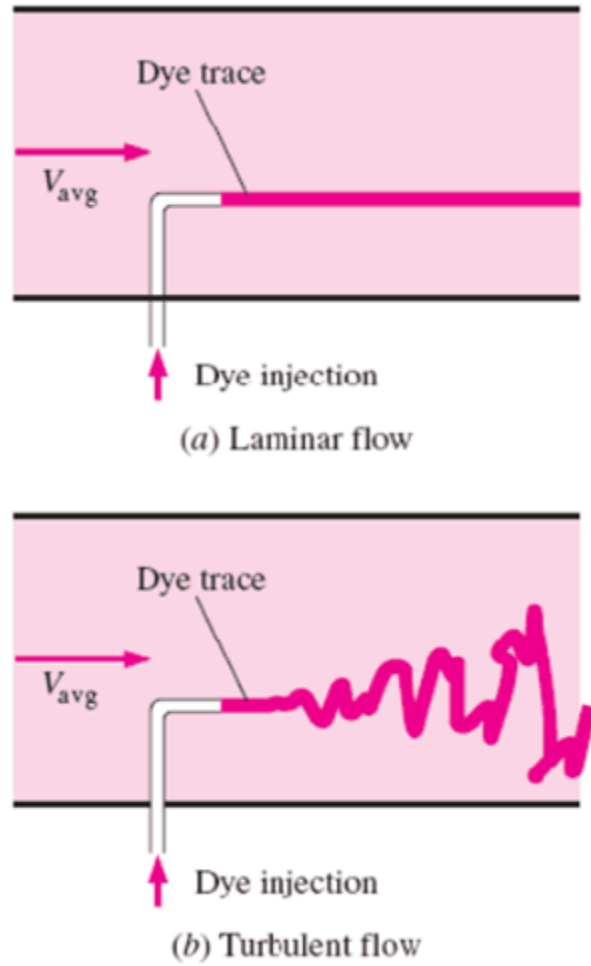


Figure 1.4: Difference in dye trace of laminar and turbulent flow.

Characteristics of turbulent flow:

- Turbulent flow tends to occur higher velocities, low viscosity and at higher characteristic linear dimensions.
- $Re > 4000$
- **Irregularity:** The turbulent flow is characterized by the irregular movement of particles of the fluid and therefore it is normally treated statistically rather than deterministically.
- **Diffusivity:** In turbulent flow, a fairly flat velocity distribution exists across the section of pipe and as a result, the entire fluid flows at a given single value and drops rapidly extremely close to the walls. The characteristic which is responsible for the enhanced

mixing and increased rate of mass, momentum and energy transports in a flow is called “diffusivity”.

- Turbulent flow is characterized by a strong three dimensional vortex generation mechanism. This mechanism is known as vortex stretching.
- The average flow velocity is approximately equal to the velocity at the center of the pipe.
- Mathematical analysis is very difficult.

1.1.4 Kays-Crawford model

Kays-Crawford model is the most used turbulence model in the treatment of industrial flows. It can be used for accurately predicting the heat transfer for liquid metal flows. This model is useful for fully developed pipe flows as well as for thermally developing pipe flows for various wall boundary conditions. The formulation of Kays-Crawford model focuses on details of the formulation of the turbulence model itself. The Kays-Crawford model for turbulence was first proposed by Kolmogorov (1942) and for stellar convection a new Kays-Crawford model was developed by Li (2012) which could reasonably describe turbulent convection both in the convectively unstable zone and overshooting regions. A revised Kays-Crawford model was developed by improving several model assumptions (including the macro-length of turbulence, convective heat flux and turbulent mixing diffusivity etc.) to make it applicable for not only convective envelopes but also convective cores. An extended Kays and Crawford turbulent Prandtl number model can be used for accurately predicting the heat transfer for liquid metal flows.

1.1.5 Heat transfer

Undulation Heat transfer is a discipline of thermal engineering that concerns the generation, use, conversion and exchange of thermal energy (heat) between physical systems. When there occurs a temperature difference between two bodies, heat flows from higher temperature to lower temperature so that they can reach at the same temperature. This state of the system is defined as the thermal equilibrium and described in the second law of thermodynamics. Heat transfer is classified into various mechanisms, such as thermal conduction, thermal convection, thermal

radiation and transfer of energy by phase changes. The transfer of mass of different chemical species, either cold or hot is also considered by engineers to achieve heat transfer. Although these mechanisms have distinct characteristics, they often occur simultaneously in the same system. Figure 1.5 is showing heat transfer system.

- **Heat conduction:** The direct microscopic exchange of kinetic energy of particles through the boundary between two systems is called heat conduction or diffusion.
- **Heat convection:** When bulk of a fluid (gas or liquid) carries heat along with the flow of matter in the fluid, then this type of heat transfer is called heat convection. All convective processes also move heat partly by diffusion, as well.
- **Heat radiation:** The heat transfer through a vacuum or any transparent medium (solid or fluid or gas) due to the transfer of energy by means of photons in electromagnetic waves is termed as heat radiation.

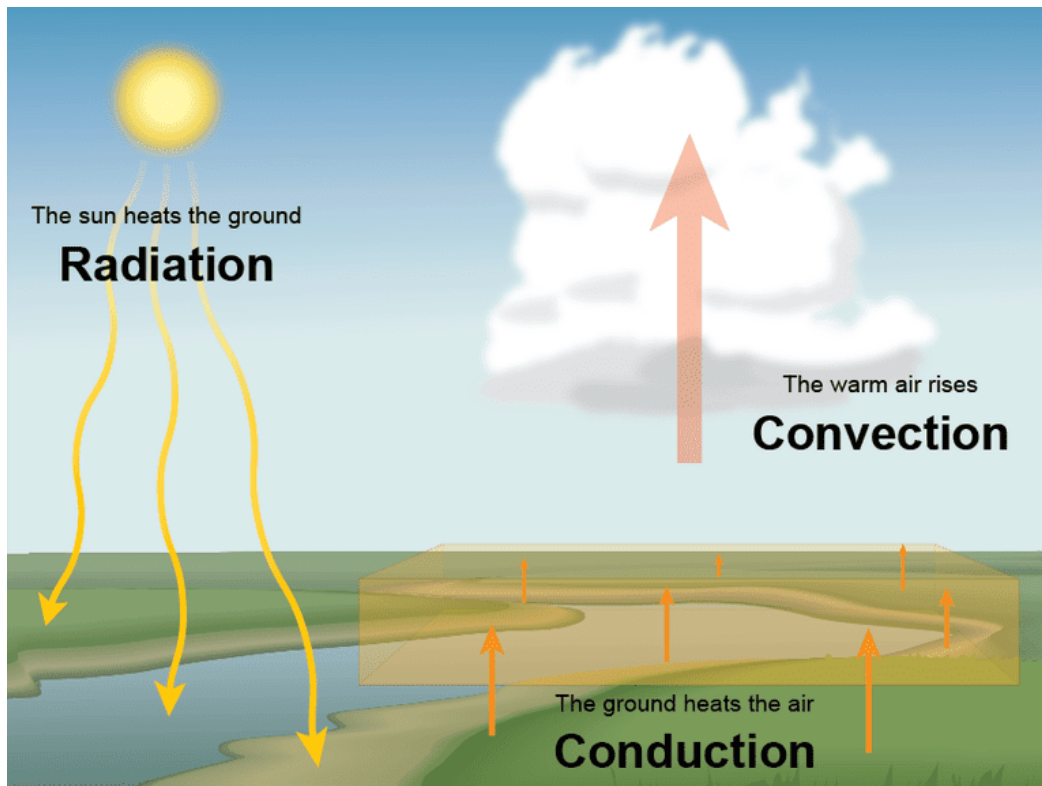


Figure 1.5: Heat transfer system

1.1.6 Conjugate heat transfer

Conjugate heat transfer is the combination of heat transfer in solids and heat transfer in fluids. It describes the processes which involve variations of temperature within solids and fluids, due to the thermal interaction between the solids and fluids. Conduction often dominates in solids whereas convection usually dominates in fluid. A typical example is the heating or cooling of a solid object by the flow of air in which it is immersed. Efficiently conjugate heat transfer is the key to designing effective coolers, heaters or heat exchangers. Heat transfer in solids and heat transfer in fluids are combined in the majority of applications as fluid flow around solids or between solid walls and also as solids are usually immersed in a fluid.

1.1.7 Forced convection

Forced convection is special type of convective heat transfer. It is a mechanism in which fluids are forced to move in order to increase heat transfer by an external source like a pump, fan, suction device or other. Forced convection can be used more effectively to create a uniform and therefore comfortable temperature throughout an entire room. Figure 1.6 and Figure 1.7 are showing examples of forced convections.



Figure 1.6: Forced convection in terms of heating/cooling a room using a fan



Figure 1.7: Forced convection by a fan in a snow machine

1.1.8 Thermal conductivity

The thermal conductivity of a material is the measurement of its ability to conduct heat. It is a physical property of a material. It is commonly denoted by κ , λ or k . The defining equation for thermal conductivity is, $q = -k\nabla T$, where q is the heat flux, k is the thermal conductivity and ∇T is the temperature gradient. This is known as Fourier's law for heat conduction. Although thermal conductivity commonly expressed as a scalar, the most general form of it is a second rank tensor. However, the tensorial description only becomes necessary in materials which are anisotropic. According to the second law of thermodynamics, heat flows from high temperature to low temperature to make the temperature difference equal to zero. Let, q be the heat flux which gives the rate per unit area at which heat flows in a certain direction (for example, X direction), T_2 be the high temperature, T_1 be the low temperature and $x = L$ be the length of separation. Then temperature difference is $T_2 - T_1$. In many materials, q is observed to be directly proportional to the temperature difference and inversely proportional to the separation. Therefore we can write,

$$q = -k \cdot \frac{T_2 - T_1}{L}$$

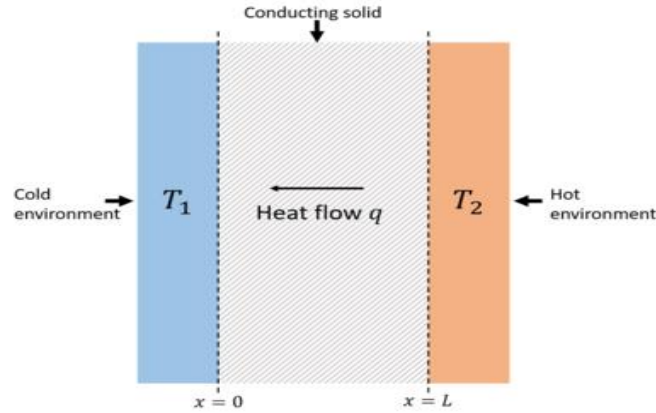


Figure 1.8: Thermal conductivity in terms of heat flow

Figure 1.8 is representing the definition of thermal conductivity in terms of heat flow. The constant of proportionality k is the thermal conductivity. In the present scenario, since $T_2 > T_1$, heat flows in the minus X direction and q is negative, which means that $k > 0$. In general k is always defined to be positive. The same definition of k can be extended to fluids, provided other modes of energy transport, such as convection and conduction are eliminated.

1.1.9 Viscosity and kinematic viscosity

The viscosity of a fluid is the measurement of its resistance to deformation at a given rate. For liquids, it corresponds to the informal concept of ‘thickness’, for example, syrup has a higher viscosity than water. In many fluids, the flow velocity is observed to vary linearly from zero at the bottom to u at the top. Moreover, the magnitude F of the force acting on the top plate is found to be proportional to the speed u and the area A of each plate and inversely proportional to their length of separation y , $F = \mu A \frac{u}{y}$

The proportionality factor μ is the viscosity of the fluid with unit of Pa.s (pascal.second). The ratio $\frac{u}{y}$ is called the rate of shear deformation or shear velocity and is the derivative of the fluid speed in the direction perpendicular to the plates. If the velocity does not vary linearly with y , then the appropriate generation is, $\tau = \mu \frac{\partial u}{\partial y}$

Figure 1.9 is showing relation between flow velocity and local shear velocity.

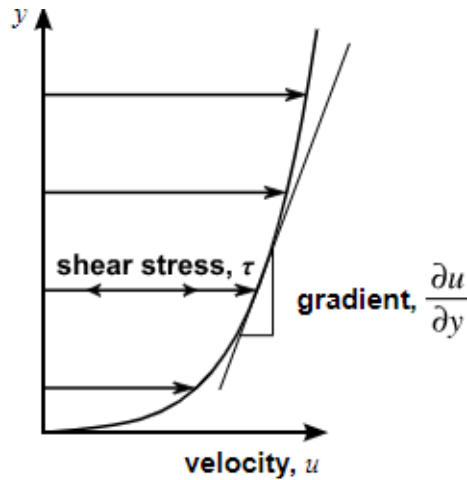


Figure 1.9: Relation between flow velocity and local shear velocity

Where, $\tau = \frac{F}{A}$ and $\frac{\partial u}{\partial y}$ is the local shear velocity. This expression is referred to as Newton's law of viscosity. Kinematic viscosity (also called "momentum diffusivity") is the measurement of a fluid's internal resistance to flow under gravitational forces. In other words, it is the measurement of the inherent resistance of a fluid to flow when no external force is exerted, except gravity. It is defined as the ratio of the viscosity μ to the density of the fluid ρ . It is usually denoted by ν and has dimension $(\text{length})^2/\text{time}$.

$$\nu = \frac{\mu}{\rho}$$

The viscosity μ is frequently called the dynamic viscosity or absolute viscosity.

1.1.10 Nanofluid and MWCNT-water nanofluid

A nanofluid is a fluid containing nanometer sized particles which are typically made of metals, oxides, carbides or carbon nanotubes. These fluids are known as colloidal suspensions of nanoparticles in a base/carrier fluid and common base/carrier fluids include water, ethylene glycol and oil. Nanofluids have novel properties for targeted changes in thermal, rheological etc. that makes them potentially useful in many applications in heat transfer including microelectronics, fuel cells, pharmaceutical processes and hybrid-powered engines, engine cooling/vehicle thermal manager, in grinding, machining and in boiler flue gas temperature

reduction. They exhibit enhanced thermal conductivity and the convective heat transfer coefficient compared to the base fluid. MWCNT-water nanofluid is a distilled water based nanofluid mixed with Multi Walled Carbon Nano Tube (MWCNT). This nanofluid is a good heat transfer fluid, with a negligible penalty in pumping power. The maximum thermal conductivity, which is highly desirable in heat transfer applications, occurred at the ultrasonication time of 60 min, solid concentration of 0.5 vol. % in water and temperature of 60 °C, was under 30%. The minimum dynamic viscosity, which is highly desirable in fluid dynamics, occurred at a 60 min ultrasonication, solid concentration of 0.1 vol. %, and temperature of 60 °C, by under 1%, while the maximum increase occurred at the highest solid concentration (0.5 vol. %) and the lowest temperature (25 °C), by higher than 3%. Figures 1.10 and 1.11 are showing SEM and TEM image of MWCNT.

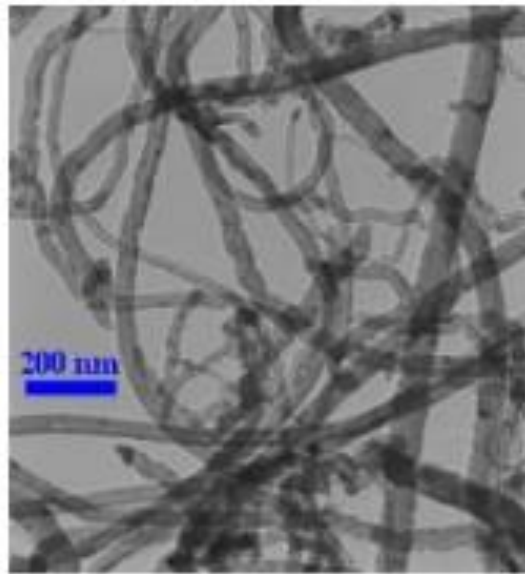


Figure 1.10: SEM image of MWCNT

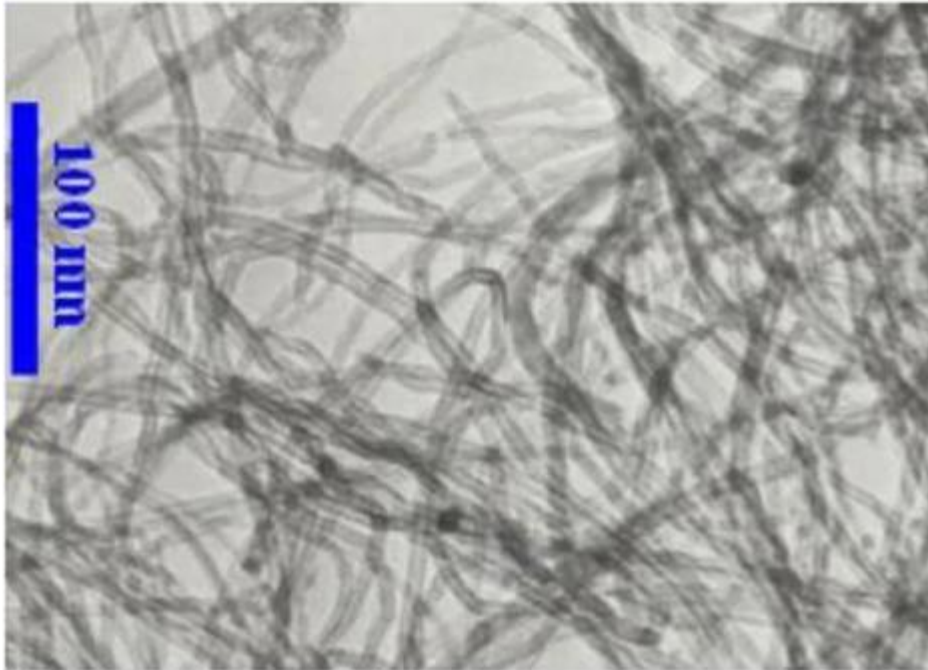


Figure 1.11: TEM image of MWCNT

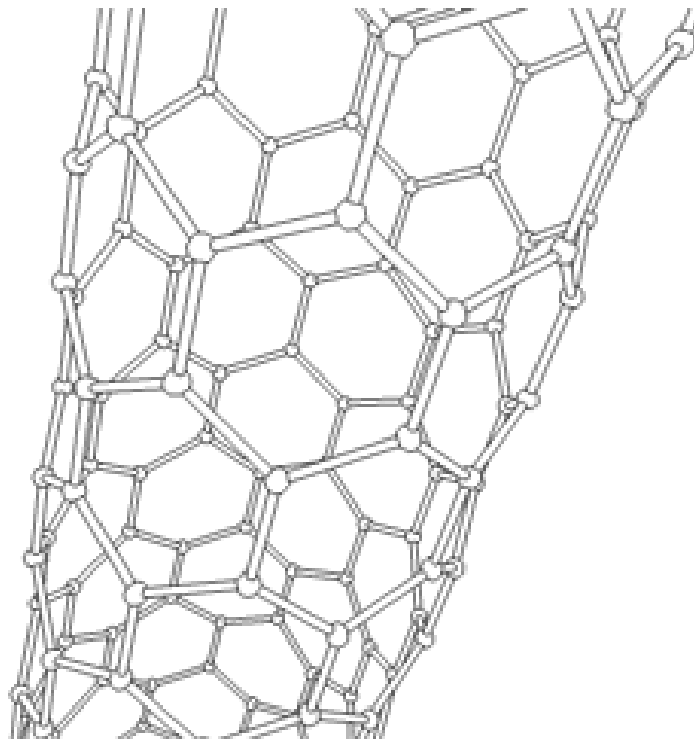


Figure 1.12: Single-walled carbon nanotube

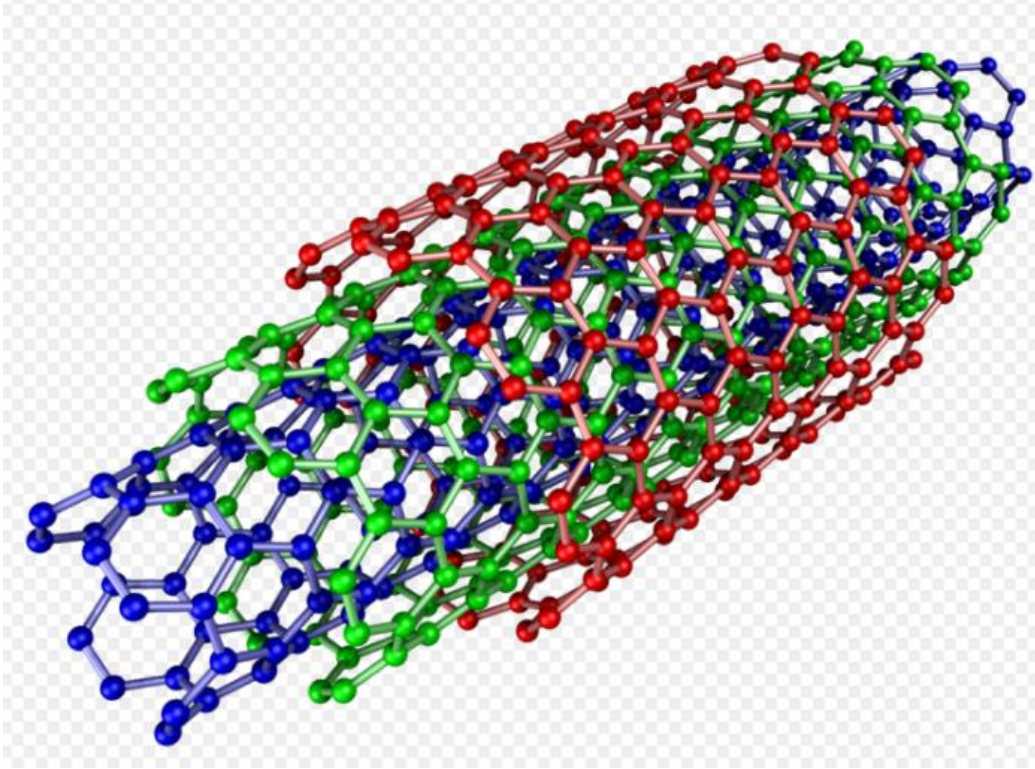


Figure 1.13: Multi-walled carbon nanotube

Figure 1.12 is the image of single walled carbon nanotube and figure 1.13 is the image of multi walled carbon nanotube here.

1.1.11 Reynolds number

Reynolds number is defined by the equation,

$$\text{Reynolds number, } Re = \frac{UL}{\nu}$$

It can easily be seen from the equation of motion that the inertia force (= terms like, ρuu_x) are order of $\frac{\rho U^2}{L}$ and the viscous forces (=terms like, $\mu \frac{\partial^2 u}{\partial x^2}$) are of order of $\frac{\mu U^2}{L^2}$.

$$\text{Therefore, } \frac{\text{inertia force}}{\text{viscous force}} \approx \frac{\frac{\rho U^2}{L}}{\frac{\mu U^2}{L^2}} = \frac{UL}{\nu} = Re$$

For this reason, Reynolds number is sometimes spoken as the ratio of inertia to viscous forces. It is in fact a parameter for viscosity. If Re is small, the viscous forces will be predominant and the

effect of viscosity will be felt in the whole flow field. On the other hand, if Re is large, the inertia force will be predominant and in such a case, the effect of viscosity will be confined in a thin layer, known as boundary layer, adjacent to the solid boundary. However, if Re is very large, the flow ceases to be laminar and becomes turbulent. The number at which this transition occurs is known as critical Reynolds number. Reynolds in 1883 found that for flow in a circular pipe becomes turbulent when Reynolds number of the flow exceeds critical value 2300. That is,

$$Re_{\text{crit}} = \left(\frac{\bar{u}d}{\nu}\right)_{\text{crit}} = 2300,$$

Where \bar{u} is the mean flow velocity, d is the diameter of the pipe.

1.1.12 Prandtl number and turbulent Prandtl number

Prandtl number is denoted by Pr and defined by the equation,

$$Pr = \frac{\text{Kinematic viscosity}}{\text{Thermal diffusivity}} = \frac{\nu}{\alpha} = \frac{\mu/\rho}{k/\rho C_p} = \frac{\mu C_p}{k}$$

It is the measure of the relative importance of viscosity of the fluid and heat conduction. The Prandtl number, like the viscosity and thermal conductivity, is a material property and it thus varies from fluid to fluid. For air, $Pr = 0.72$ (approx.) and for water at 60°F , $Pr = 7.00$ (approx.). For mercury, $Pr = 0.044$, but for high viscous fluid it may be very large, e.g. for glycerin, $Pr = 7250$.

The turbulent Prandtl number (Pr_t) is a non-dimensional term defined as the ratio between the momentum eddy diffusivity and heat transfer eddy diffusivity. It is useful for solving the heat transfer problem of turbulent boundary layer flows. The simplest model for Pr_t is the Reynolds analogy which yields a turbulent Prandtl number of 1. From experimental data, Pr_t has an average value of 0.85, but ranges from 0.7 to 0.9 depending on the Prandtl number of the given fluid.

The turbulent Prandtl number is then defined as,

$$Pr_t = \frac{\varepsilon_M}{\varepsilon_H}$$

where, ε_M is the eddy diffusivities for momentum transfer and ε_H is the diffusivities for heat transfer.

1.1.13 Nusselt number

Nusselt number is denoted by Nu. It is the ratio of heat flow rate by convection under unit temperature gradient to the heat flow rate by conduction process under unit temperature gradient through a characteristic length.

$$\text{Nu} = \frac{hL}{k}$$

1.2 Literature Review

Shell and tube heat exchangers are used widely in the chemical process industries, especially in refineries for their numerous advantages over other types of heat exchangers. Heat exchanger's efficiency can be increased by increasing working fluid's efficiency. Different investigations have been done on the enhancement of the thermal properties of the working fluid by researchers [1-4]. Working fluid's main property for the heat transfer application depends upon the thermal conductivity of that particular material [5]. Increase of nanoparticle concentration enhances heat transfer coefficient [6-8]. Increasing nanoparticle concentration increases thermal conductivity of fluid and consequently heat transfer coefficient on the laminar by 7 and 22% in turbulent regions [9-10]. Experimental investigation using nanofluid inside a horizontal shell and tube heat exchanger was conducted by Aghabozorg *et al.* [11]. A review report on heat transfer enhancement of shell and tube heat exchangers using different nanofluids has been expressed by Krishnan and Kumar [12].

Researchers [13-16] investigated pressure drop, tubeside flow and heat transfer considering different forms of shell and tube heat exchangers like segmentally baffled, helically coiled, arranged in a triangular pitch etc. An investigation had done on the characteristics of (Ethelene Glycol+Al₂O₃) nanofluid and Ethelene Glycol fluid which cross a rectangular arrangement of tubes in a shell and tube heat exchanger by Khoddamrezaee *et al.* [17]. Hasanuzzaman *et al.* [18] showed in a research that convective heat transfer coefficient of Cu-water, Al-water, Al₂O₃-

water and TiO_2 -water nanofluids are 81, 6, 66 and 64% higher compared to pure water respectively. A comparison of the thermo-physical properties of the fluids conventional water and ethelene glycol with nanofluids Al_2O_3 and CuO immersed in water and ethelene glycol was studied by Gurrieri *et al.* [19].

An experimental study was conducted by Cox *et al.* [20] in a laboratory scale industrial type shell and tube heat exchanger with three mass particle concentrations, 2, 4 and 6% of SiO_2 -water nanofluids formulated by dispersing 20 nm diameter nanoparticles in desalinated water. This study represented that the measured pressure drop in the nanofluids flow shows an increase when compared to that of base fluid that could limit the use of nanofluids in heat exchangers for industrial applications. Albadr *et al.* [21] reports an experimental study on forced convective heat transfer and flow characteristics of a nanofluid consisting of water and different volume concentrations of Al_2O_3 -water nanofluid (0.3-2%) flowing in a horizontal shell and tube heat exchanger counter flow under turbulent flow conditions. This study represented that the convective heat transfer coefficient of nanofluid is slightly higher than that of the base liquid at some mass flow rate and at some inlet temperature.

The effect of using Al_2O_3 -water nanofluid on thermal performance of a commercial shell and tube heat exchanger with segmental baffles is assessed experimentally by Barzegarian *et al.* [22]. According to the analysis results of this research, utilizing nanofluid at minimum and maximum nanoparticles volume fraction ($\varphi = 0.03$ and 0.3%) results in average augmentation of around 6.5% and 18.9% in thermal performance fator (η) of the heat exchanger compared to the base liquid respectively. Ullah *et al.* [23] numerically investigated the heat transfer characteristics of $\gamma\text{-Al}_2\text{O}_3$ -water and TiO_2 -water nanofluids in a shell and tube heat exchanger under turbulent flow condition and found that, for $\gamma\text{-Al}_2\text{O}_3$ -water maximum improvement in convective heat transfer coefficient is 41.8% while TiO_2 -water shows maximum 37% increment.

Majdi *et al.* [24] conducted a research in a double pipe heat exchanger under turbulent flow conditions where aluminium oxide nanoparticles were used with different concentrations (0.6-3g/l) in hot water to increase the heat transfer rate. Again, Saffarian *et al.* [25] used a shell and tube heat exchanger with a 25% baffle cut in which heat transfer performance through tubes of different cross sections (circular, elliptical with an attack angle of 90° and elliptical with an

attack angle of 0°) were studied. This study represented that a heat exchanger with ellipsoidal tubes near the shell with an attack angle of 90° and circular tubes in the center of the shell showed the highest heat transfer compared with the shell and tube heat exchangers with circular tubes and elliptical tubes with an attack angle of 90° and 0° . Rao *et al.* [26] has investigated the heat transfer rate of different concentrations of alumina nanofluids using a shell and tube heat exchanger in single and multi-tubes under turbulent flow condition by a forced convection mode. An investigation was conducted by Albadr [27] to experiment the thermal performance of propylene glycol/water with a concentration of (10/90) % and Al_2O_3 -water nanofluid with a volume concentration of (0.1, 0.4, 0.8, 1.5 and 2.5%) under turbulent flow inside a horizontal shell and tube heat exchanger.

Experiments under turbulent flow conditions were executed using distilled water and Al_2O_3 -water nanofluid with 0.2, 0.5, and 1% particle volume concentrations for different type of heat exchanger including shell and tube heat exchanger by Mansoury *et al.* [28]. Etaig *et al.* [29] conducted a three-dimensional analysis for a co-current heat exchanger with inclined baffles where Magnesium Oxide-copper Oxide-water hyper nanofluid is the cooling fluid. An experimental study is performed with a volume fraction between 0.1, 0.2, and 0.3% of Al_2O_3 and Reynolds number between 3000 and 10500 to investigate Nusselt number and friction factor of nanofluids through a shell and tube heat exchanger [30].

Researchers showed that Kays Crawford model is mostly used for liquid metal turbulent flows and useful for fully developed and thermally developing pipe flows for various wall boundary conditions [31-32]. This is the superiority of the Kays-Crawford model over conventional model to conduct the present research.

1.3 Objectives

The objective of this research is to investigate numerically velocity, pressure, temperature and heat transfer rate for different variations of relevant parameters which will be carried out with the turbulent flow through a shell and tube heat exchanger using water-MWCNT nanofluid. The specific aims of this research are as follows:

- To modify the mathematical model using Reynolds Averaged Navier-Stokes (RANS) equations, Kays-Crawford model of turbulent Prandtl number and nanofluid's effective properties.
- To solve the mathematical model numerically.
- To obtain the effects of turbulent flow and nanofluid on velocity, pressure, temperature and heat transfer rate.

1.4 Outline of the Thesis

A brief description of the numerical investigation of heat transfer performance through a shell and tube heat exchanger using pure water and water based MWCNT nanofluid has been presented in this thesis. This thesis consists of four chapters as stated below:

Chapter 1 contains introduction of the present work including a literature review of the past studies on heat transfer performance through different types of shell and tube heat exchanger using nanofluids which are relevant to the present work. Objectives of the present study have also been incorporated in this chapter.

Chapter 2 explains the two dimensional model of a shell and tube heat exchanger which consists of a bundle of circular tubes containing abundant supply of cooling water at constant temperature. Besides, mathematical formulation has been given for numerical computation in this chapter. This chapter also presents a detailed description for the numerical simulation of heat transfer and fluid flow characteristics of heat transfer through the external region of the circular tubes using water and water based MWCNT nanofluids.

In Chapter 3, the effects of solid concentration, velocity and temperature of water based MWCNT nanofluides have been investigated. Results have been shown in isothermal lines, streamlines to better understand the heat transfer mechanism through the considered model of shell and tube heat exchanger. The comparison of obtained mean Nusselt number for various volume fractions from present numerical research with Yang and Liu [44] has been also shown.

Chapter 4 concludes remarks of the whole research and presents the recommendations for the future research systematically.

Chapter 2

Numerical Analysis

2.1 Introduction

Numerical analysis is the study of algorithms that uses numerical approximation (as opposed to symbolic manipulations) for the problems of mathematical analysis (as distinguished from discrete mathematics). Numerical analysis naturally finds application in all fields of engineering and the physical sciences, but in the 21st century also the life sciences, social sciences, medicine, business and even the arts have adopted elements of scientific computations.

2.2 Finite Element Method

The finite element method (FEM) is a numerical method for solving problems of engineering and mathematical physics. Typical problem areas of interest include structural analysis, heat transfer, fluid flow, mass transport, and electromagnetic potential. The analytical solution of these problems generally requires the solution to boundary value problems for partial differential equations. The finite element method formulation of the problem results in a system of algebraic equations. The method approximates the unknown function over the domain. To solve the problem, it subdivides a large system into smaller, simpler parts that are called finite elements. The simple equations that model these finite elements are then assembled into a larger system of equations that models the entire problem. The FEM then uses variational methods from the calculus of variations to approximate a solution by minimizing an associated error function. Studying or analyzing a phenomenon with the FEM is often referred to as finite element analysis (FEA).

A finite element method is characterized by a variational formulation, a discretization strategy, one or more solution algorithms and post-processing procedures. Examples of variational formulation are the Galerkin method, the discontinuous Galerkin method, mixed methods, etc. A discretization strategy is understood to mean a clearly defined set of procedures that cover (a) the creation of finite element meshes, (b) the definition of basis function on reference elements (also

called shape functions) and (c) the mapping of reference elements onto the elements of the mesh. Examples of discretization strategies are the h-version, p-version, hp-version, x-FEM, isogeometric analysis, etc. Each discretization strategy has certain advantages and disadvantages. A reasonable criterion in selecting a discretization strategy is to realize nearly optimal performance for the broadest set of mathematical models in a particular model class. There are various numerical solution algorithms that can be classified into two broad categories; direct and iterative solvers. These algorithms are designed to exploit the sparsity of matrices that depend on the choices of variational formulation and discretization strategy.

Post-processing procedures are designed for the extraction of the data of interest from a finite element solution. In order to meet the requirements of solution verification, postprocessors need to provide for a posteriori error estimation in terms of the quantities of interest. When the errors of approximation are larger than what is considered acceptable then the discretization has to be changed either by an automated adaptive process or by action of the analyst. There are some very efficient postprocessors that provide for the realization of super convergence.

The figure 2.1 is an example of a two dimensional FEM (finite element method) mesh for a cylindrically shaped magnetic shield. The mesh is created by an analyst prior to solution by the FEM software. In this case "two dimensional" means that the picture shows a flat cross section of an assembly that extends to a large distance at right-angles to the paper (Cartesian coordinates). The rectangle outlined at the right of the picture has been designated the conducting component, which carries the electric current that creates the magnetic field. The cylindrical part has been designated to be a material of high magnetic permeability (for example iron). The gray areas have been designated air. The mesh is divided into smaller triangles inside the cylinder, which is an area where the lines of magnetic flux will be more concentrated.

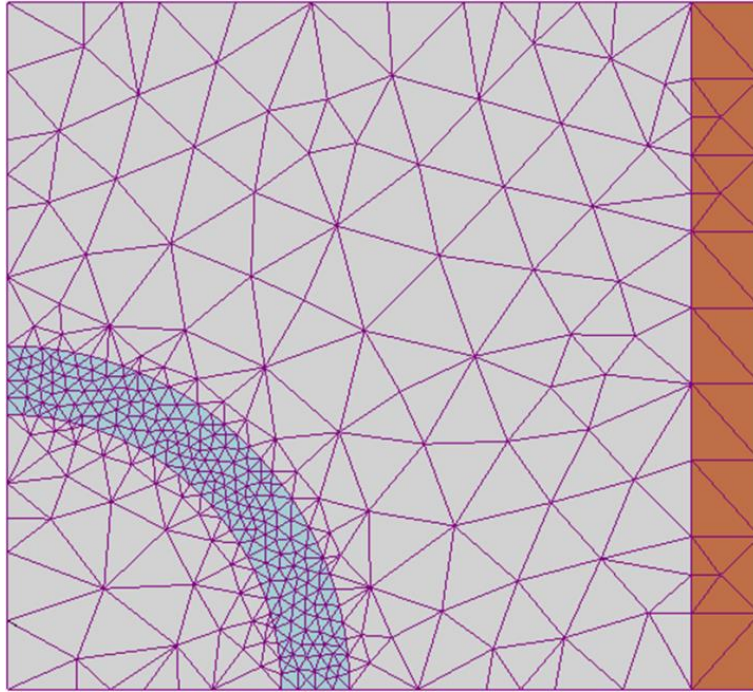


Figure 2.1: FEM mesh

2.3 Problem Formulation

The schematic diagram of the studied configuration has been depicted in the Figure 2.2. This model describes a part of a shell and tube heat exchanger, where hot water enters from above. The cooling medium, commonly water, flows through the pipes and enters from the side. The tubes assumed to be made of stainless steel. The arrows indicate the flow directions.

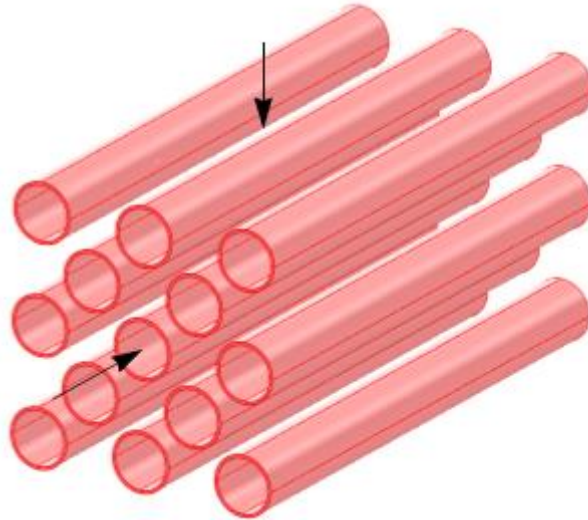


Figure 2.2: A tube bundle from a shell and tube heat exchanger

Assuming that the cooling water is in abundant supply, the flow through the pipes has a constant temperature. Under that assumption, we can model this heat exchanger by a two dimensional (2D) model as shown in Figure 2.3.

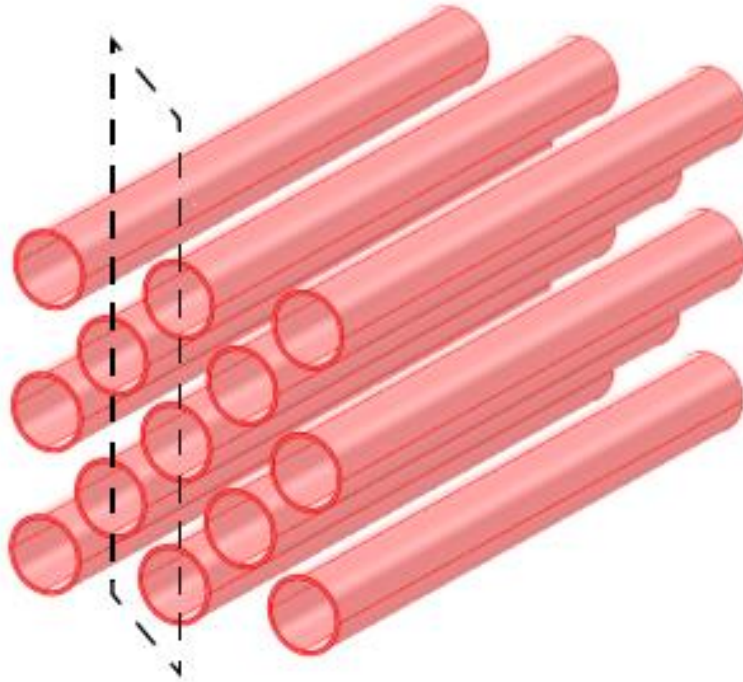


Figure 2.3: The model region

The dashed line marks the model region. The corresponding 2D domain appears in Figure 2.4. In this figure it is noticed that total length of x and y axes are 50 and 1000 mm, respectively. It is noted that the pipe interiors are not part of the domain because the model assumes the temperature to be constant there.

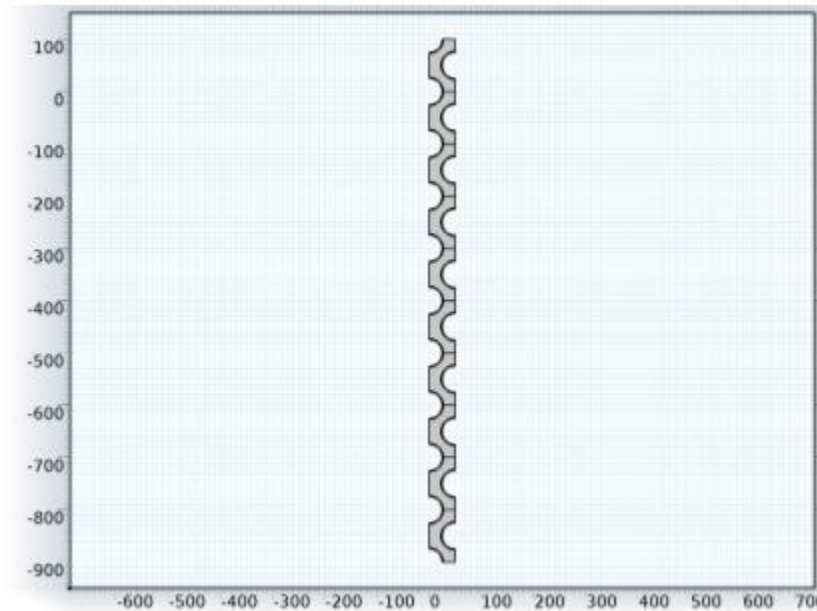


Figure 2.4: The modeled 2D region (Total arc length of the region is considered as 1000 mm)

An important characteristic of the flow is the Reynold number, Re , defined as,

$$Re = \frac{UL}{\eta}$$

where U is a velocity scale, L is a length scale and η is a kinematic viscosity. If the Reynolds number is low, no turbulence model is needed. If, on the other hand, the Reynolds number is high, then the flow is dominated by convection and a turbulence model is necessary.

In this case, a suitable velocity scale is the mean inlet velocity, which is 1.5 m/s and L is to set to the pipe radius. Then, using standard values for water for the density and viscosity, the equation

gives an approximate Reynolds number of 75,000, which is high enough to warrant the use of a turbulence model.

Figure 2.5 shows the close view of the modeled 2D region where the arrows indicate the flow. This numerical study demonstrates how to model a conjugate heat transfer problem with COMSOL Multiphysics, using the Turbulent Fluid-Thermal Interaction predefined Multiphysics coupling from the Heat Transfer Module. It also demonstrates how to generate a fully developed flow field when you know the mass flow rate but not the pressure drop.

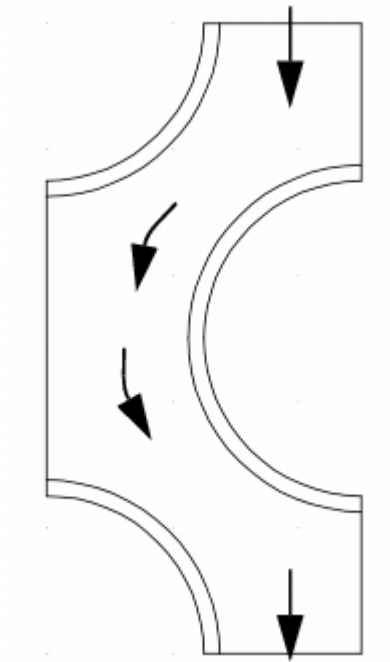


Figure 2.5: Close view of the modeled 2D region

Figure 2.6 expresses the CAD (Computer Aided Design) model loaded in COMSOL Multiphysics geometry file.

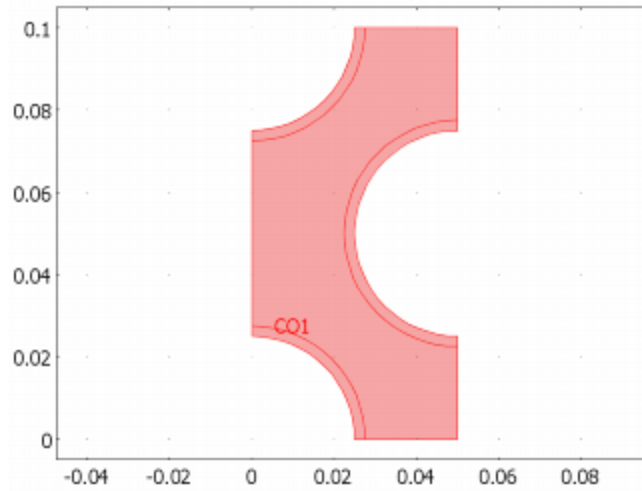


Figure 2.6: Loaded CAD model in COMSOL Multiphysics geometry

This model studies a part of a shell-and-tube heat exchanger where hot water enters from above. The cooling medium flows through the tubes that, in this model, impose a constant temperature at the walls. Furthermore, the tubes are assumed to be made of stainless steel and the heat flux is also modeled through them. The purpose of the model is to show the coupling between the k-omega turbulence model and the heat transfer modeling interfaces in the Heat Transfer Module.

2.4 Mathematical Modeling

The governing equations in this model are

- The Reynolds-averaged Navier-Stokes (RANS) equations and a $\kappa - \varepsilon$ turbulence model in the water-MWCNT domain.
- Keys-Crowford heat transport turbulence model in the water-MWCNT and the solid (steel) tube walls.

The non-isothermal flow interface sets up both sets of equations together with the applicable couplings, making it easy to model the fluid-thermal interaction. The model uses temperature-dependent properties for water and steel from the built-in material library. It incorporates the influence of the turbulent fluctuations on the temperature field using the Kays-Crawford model

for the turbulent Prandtl number. Furthermore, to account for the effect of mixing due to eddies, it is necessary to correct the fluid's thermal conductivity. The turbulence results in an effective thermal conductivity. The turbulence results in an effective thermal conductivity, κ_{eff} , according

$$\text{to the equation.}, \kappa_{eff} = \kappa + \kappa_T \kappa_T = \frac{C_p \mu_T}{Pr_T}$$

where κ is the fluid's physical thermal conductivity and κ_T is the turbulent thermal conductivity. Furthermore, μ_T denotes the turbulent dynamic viscosity, C_p is the heat capacity and Pr_T refers to the turbulent Prandtl number. The 2D numerical simulation has been performed in steady state conditions. The governing partial differential equations [33-36] in terms of non-isothermal flow and thermal energy equations using water-MWCNT nanofluid are given below:

Continuity Eqⁿ

$$\frac{\partial u}{\partial x} + \frac{\partial v}{\partial y} = 0 \quad (1)$$

Momentum Eqⁿ

$$\rho_{nf} \left(u \frac{\partial u}{\partial x} + v \frac{\partial u}{\partial y} \right) = -\frac{\partial p}{\partial x} + (\mu_{nf} + \mu_T) \left(\frac{\partial^2 u}{\partial x^2} + \frac{\partial^2 u}{\partial y^2} \right) \quad (2)$$

$$\rho_{nf} \left(u \frac{\partial v}{\partial x} + v \frac{\partial v}{\partial y} \right) = -\frac{\partial p}{\partial y} + (\mu_{nf} + \mu_T) \left(\frac{\partial^2 v}{\partial x^2} + \frac{\partial^2 v}{\partial y^2} \right) \quad (3)$$

Turbulent Kinetic Energy Eqⁿ

$$\rho_{nf} \left(u \frac{\partial \kappa}{\partial x} + v \frac{\partial \kappa}{\partial y} \right) = \left(\mu_{nf} + \frac{\mu_T}{\sigma_\kappa} \right) \left(\frac{\partial^2 \kappa}{\partial x^2} + \frac{\partial^2 \kappa}{\partial y^2} \right) + p_\kappa - \rho \epsilon \quad (4)$$

Turbulent Energy Dissipation Eqⁿ

$$\rho_{nf} \left(u \frac{\partial \epsilon}{\partial x} + v \frac{\partial \epsilon}{\partial y} \right) = \left(\mu_{nf} + \frac{\mu_T}{\sigma_\epsilon} \right) \left(\frac{\partial^2 \epsilon}{\partial x^2} + \frac{\partial^2 \epsilon}{\partial y^2} \right) + C_{\epsilon 1} \frac{\epsilon}{\kappa} p_\kappa - C_{\epsilon 2} \rho \frac{\epsilon^2}{\kappa} \quad (5)$$

Energy Eqⁿ

$$(\rho C_p)_{nf} \left(u \frac{\partial T}{\partial x} + v \frac{\partial T}{\partial y} \right) = k_{nf} \left(\frac{\partial^2 T}{\partial x^2} + \frac{\partial^2 T}{\partial y^2} \right) \quad (6)$$

where,

$$p_\kappa = \mu_T [\nabla \mathbf{u} : (\nabla \mathbf{u} + (\nabla \mathbf{u})^T) - \frac{2}{3} (\nabla \cdot \mathbf{u})^2] - \frac{2}{3} \rho \kappa (\nabla \cdot \mathbf{u}) \text{ and } \mu_T = \rho C_\mu \frac{\kappa^2}{\epsilon},$$

$$C_{\epsilon 1} = 1.44, C_{\epsilon 2} = 1.92, C_\mu = 0.09, \sigma_\kappa = 1.0, \sigma_\epsilon = 1.3 \quad (7)$$

The following models of effective properties of nanofluids have been chosen as:

$$\text{Thermal diffusivity, } \alpha_{nf} = k_{nf}/(\rho C_p)_{nf} \quad (8)$$

$$\text{Density, } \rho_{nf} = (1 - \phi)\rho_f + \phi\rho_s \quad (9)$$

$$\text{Heat capacitance, } (\rho C_p)_{nf} = (1 - \phi)(\rho C_p)_f + \phi(\rho C_p)_s \quad (10)$$

$$\text{Specific heat at constant pressure, } C_{pnf} = \frac{(1-\phi)(\rho C_p)_f + \phi(\rho C_p)_s}{(1-\phi)\rho_f + \phi\rho_s} \quad (11)$$

$$\text{Viscosity of Brinkman model [37], } \mu_{nf} = \frac{\mu_f}{(1-\phi)^{2.5}} \quad (12)$$

Thermal conductivity of Maxwell-Garnett model [38]

$$k_{nf} = k_f \frac{k_s + 2k_f - 2\phi(k_f - k_s)}{k_s + 2k_f + \phi(k_f - k_s)} \quad (13)$$

The mean Nusselt number at the top surface of the shell and tube heat exchanger,

$$Nu = -\frac{k_{nf}}{k_f} \frac{1}{L_{in}} \int_0^{L_{in}} \frac{\partial T}{\partial y} dx \quad (14)$$

2.4.1 Boundary conditions

Figure 2.7 displays the appropriate boundary conditions for the present numerical investigation.

The boundary conditions for the problem are as follows:

- $\kappa - \varepsilon$ equations in the fluid domain:
 - Specified initial velocity, v_{in} m/s
 - Symmetry at the region borders
 - Logarithmic wall function at the pipe/fluid interfaces
 - Fixed outlet pressure, $p = 0$ Pa
 - Normal flow at the inlet and outlet

- Heat transport equations:
 - Fixed temperature at the inlet, T_{in} K
 - Convection-dominated transport at the outlet
 - Symmetry (thermal insulation) at the region borders
 - Thermal wall function at the pipe/fluid interfaces
 - Fixed temperature at the inner pipe surfaces, T_{pipe} K

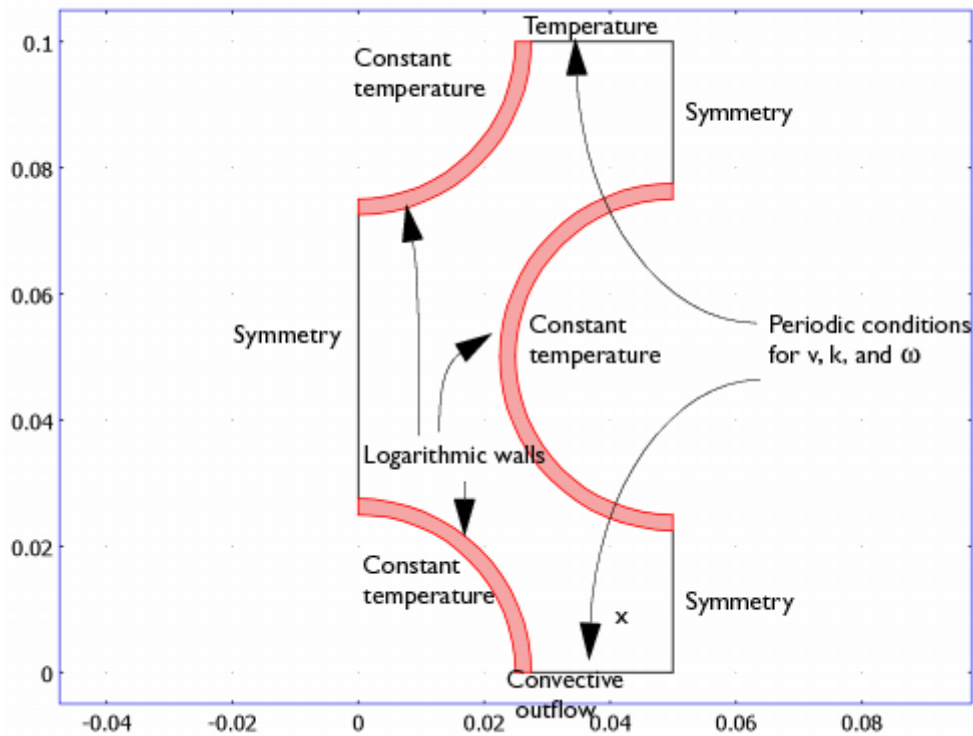


Figure 2.7: Modeled 2D geometry with boundary condition

The periodicity of the flow is important because we are modeling a part of the heat exchanger where the flow is fully developed. It is hard to make a periodic configuration converge from a homogeneous initial guess, however, and therefore, an initial calculation with constant inlet velocity and fixed outlet pressure is first performed.

The logarithmic wall function boundary condition for turbulent flow is used to model the solid-fluid interfaces. An algebraic relationship—the logarithmic wall function—describes the

momentum transfer at the solid-fluid interface. This means that the solid-fluid boundaries in the model actually represent lines within the logarithmic regions of the boundary layers. Similar to the fluid velocity, the temperature is not modeled in innermost part of the boundary layer. Instead of assuming continuity of the temperature across the layer, a thermal “wall function” is used. There is a jump in temperature from the solid surface to the fluid due to the omitted innermost part of the boundary layer. The predefined group for the wall domains defines this wall function in the following way.

To achieve the thermal wall function, the model uses two heat transfer application modes: one for the solid, and one for the fluid. These are connected through a heat flux boundary condition, the thermal wall function. This means that the resistance to heat transfer through the innermost part of the boundary layer is related to that for momentum transfer for the fluid. The heat flux, q , is determined by the equation

$$q = \frac{\rho C_p C_\mu^{1/4} k_w^{1/2} (T_w - T)}{T^+}$$

Where ρ and C_p are the fluid’s density and heat capacity, respectively; C_μ is a constant of the turbulence model; and k_w is the value of the turbulent kinetic energy at the wall. T_w equals the temperature of the solid at the wall, while T is the temperature of the fluid on the other side of the omitted laminar sublayer. The dimensionless quantity $T^+ = T^+(\delta_w^+)$ is the dimensionless temperature and depends on the dimensionless wall offset, δ_w^+ .

Table 2.1 demonstrates the values of different constants imposed in this model.

Table 2.1: Different constants values

Name	Expression	Description
T_{in}	323[K]	Inflow temperature
T_{pipe}	278[K]	Pipe temperature
v_{in}	-1.5[m/s]	Inflow velocity
ρ	988[kg/m ³]	Reference density
L_{in}	0.025[m]	Width of inflow boundary
mf_{in}	$L_{in} * \rho * v_{in}$	Mass inflow

2.4.2 Thermo-physical properties

Thermo-physical properties [39-41] of base fluid and different nanoparticles have been shown in Table 2.2, assumed constant except for the density variation, which is maintained on Boussinesq approximation.

Table 2.2: Thermo- physical properties of base fluid, nanoparticle and pipe material

Physical properties	Fluid phase (water)	MWCNT	Steel
C_p (J/kgK)	4179	796	475
ρ (kg/m ³)	988	1600	7850
k (W/mK)	0.6	3000	44.1

2.5 Computational Procedure

Using the Galerkin weighted residual finite element technique [42-43] the momentum and energy balance equations have been solved using COMSOL Multiphysics. In this method, the solution domain has been discretized into finite element meshes, which have been composed of non-uniform triangular elements. Then the nonlinear and dimensional governing partial differential equations have been transferred into a system of integral equations by applying Galerkin weighted residual method. The basic unknowns for the governing partial differential

equations (1-6) are the velocity components u , v , the turbulent kinetic energy, κ , turbulent dissipation rate, ε , the temperature T and the pressure p . The six nodes with triangular element have been used in this numerical research. All six nodes have been associated with velocities as well as temperature while three corner nodes with pressure. The nonlinear algebraic equations so obtained have been modified by imposition of boundary conditions. These modified nonlinear equations have been transferred into linear algebraic equations by using Newton's method. Finally, these linear equations have been solved by using triangular factorization method. The convergence criterion for the solution procedure has been defined as $|\psi^{n+1} - \psi^n| \leq 10^{-6}$, where n is the number of iteration and ψ is a function of u , v , κ , ε and T .

2.5.1 Mesh generation

The discrete locations at which the variables are to be calculated are defined by a mesh which covers the geometric domain on which the problem is to be solved. It divides the solution domain into a finite number of sub-domains called finite elements. The computational domains with irregular geometries by a collection of finite elements make the method a valuable practical tool for the solution of boundary value problems arising in various fields of engineering.

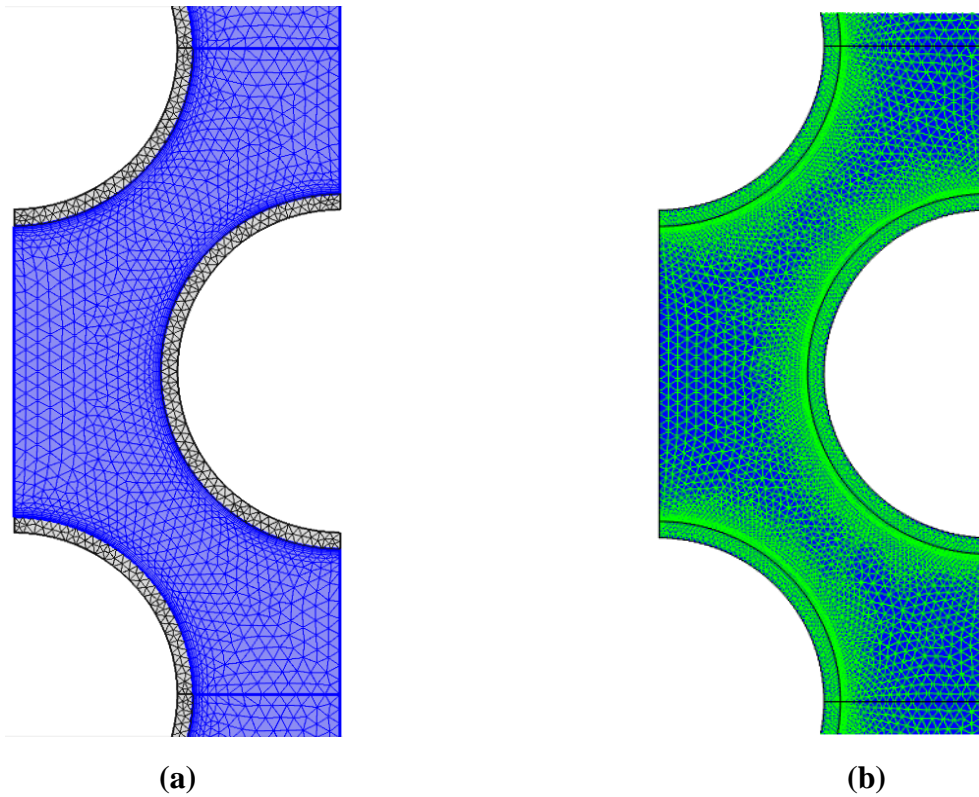


Figure 2.8: FEM mesh generation (a) normal and (b) fine mesh type

Figure 2.8 displays the finite element mesh of the present physical domain. The mesh consists of tetrahedral element with ten nodes in subdomain and triangular element with six nodes in boundaries.

2.5.2 Grid sensitivity test

In order to determine the proper grid size for this study, a grid independence test has been conducted with five types of mesh for water-MWCNT nanofluid of solid volume fraction 1%, inlet velocity -1.5 m/s, temperature 323 K and mass flow rate 2.91 kg/s. This test result has been shown in Table 2.3. Corresponding grid densities are 51198 nodes, 14036 elements, time 65 s; 73885 nodes, 21026 elements, 113 s; 107039 nodes, 31678 elements, 217 s; 284771 nodes, 93224 elements, 384 s; and 701802 nodes, 250676 elements, 739 s. The extreme value of Nu is used as the monitoring variable for sensitivity measure of the accuracy of the solution. Taking into account both the precision of numerical values and computational time, the present

calculations are performed with 284771 nodes, 93224 elements grid system. In the Table 2.3, it is observed that no further improvement in accuracy occur using higher number of elements.

Table 2.3: Grid sensitivity check at $\phi = 0.01$, $v_{in} = -1.5$ m/s and $T_{in} = 323$ K

Mesh type	Coarser	Coarse	Normal	Fine	Finer
Elements	14036	21026	31678	93224	250676
Nu	1080	1083	1087	1088	1088.43
Time (s)	42	95	153	212	464

Chapter 3

Results and Discussions

3.1 Introduction

Heat transfer performance for different concentration of water-MWCNT nanofluid flow through a shell and tube heat exchanger has been investigated numerically where the heat transfer is conjugate and the flow is turbulent. We have used the Kays-Crawford model for the turbulent Prandtl number. To explain the numerical results of the previous chapter and investigate the effect of solid concentration, inflow velocity and inlet temperature on heat transfer performance, we have been used different solid concentration of nanoparticles (0-3%), inflow velocities (- 0.1, - 0.5, - 1 and - 1.5 m/s) and inlet temperatures (323, 318, 313 and 308 K). The effects for the variation of mentioned physical parameters have been presented graphically via stream function contours (streamlines) and temperature contours (isotherms) in this chapter.

3.2 Effect of Solid Concentration

We have used water and water-MWCNT nanofluid of solid volume fraction (0.1, 1, 2 and 3%) to identify the effect of solid concentration with fixed value of inflow velocity, temperature and mass flow rate of working fluid - 1.5 m/s, 323 K and 2.91 kg/s respectively. We have checked the changes in velocity and temperature contours, surface plot for velocity magnitude. Also, velocity, pressure and temperature at $y = 400, 500, 600$ and 700 mm arc length for water and all above mentioned concentrations of water-MWCNT nanofluid have been displayed.

Figure 3.1 (a-c) is representing the streamlines, isothermal lines and surface plot for velocity magnitude of the tabular heat exchanger using HTF as water i.e. base fluid. It is shown from the figure 3.1(a) that the velocity is very low at the opposite parts of circular pipes' wall in the exterior region. Again, the velocity is the maximum at the quarter part adjacent region to the exterior wall of the pipes. From figure 3.1(b) it can be understood that the temperature is very low at the lower portion of the circular pipes in the exterior region. The velocity is the minimum at each corner of the exterior region of the circular pipes which is realized from figure 3.1(c).

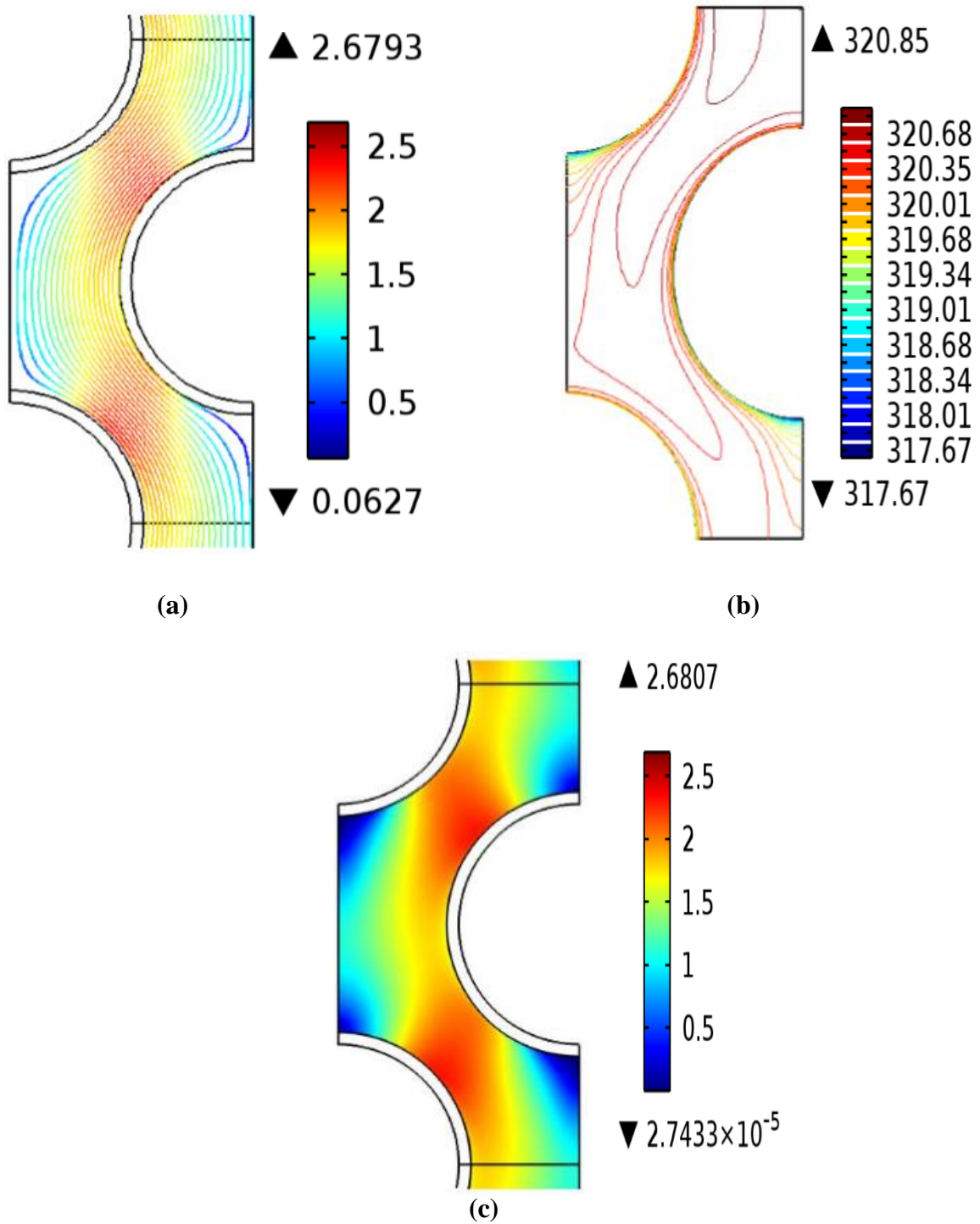


Figure 3.1: (a) Streamlines, (b) isothermal lines and (c) surface plot for velocity magnitude of tabular heat exchanger using water

Figure 3.2 (a-d) displays streamlines using different concentrations of nanofluid which are 0.1, 1, 2 and 3% concentrated water-MWCNT nanofluids.

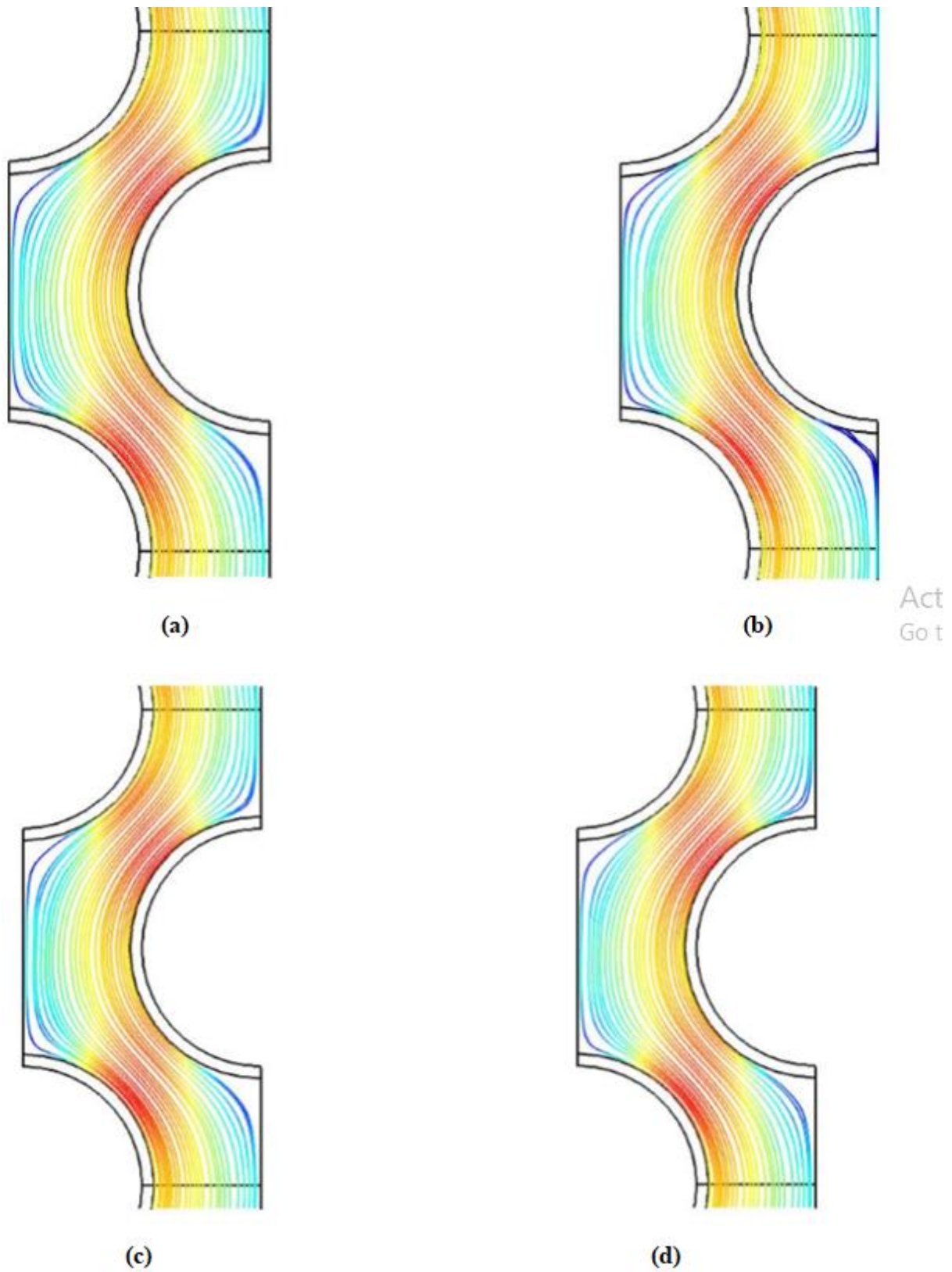


Figure 3.2: Velocity contours using (a) 0.1, (b) 1, (c) 2 and (d) 3% concentrated water-MWCNT nanofluid

The streamlines for water (figure 3.1a) and different concentrations of nanofluid (figure 3.2 a-d) are showing significant changes. It is clear that, velocities at the corners of the exterior region of the circular pipes are comparatively more in 0.1% water-MWCNT nanofluid than water. Similarly, for 2 and 3% water-MWCNT nanofluids, these velocities are more than water which can be understood from figures 3.2(c), 3.2(d) and 3.1(a). Among 0.1, 2 and 3% concentrated water-MWCNT nanofluids, these velocities increase with concentration. Again, figures 3.2(b) and 3.1(a) are showing that the velocity at the lower corner of the exterior region of the circular pipes is comparatively less for 1% concentrated water-MWCNT nanofluid than water.

Figure 3.3(a-d) represents the temperature contours for working fluid 0.1, 1, 2 and 3% concentrated water-MWCNT nanofluids.

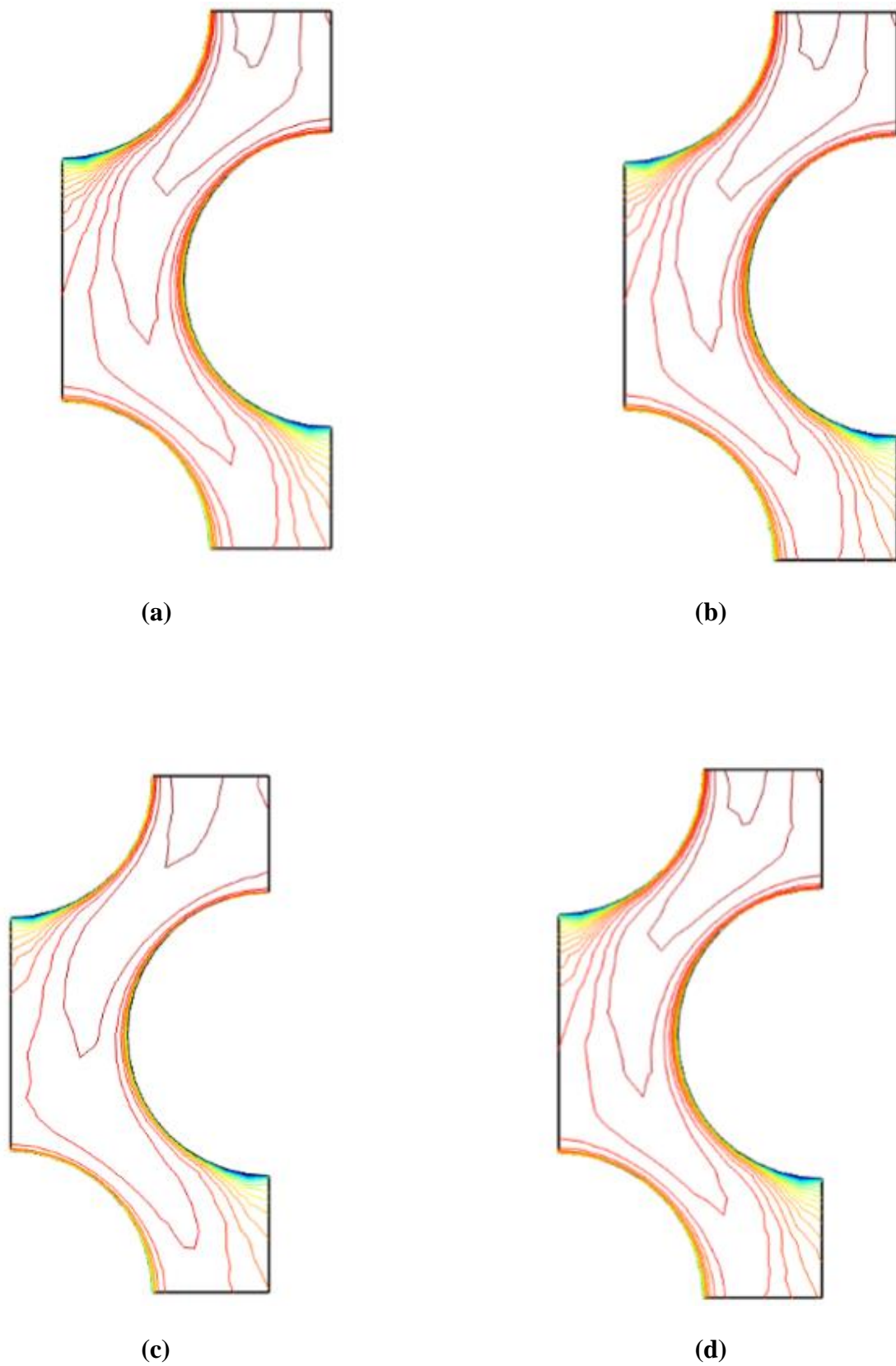


Figure 3.3: Temperature contours using (a) 0.1, (b) 1, (c) 2 and (d) 3% concentrated water-MWCNT nanofluid

Figure 3.1(b) is showing us that the temperature is lowest at the lowest portion of the circular pipes of their exterior region for water. This case is similar for all considered concentrations of water-MWCNT nanofluids which can be realized from figures 3.3(a)-3.3(d). Temperature is the highest in the middle portion of the exterior region of the circular pipes. The contours are almost similar for all the figures. From figure 3.1(b) and figure 3.3(c), the contours are closely similar for water and 2% concentrated water-MWCNT nanofluid. Again, the contours for 0.1, 1 and 3% concentrated water-MWCNT nanofluids are closely similar.

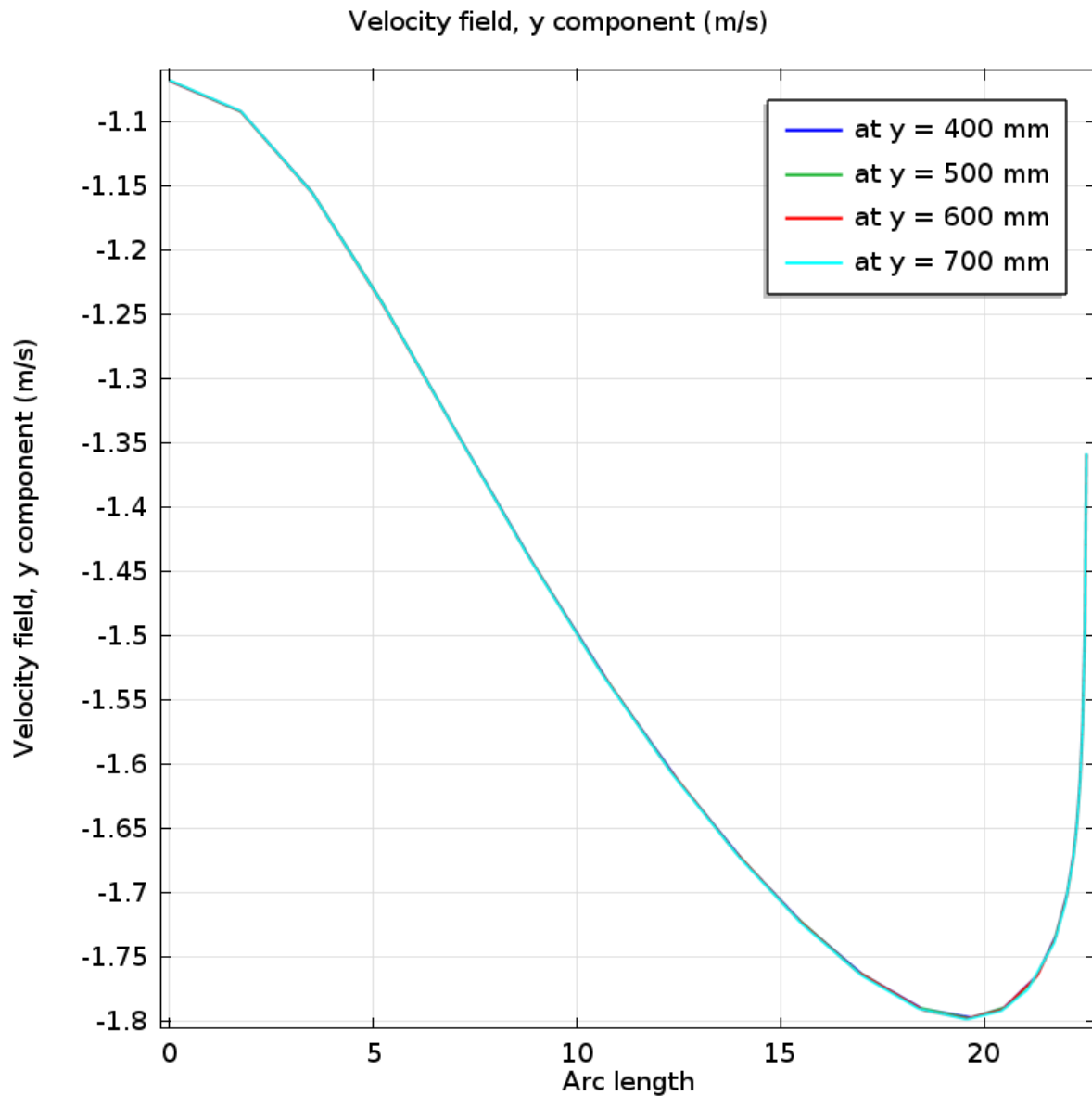


Figure 3.4(a): Velocity field of y-component at y = 400, 500, 600 and 700 mm for water

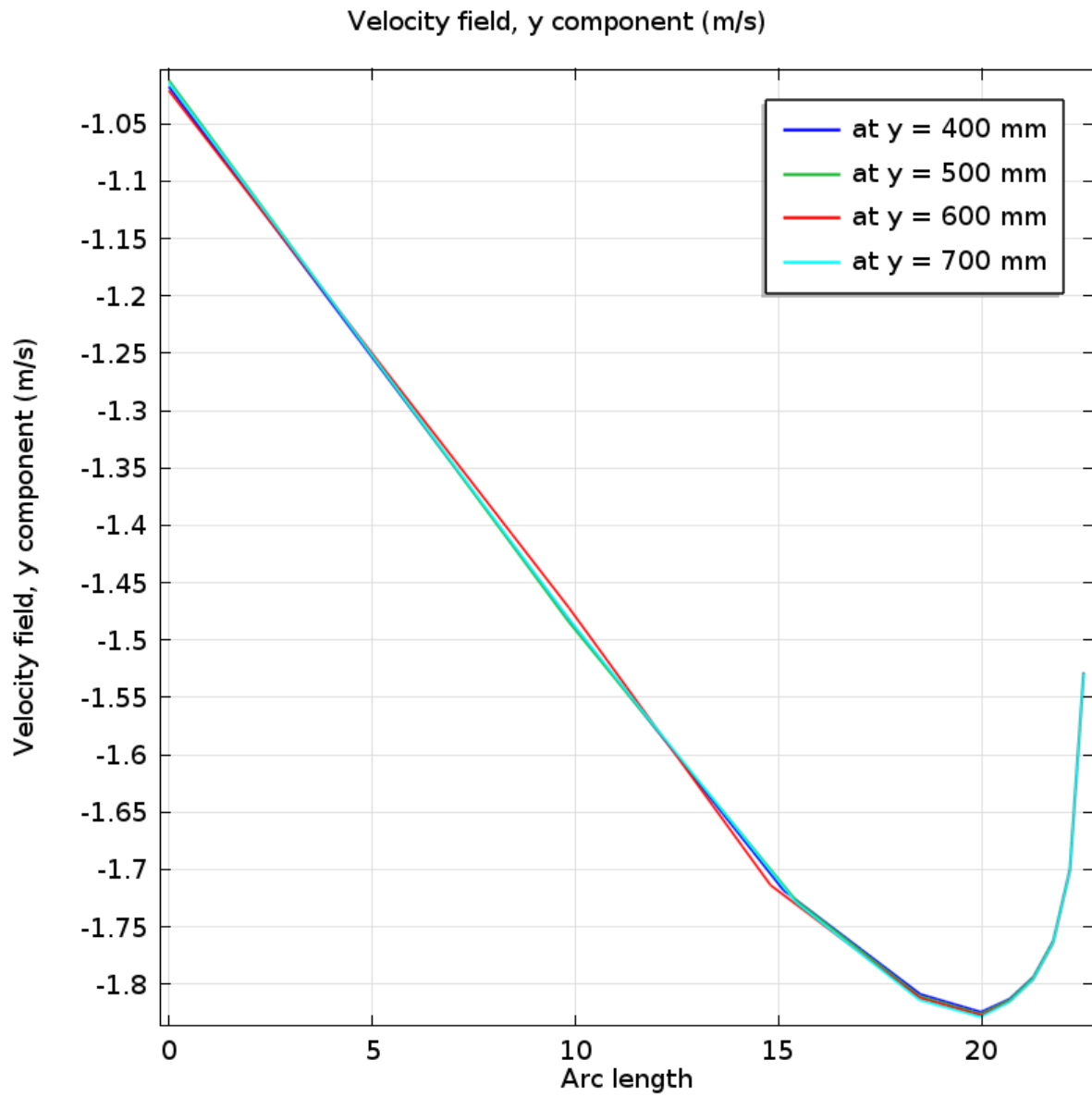


Figure 3.4(b): Velocity field of y-component at y = 400, 500, 600 and 700 mm for 0.1% concentrated water-MWCNT nanofluid

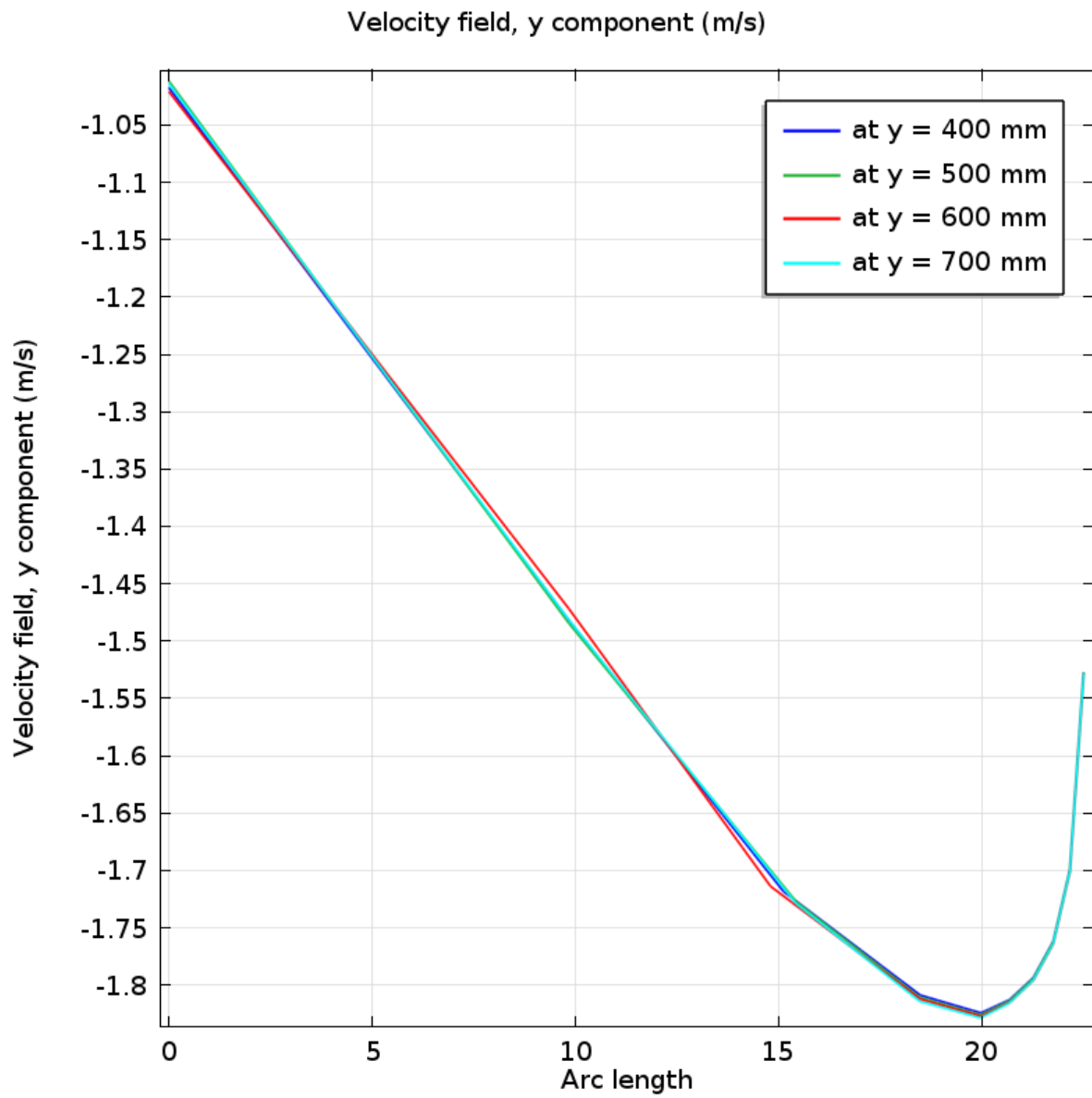


Figure 3.4(c): Velocity field of y-component at y = 400, 500, 600 and 700 mm for 1% concentrated water-MWCNT nanofluid

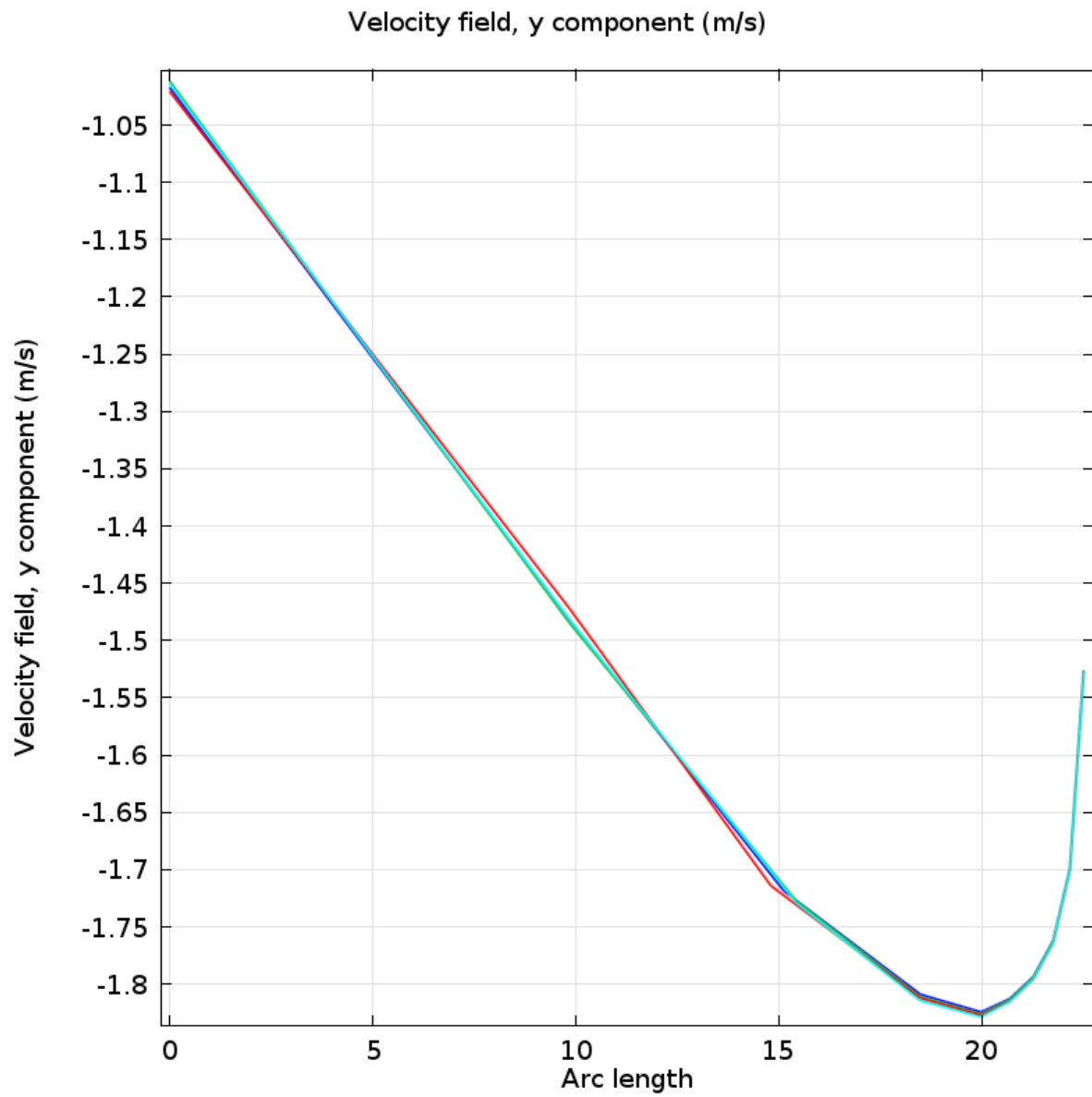


Figure 3.4(d): Velocity field of y-component at $y = 400, 500, 600$ and 700 mm for 2% concentrated water-MWCNT nanofluid

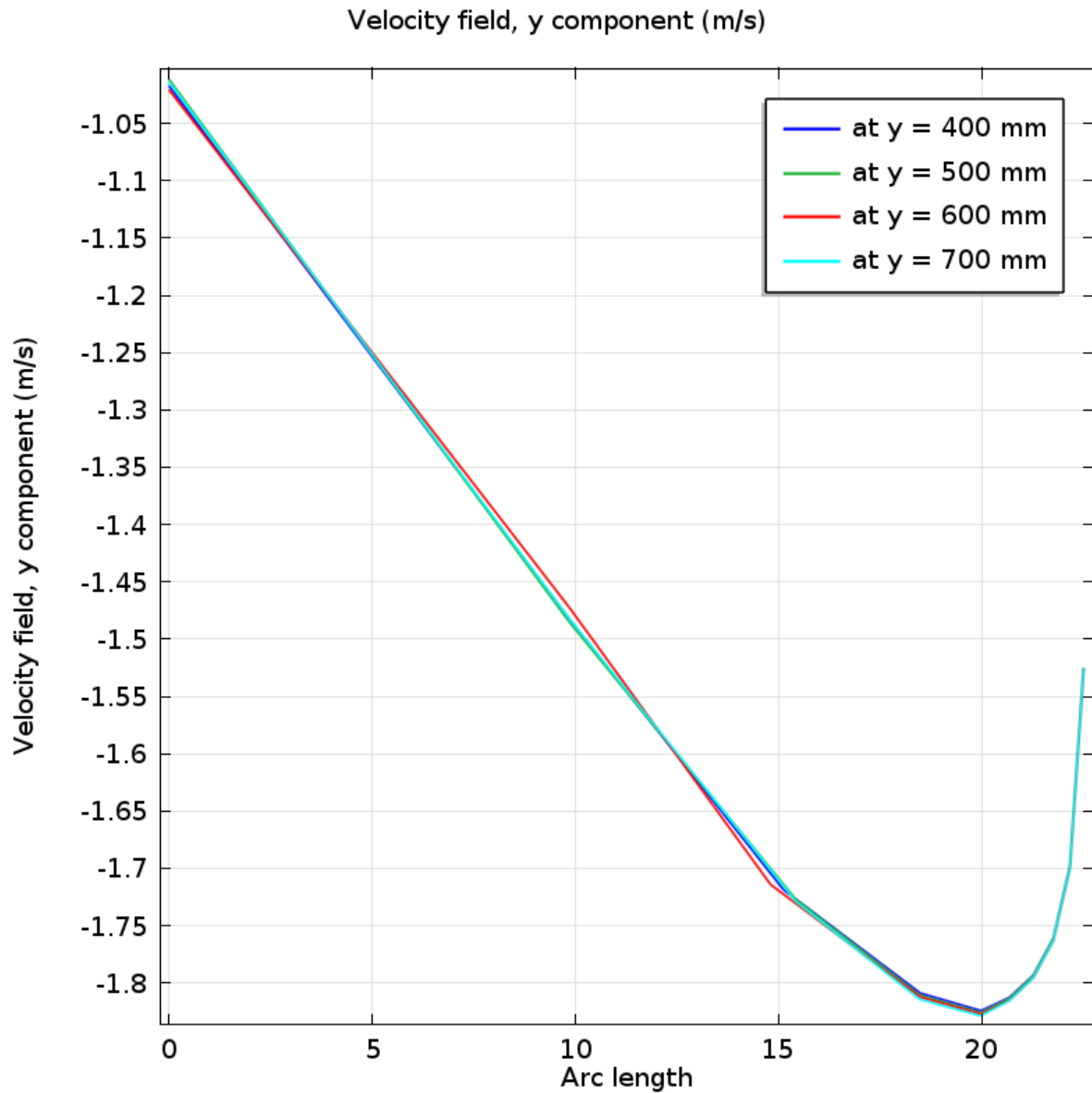


Figure 3.4(e): Velocity field of y-component at $y = 400, 500, 600$ and 700 mm for 3% concentrated water-MWCNT nanofluid

Figure 3.4(a-e) are showing velocity field of y-component at $y = 400, 500, 600$ and 700 mm along arc length using water, 0.1, 1, 2 and 3% concentrated water-MWCNT nanofluids, as heat transferring fluid respectively. For water, the curves at $y = 400, 500, 600$ and 700 mm coincide almost fully. But for 0.1, 1, 2 and 3% concentrated water-MWCNT nanofluids, they are coincided partially and the figures in these cases are similar.

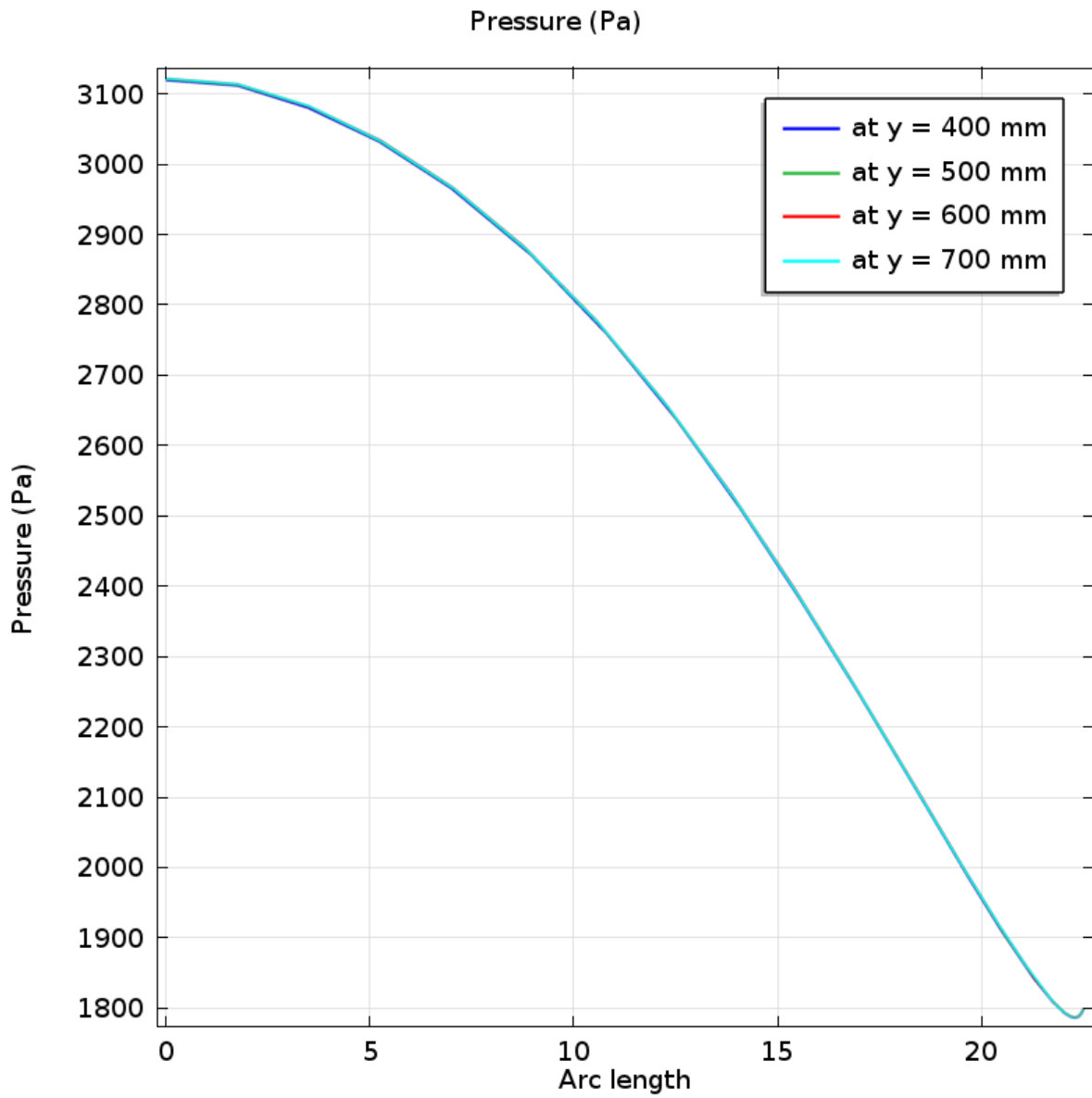


Figure 3.5(a): Pressure at y = 400, 500, 600 and 700 mm for water

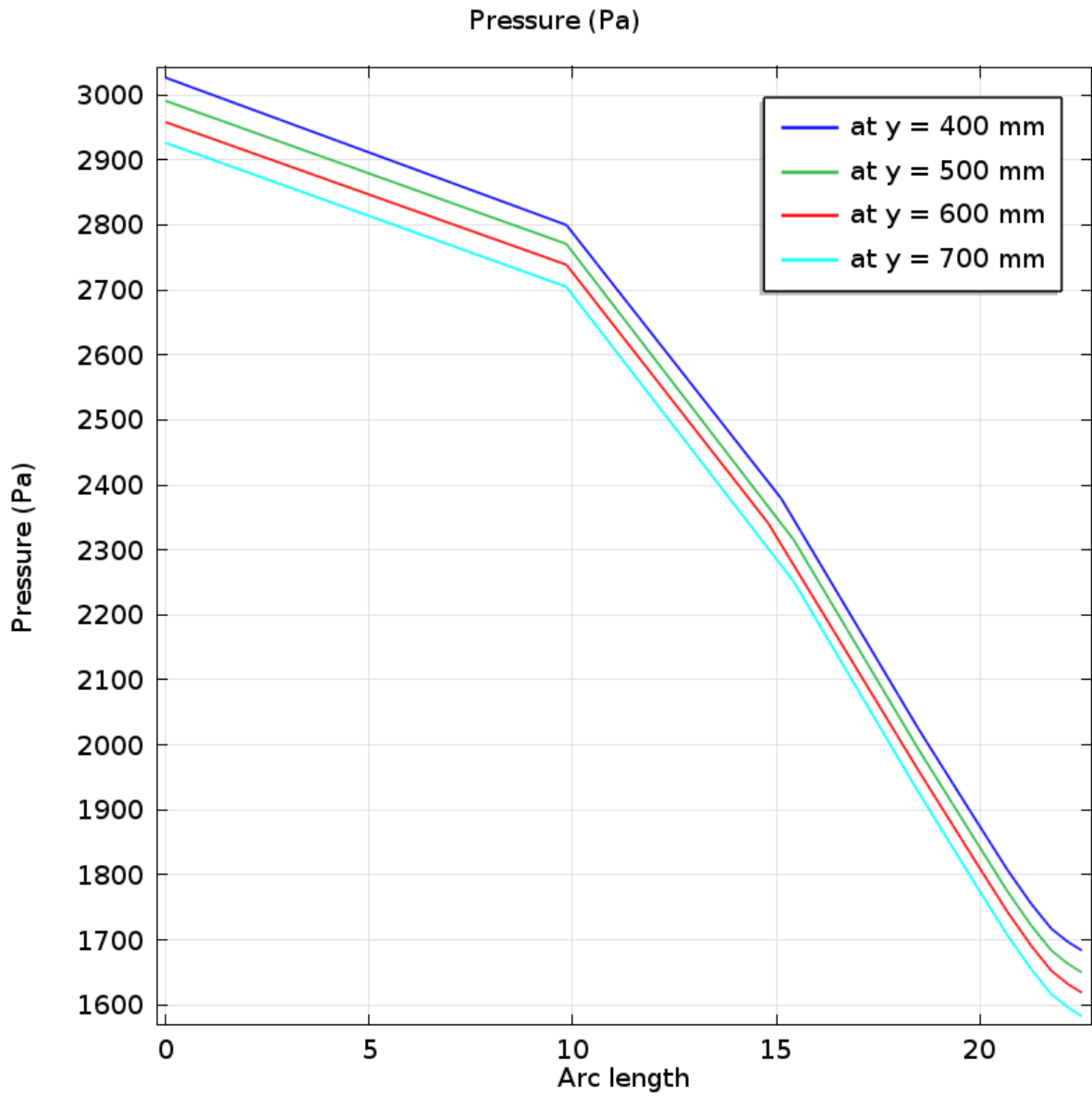


Figure 3.5(b): Pressure at y = 400,500,600 and 700 mm for 0.1% concentrated water-MWCNT nanofluid

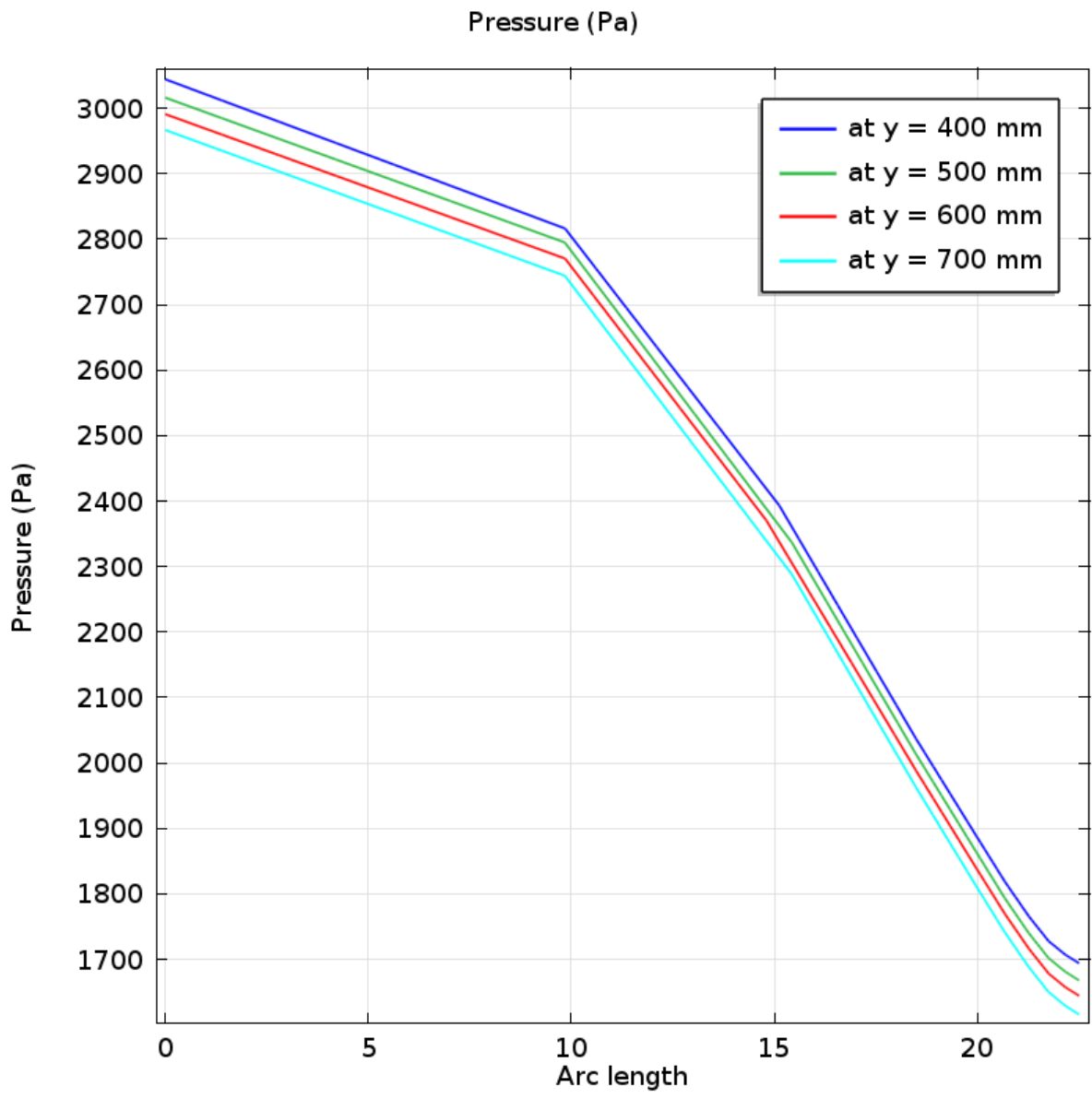


Figure 3.5(c): Pressure at y = 400, 500, 600 and 700 mm for 1% concentrated water-MWCNT nanofluid

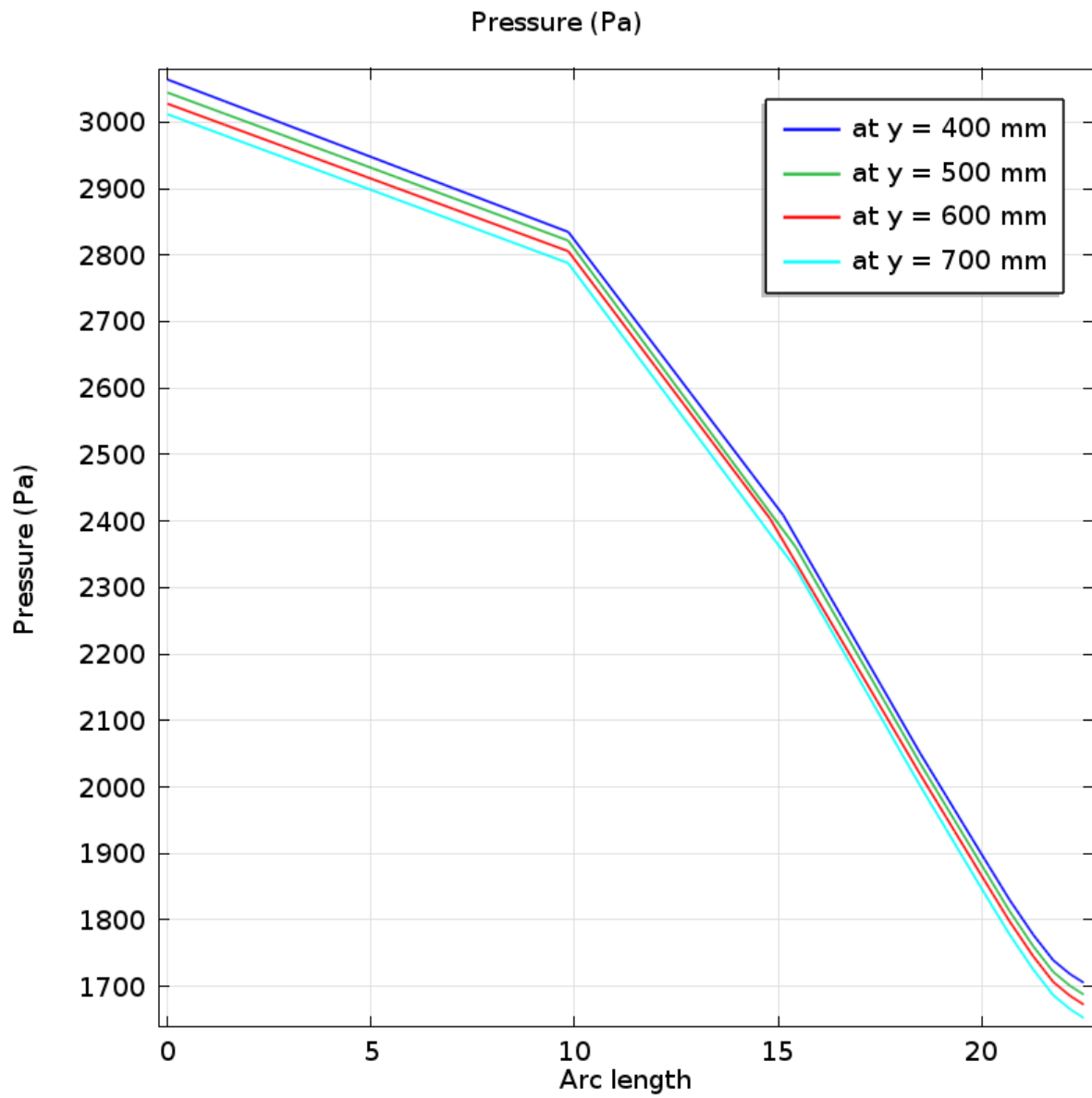


Figure 3.5(d): Pressure at y = 400, 500, 600 and 700 mm for 2% concentrated water-MWCNT nanofluid

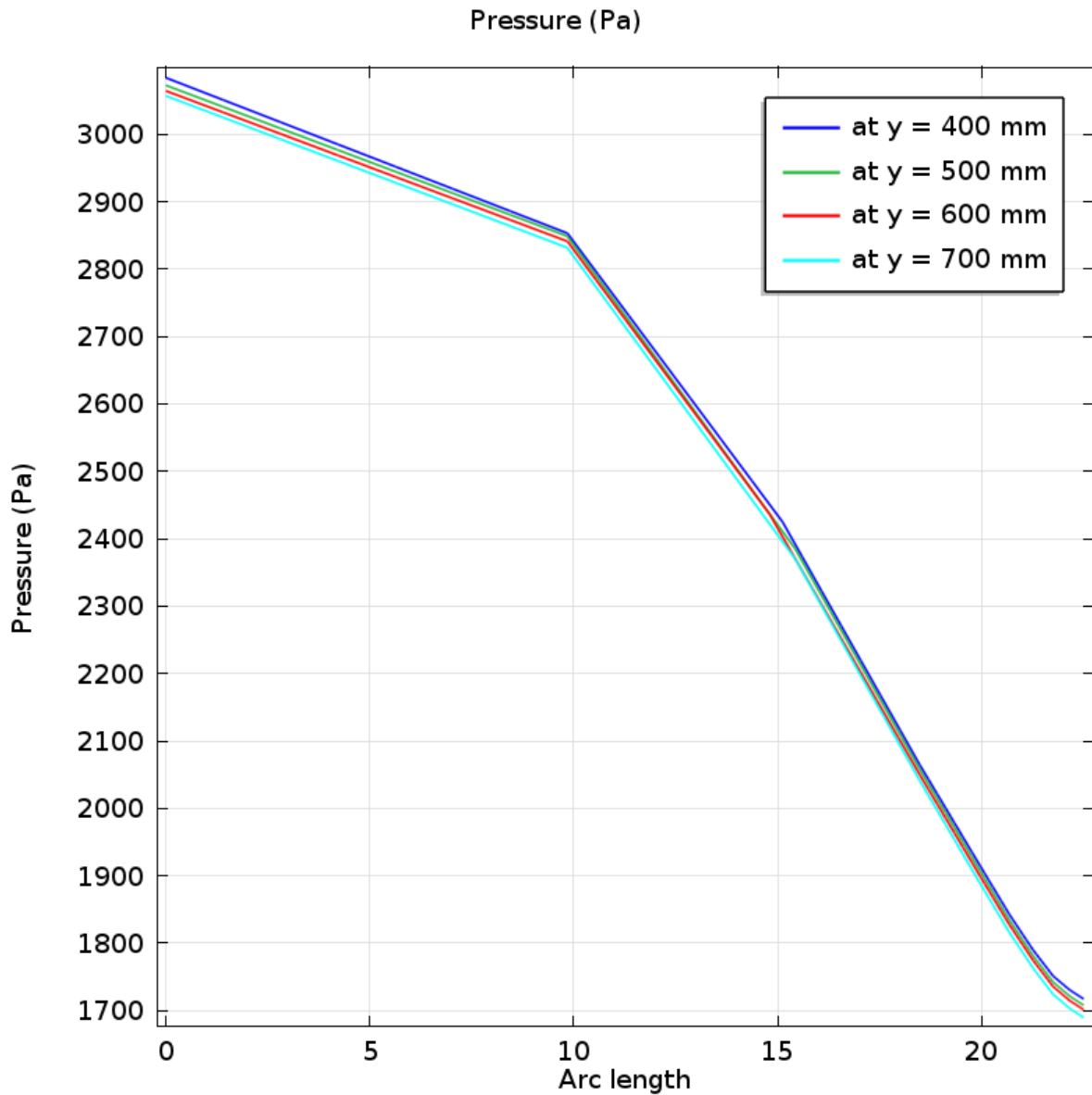


Figure 3.5(e): Pressure at y = 400, 500, 600 and 700 mm for 3% concentrated water-MWCNT nanofluid

The pressure at y = 400, 500, 600 and 700 mm are shown in figures 3.5(a-e) for water, 0.1%, 1%, 2% and 3% water-MWCNT nanofluids. For water as shown in figure 3.5(a), the curves for y = 400, 500, 600 and 700 mm are coincided fully. But from figures 3.5(b), 3.5(c), 3.5(d) and 3.5(e), it is shown that, the curves are separated from each other. The figures for 0.1%, 1%, 2% and 3% nanofluids are similar and the space between any two curves is decreasing with concentration.

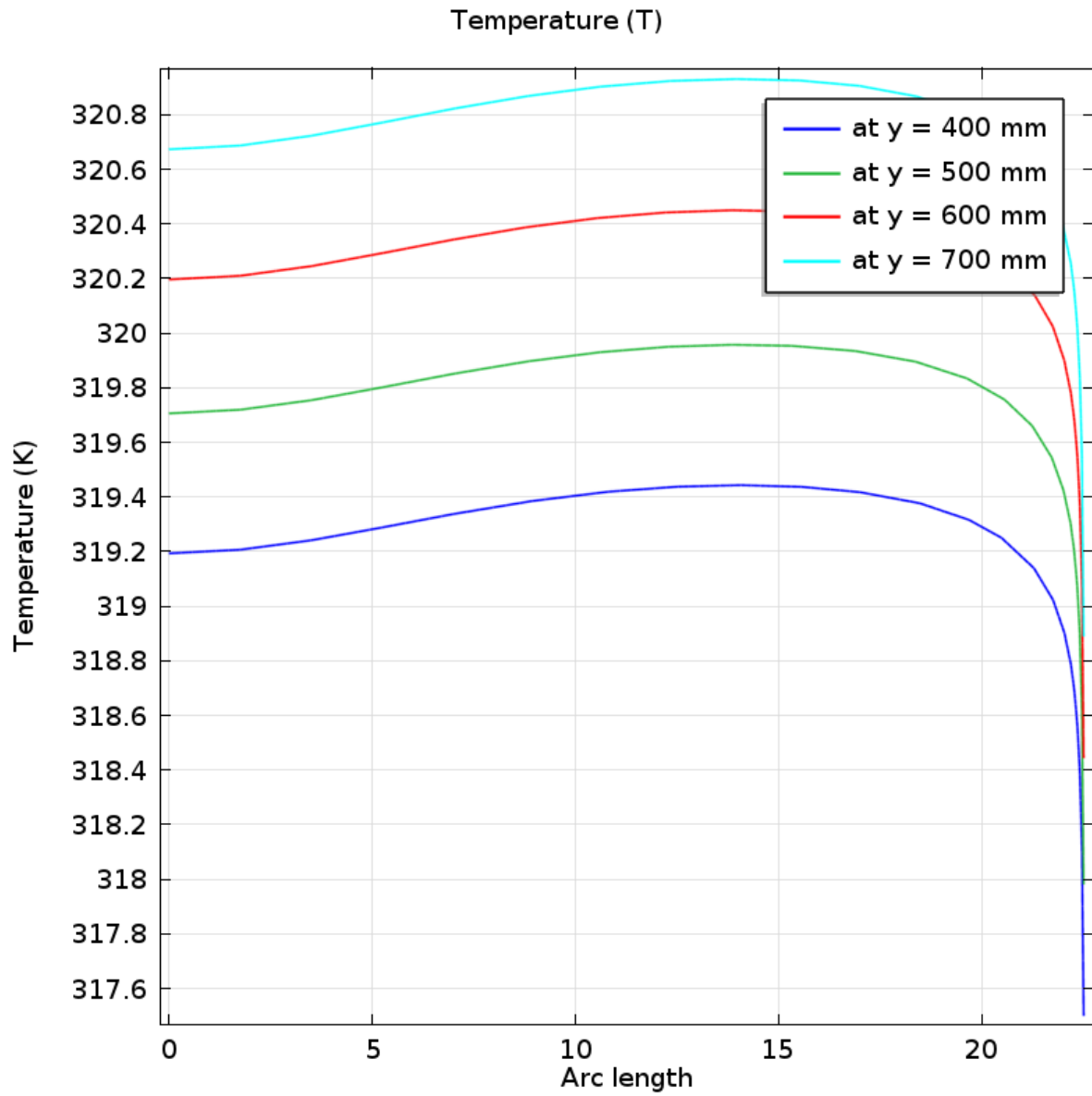


Figure 3.6(a): Temperature at y = 400, 500, 600 and 700 mm for water

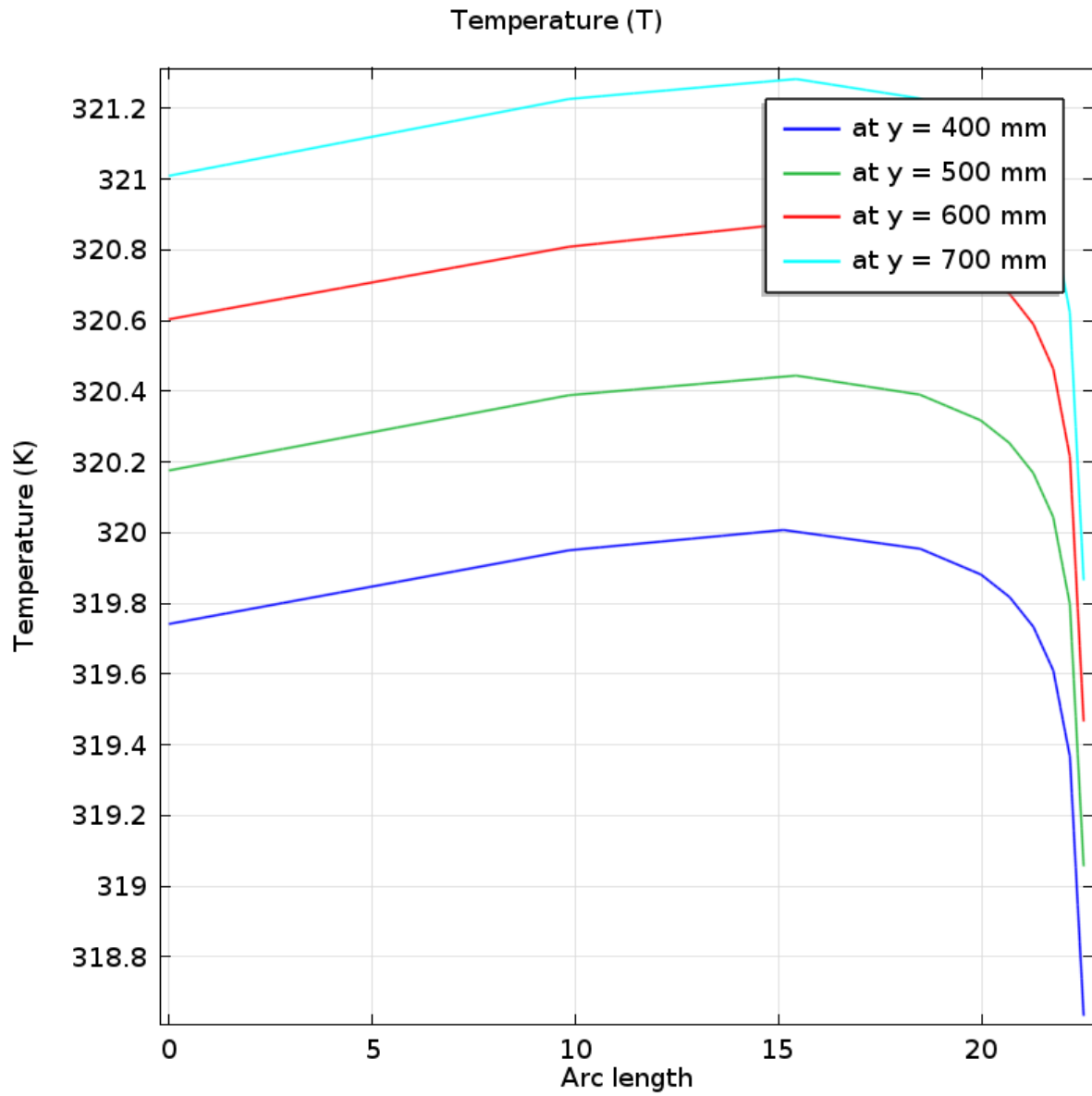


Figure 3.6(b): Temperature at y = 400, 500, 600 and 700 mm for 0.1% concentrated water-MWCNT nanofluid

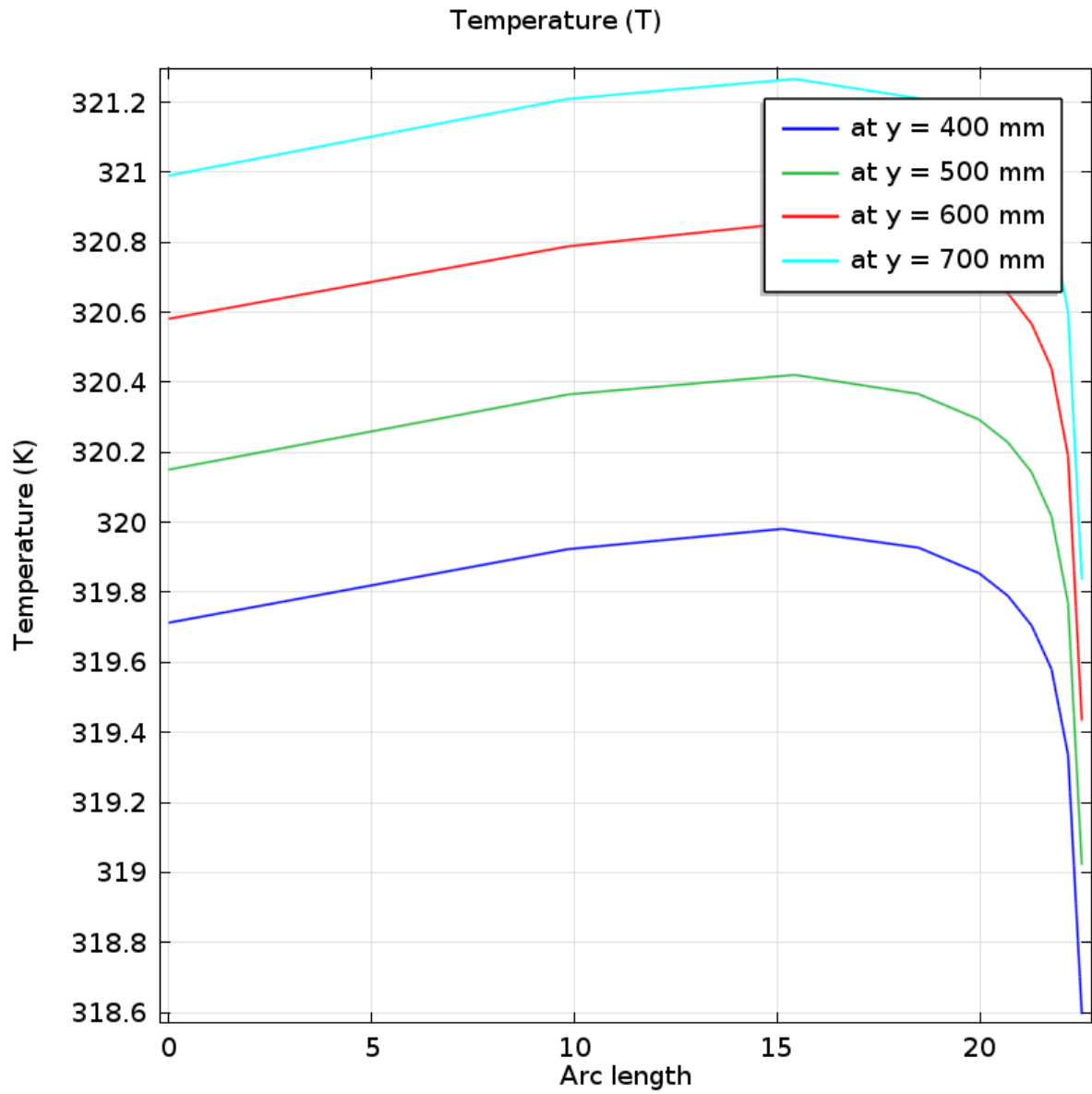


Figure 3.6(c): Temperature at y = 400, 500, 600 and 700 mm for 1% concentrated water-MWCNT nanofluid

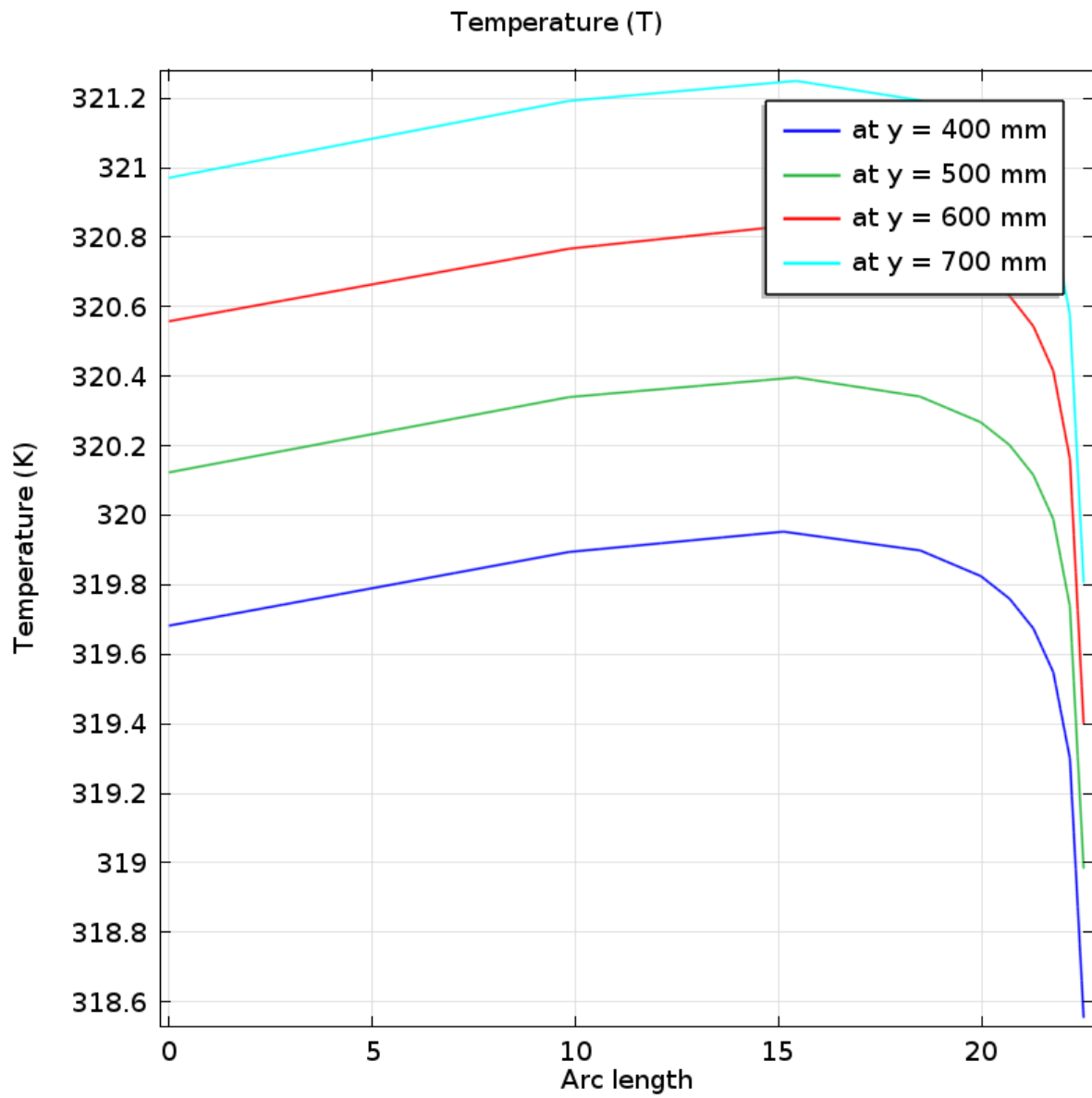


Figure 3.6(d): Temperature at y = 400, 500, 600 and 700 mm for 2% concentrated water-MWCNT nanofluid

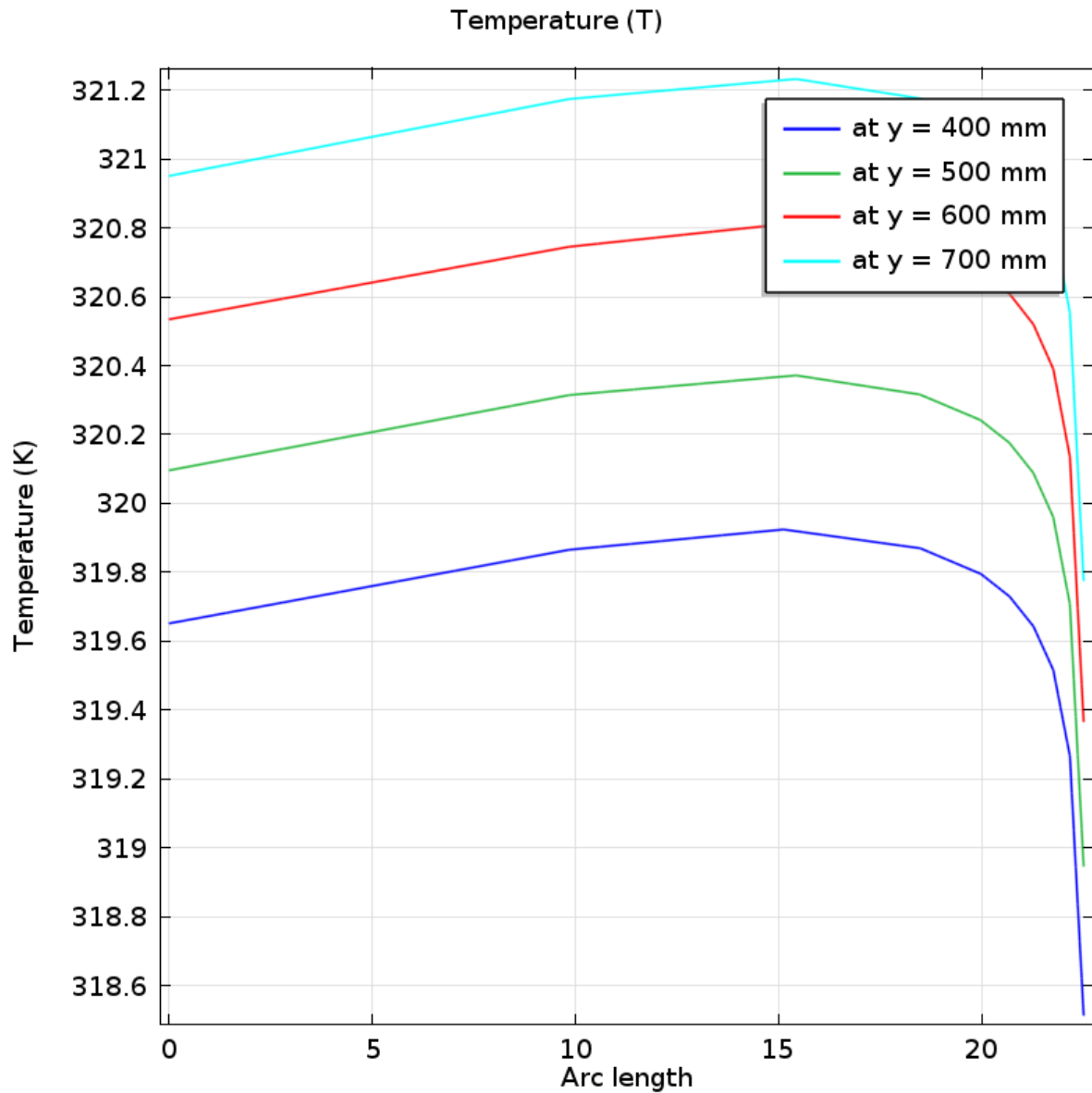


Figure 3.6(e): Temperature at $y = 400, 500, 600$ and 700 mm for 3% concentrated water-MWCNT nanofluid

Figures 3.6(a-e) are representing temperature distribution at $y = 400, 500, 600$ and 700 mm for water, 0.1, 1, 2 and 3% water-MWCNT nanofluids respectively. The temperature distribution shapes look like similar but the values of temperature are different for all kinds of variations of heat transferring fluids.

3.3 Effect of velocity

In this section, the effects of different inflow velocities (- 0.1, - 0.5, - 1 and - 1.5 m/s) of fixed concentrated water-MWCNT nanofluid with fixed inlet temperature of nanofluid (the negative sign in inflow velocities is used as the fluid is flowing downward) will be analyzed. These values of inlet fluid velocity indicate the values of Reynolds number as 5000, 25000, 50000 and 75000 respectively. In this case, fixed values of inlet temperature and solid volume fraction of working fluid are 323 K and 1%, respectively. To identify the effects of inflow velocity on flow and temperature field it is needed to notice the streamlines and isothermal lines pattern. In addition, nanofluid velocity, pressure and temperature at the position $y = 400, 500, 600$ and 700 mm of arc length against arc length have been depicted for different inlet velocities.

Figures 3.7(a-d) shows the streamlines of 1% concentrated water-MWCNT nanofluid for different inflow velocities which are - 0.1, - 0.5, - 1 and - 1.5 m/s.

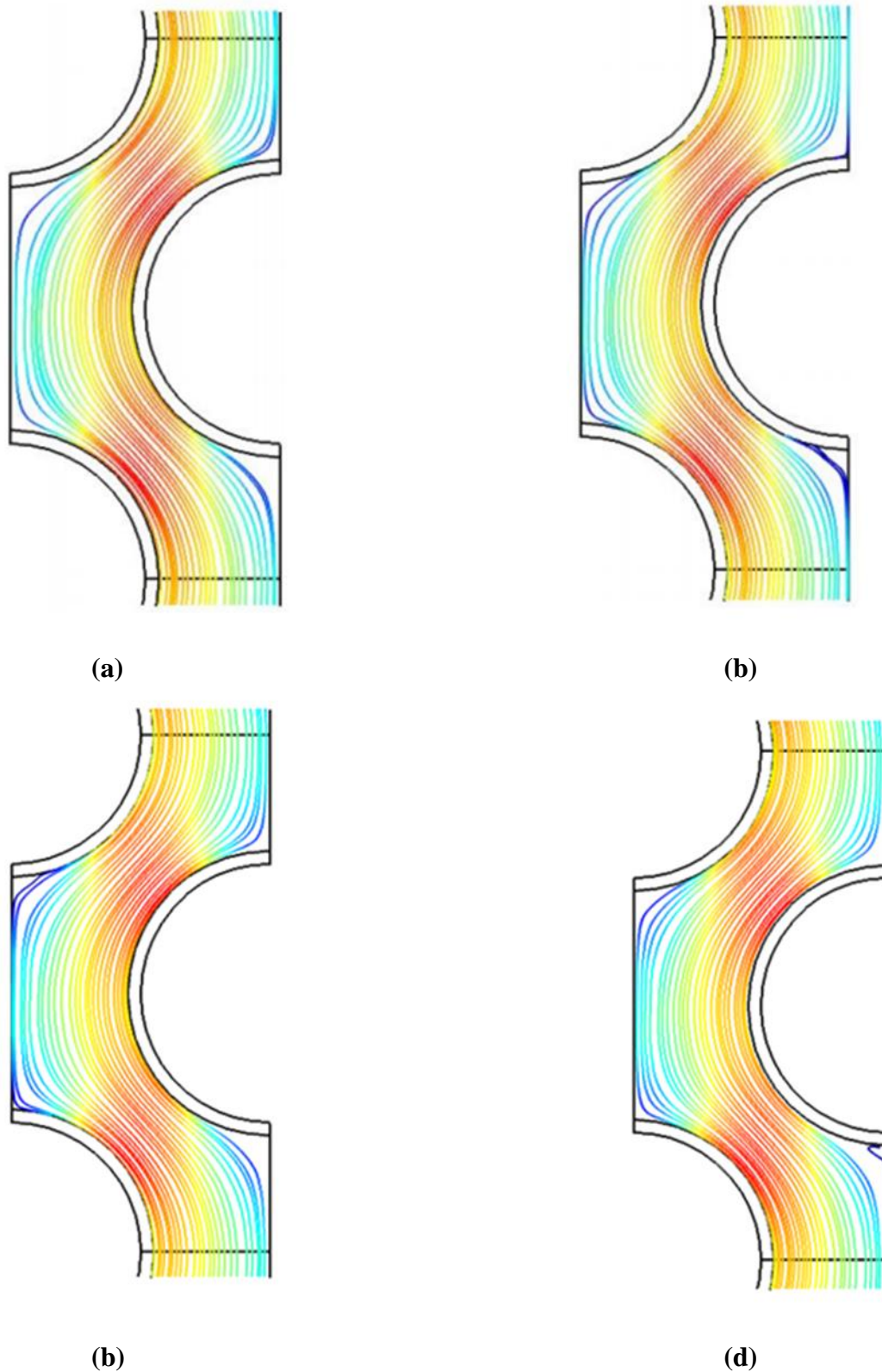


Figure 3.7: Velocity contours using v_{in} (a) - 0.1, (b) - 0.5, (c) - 1 and (d) - 1.5 m/s

From these figures, we can see that the velocity at the lowest corner of the exterior region of the circular pipes is the lowest at figure 3.7(b) for inlet velocity - 0.5 m/s and then lowest in

figure 3.7(a) for inlet velocity - 0.1 m/s. The velocity at the opposite portion of circular pipe's exterior region is lowest at figure 3.7(c) for inlet velocity - 1 m/s. Otherwise, the figures are almost similar.

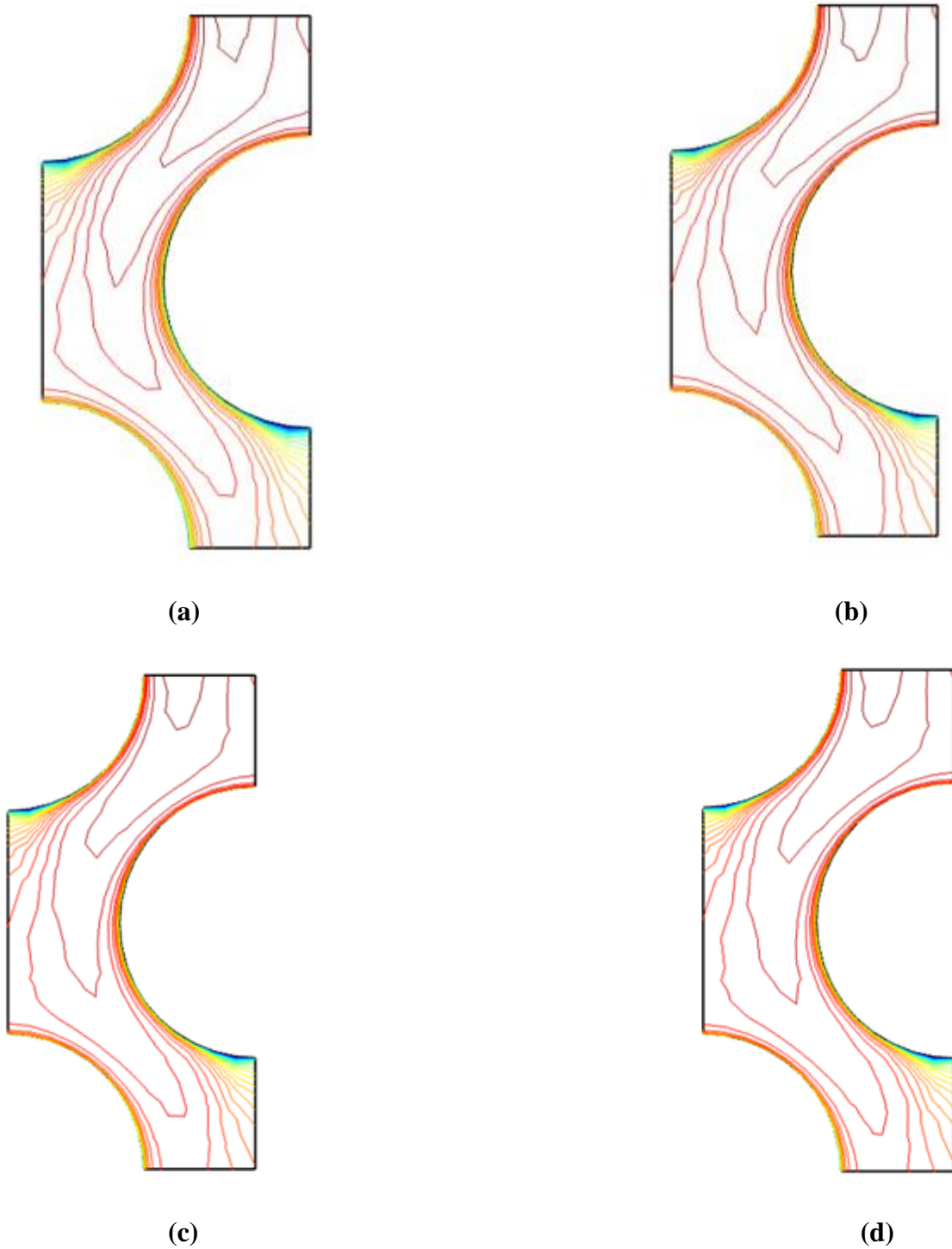


Figure 3.8: Temperature contours using v_{in} (a) - 0.1, (b) - 0.5, (c) - 1 and (d) - 1.5 m/s

Temperature contours for inflow velocities - 0.1, - 0.5, - 1 and - 1.5 m/s are shown in figures 3.8(a-d) for concentrated water-MWCNT nanofluid with solid volume fraction of 1%. The figures are almost similar for inlet velocities - 0.5, - 1 and - 1.5 m/s. It is found that the temperature at the lower external region of circular pipes is the lowest for inlet velocity - 0.1 m/s.

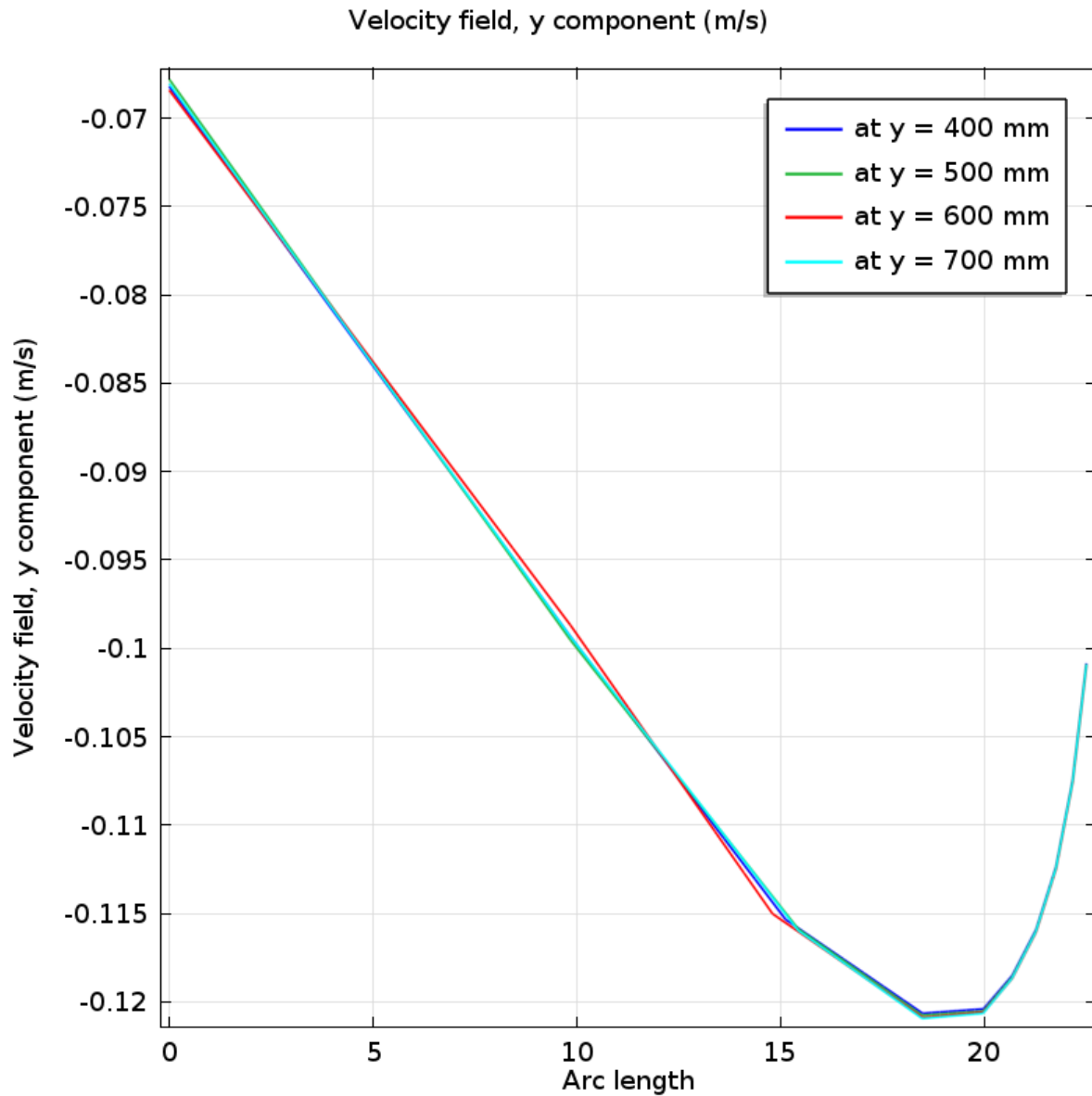


Figure 3.9(a): Velocity field of y-component at y = 400, 500, 600 and 700 mm using $v_{in} = - 0.1$ m/s

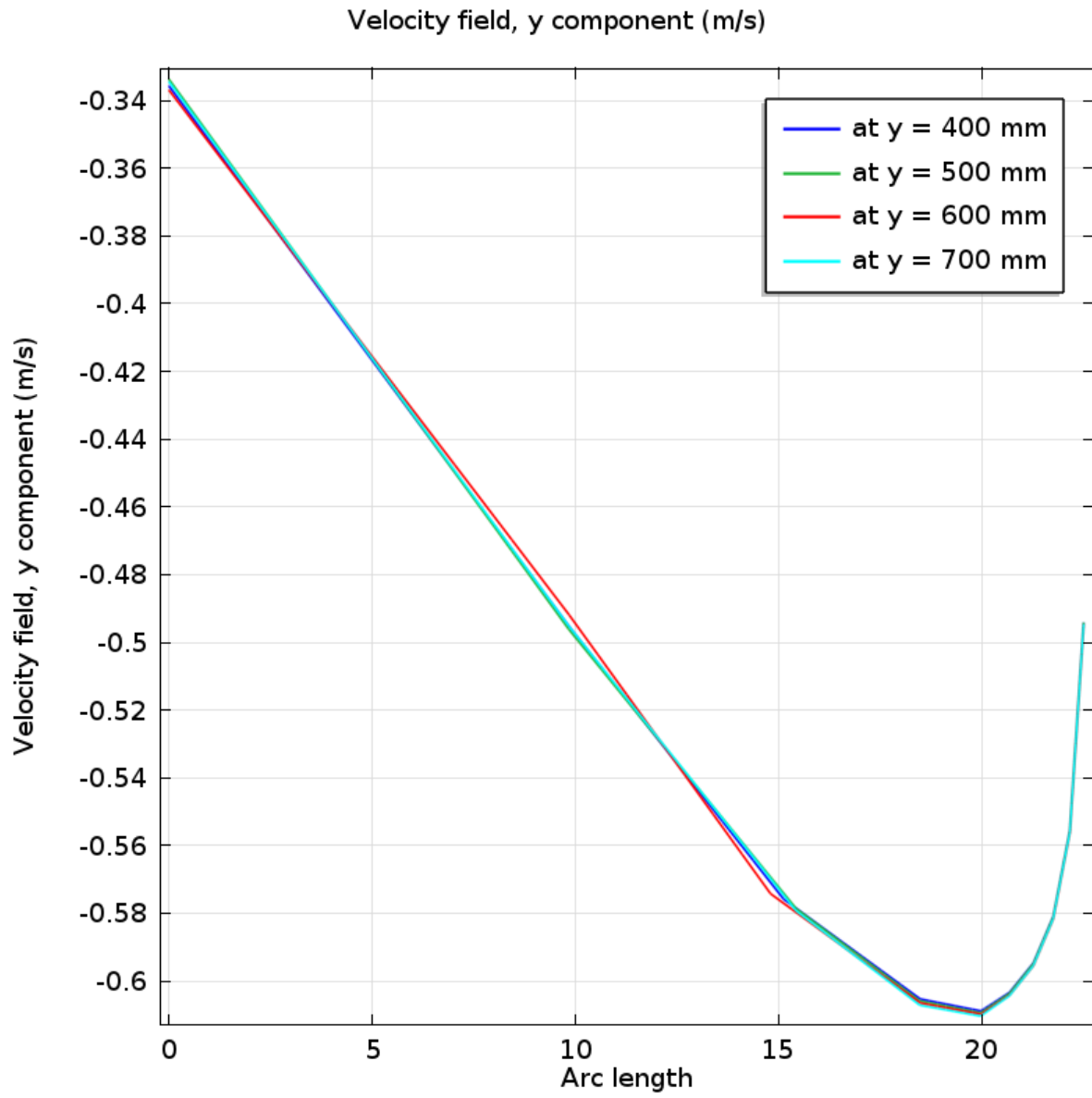


Figure 3.9(b): Velocity field of y-component at y = 400, 500, 600 and 700 mm using $v_{in} = -0.5$ m/s

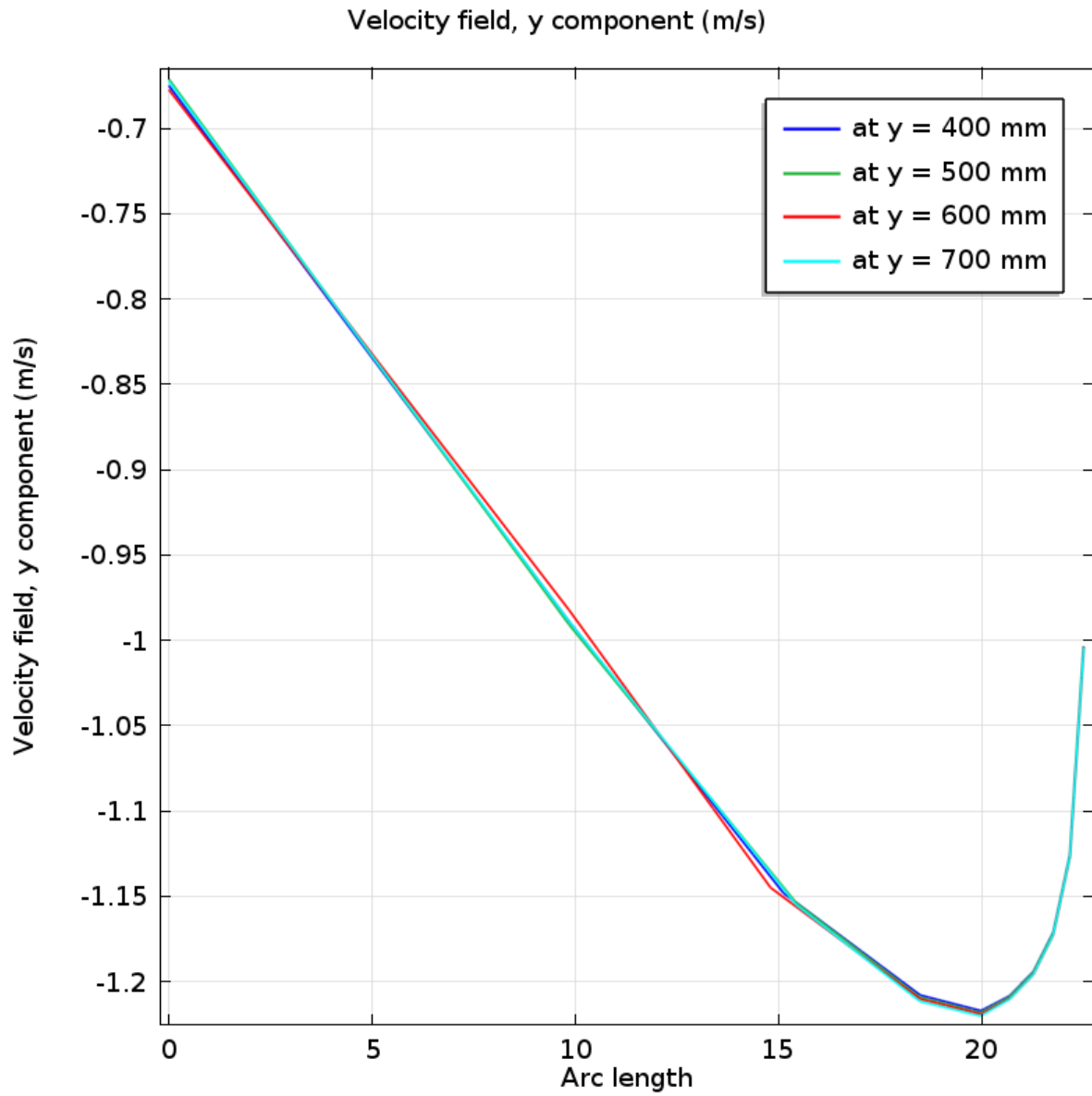


Figure 3.9(c): Velocity field of y-component at y = 400, 500, 600 and 700 mm using $v_{in} = -1$ m/s

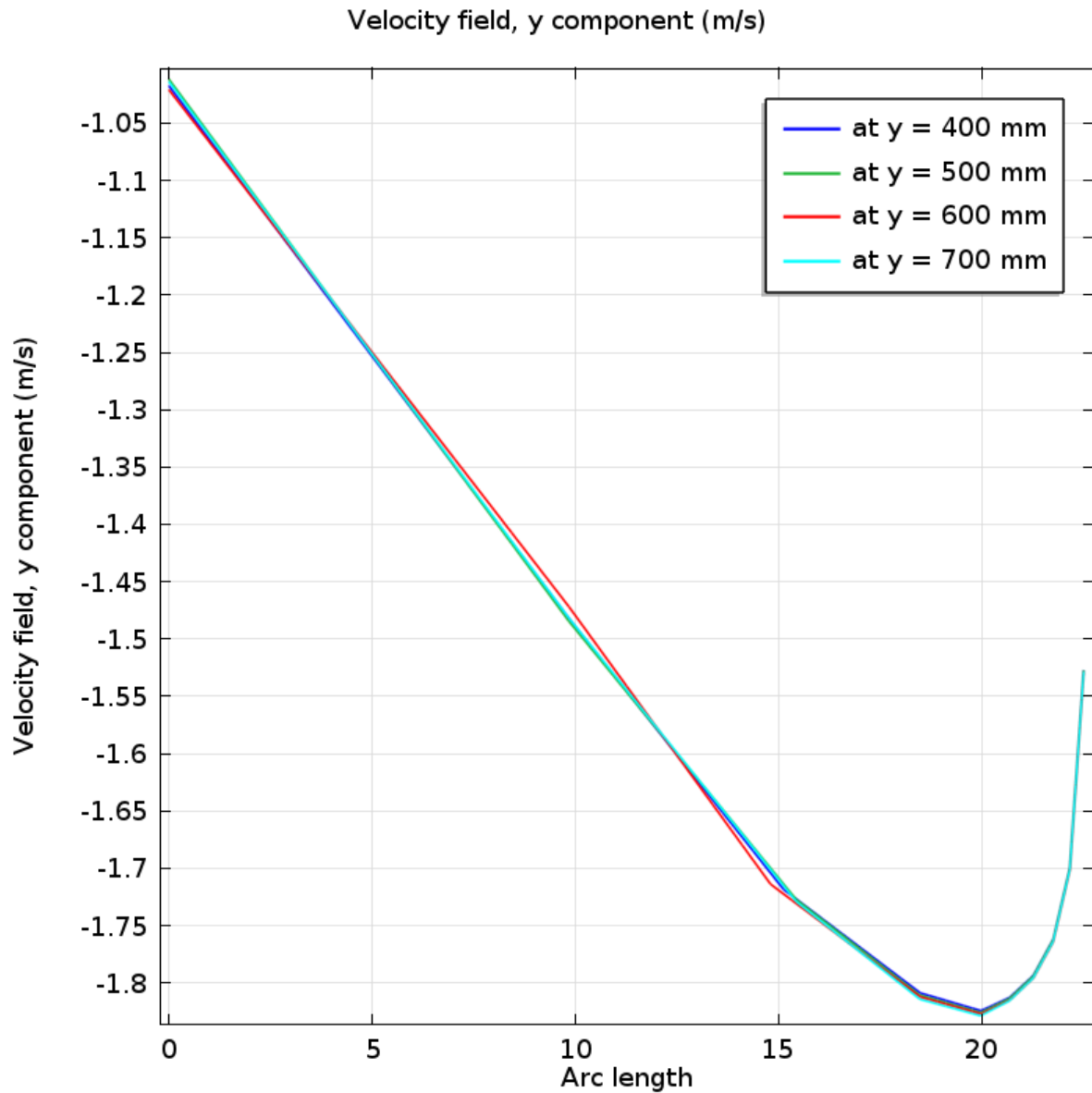


Figure 3.9(d): Velocity field of y-component at y = 400, 500, 600 and 700 mm using $v_{in} = -1.5$ m/s

Figures 3.9(a-d) represent the velocity at y = 400, 500, 600 and 700 mm for inflow velocities - 0.1, - 0.5, - 1 and - 1.5 m/s respectively of 1% MWCNT nanofluid. The figures are similar for all considered inflow velocities. The maximum velocities at y = 400, 500, 600 and 700 mm are - 0.065, - 0.35, - 0.65 and - 1 m/s for inflow velocities - 0.1, - 0.5, - 1 and - 1.5 m/s respectively.

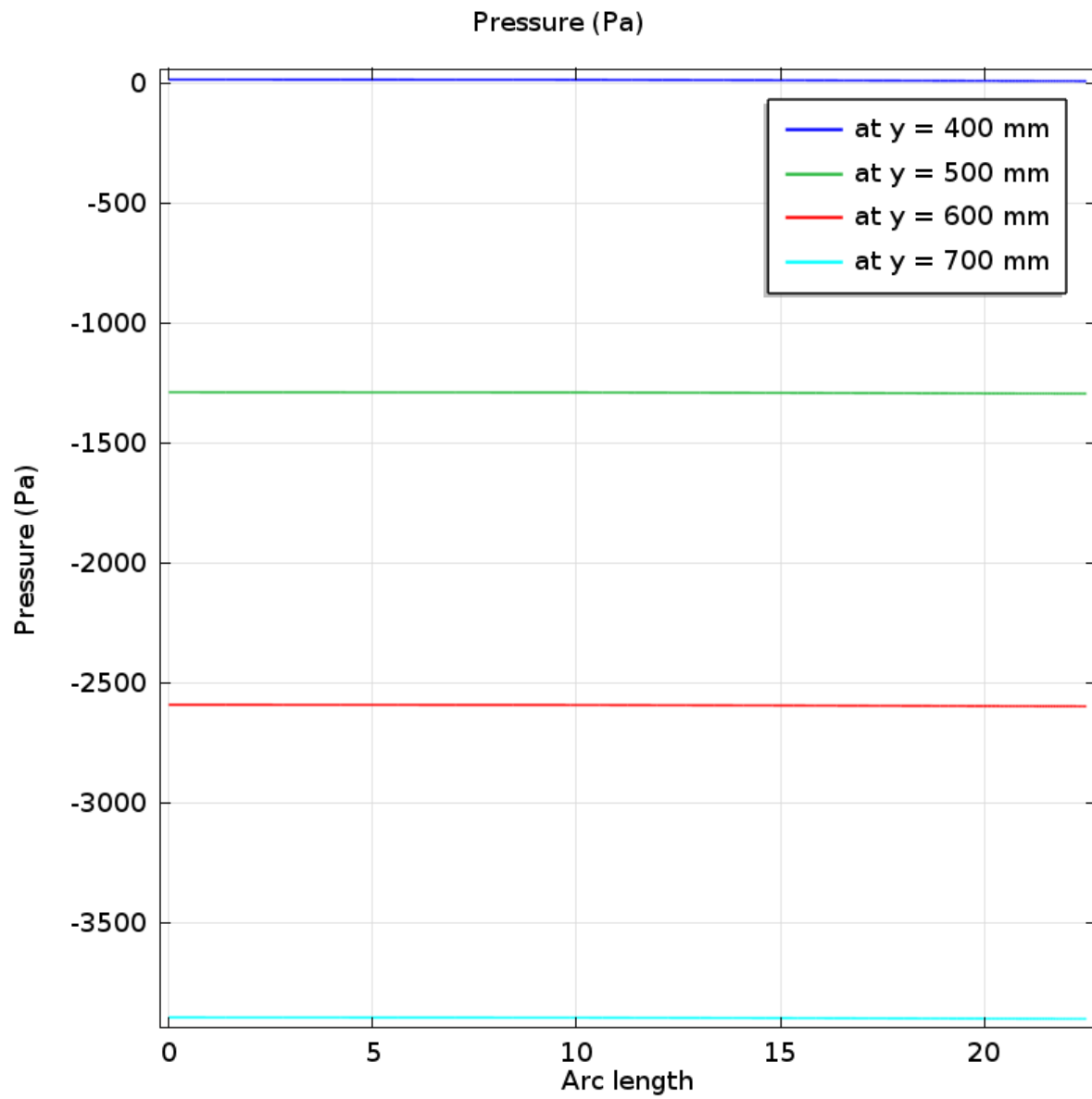


Figure 3.10(a): Pressure at $y = 400, 500, 600$ and 700 mm using $v_{in} = -0.1$ m/s

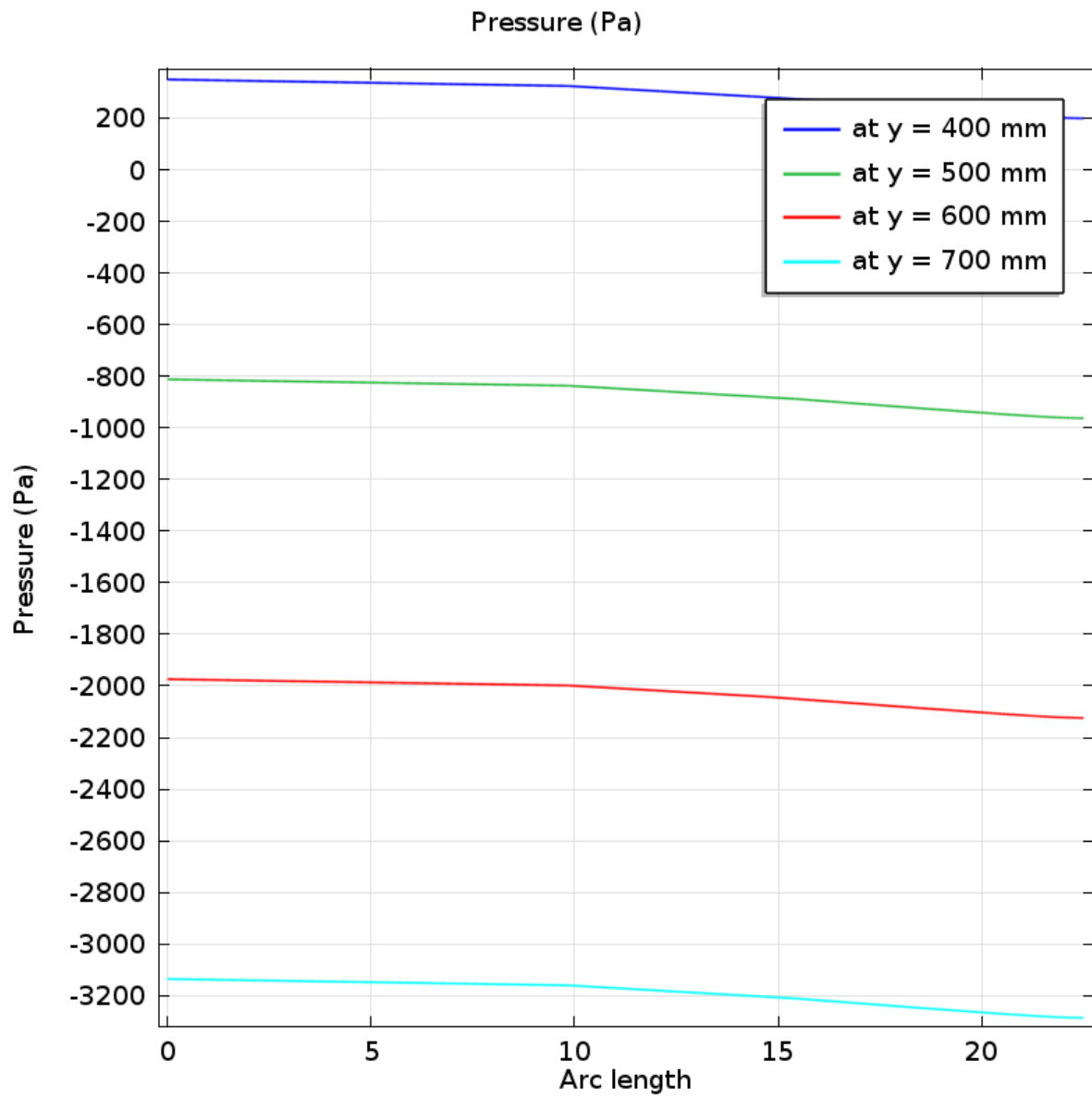


Figure 3.10(b): Pressure at y = 400, 500, 600 and 700 mm using $v_{in} = -0.5$ m/s

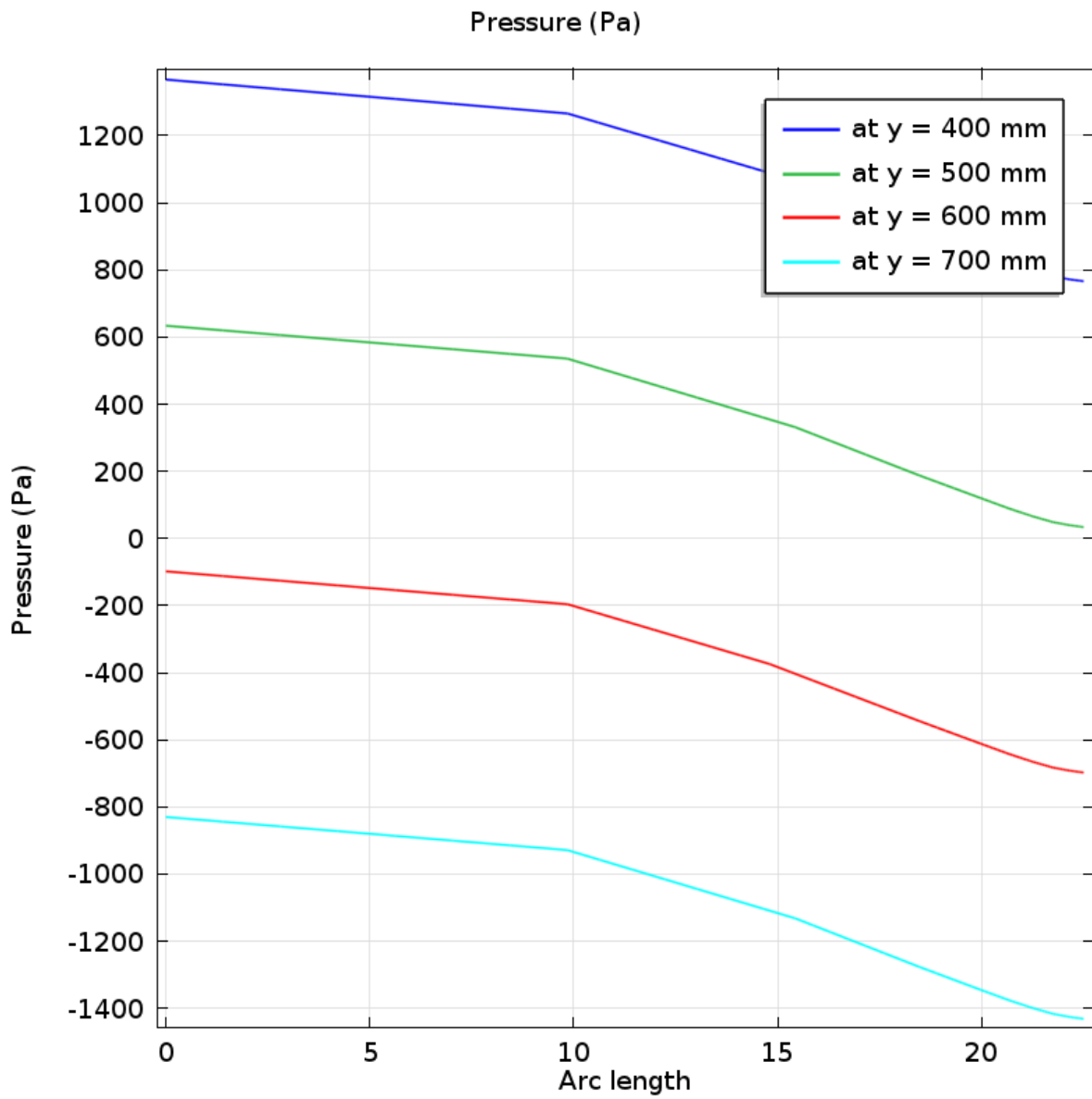


Figure 3.10(c): Pressure at y = 400, 500, 600 and 700 mm using $v_{in} = -1$ m/s

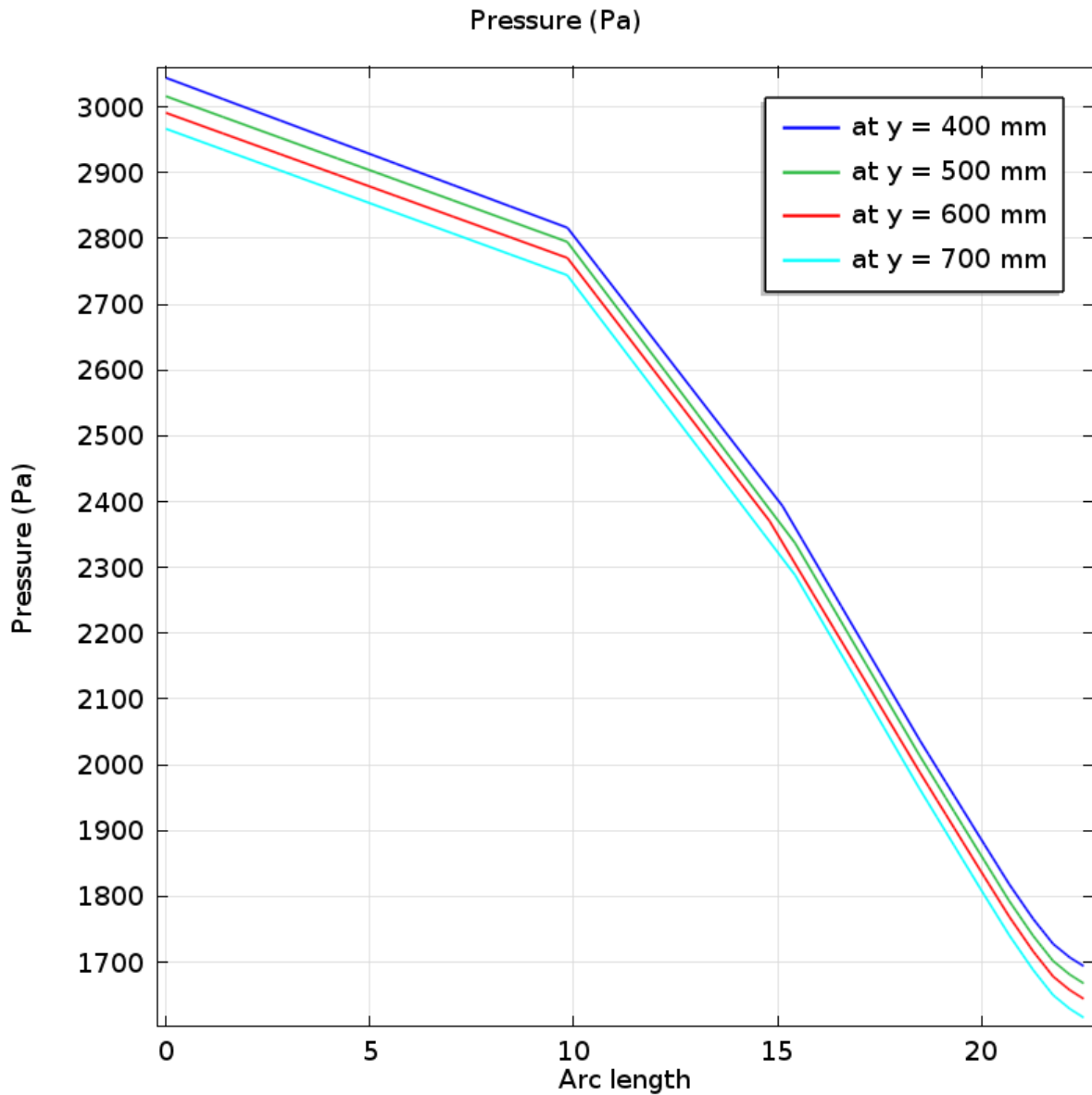


Figure 3.10(d): Pressure at y = 400, 500, 600 and 700 mm using $v_{in} = -1.5$ m/s

Pressure at y = 400, 500, 600 and 700 mm for inflow velocities - 0.1, - 0.5, - 1 and - 1.5 m/s of 1% concentrated water-MWCNT nanofluid are represented in figures 3.10(a-d). It is seen that the significant changes occur in the curves for different figures. The curves are of similar pattern but the separation between any two curves is decreasing with inflow velocities. The curves for inflow velocity - 0.1 m/s become almost straight lines as shown in figure 3.10(a).

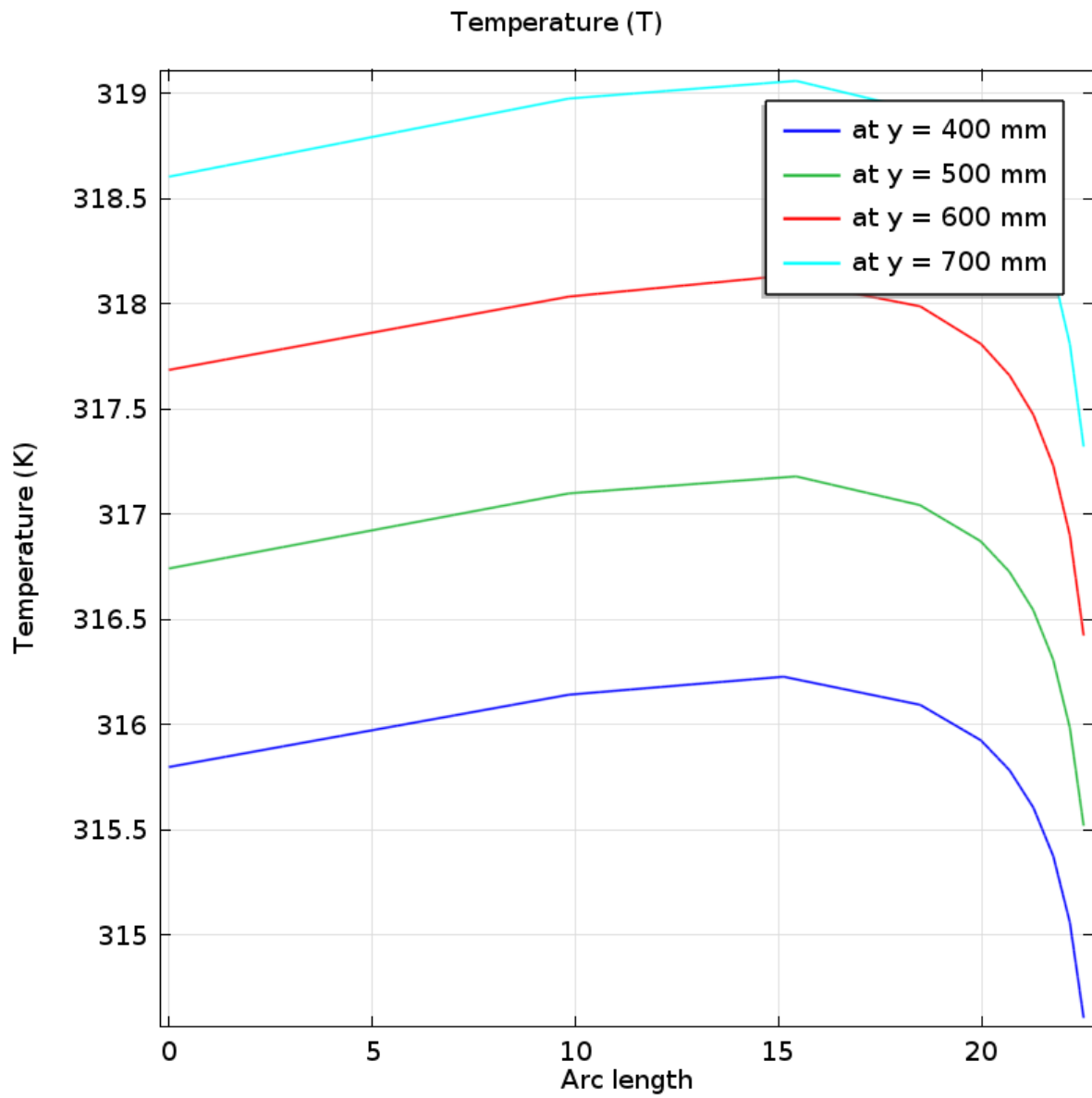


Figure 3.11(a): Temperature at y = 400, 500, 600 and 700 mm using $v_{in} = -0.1$ m/s

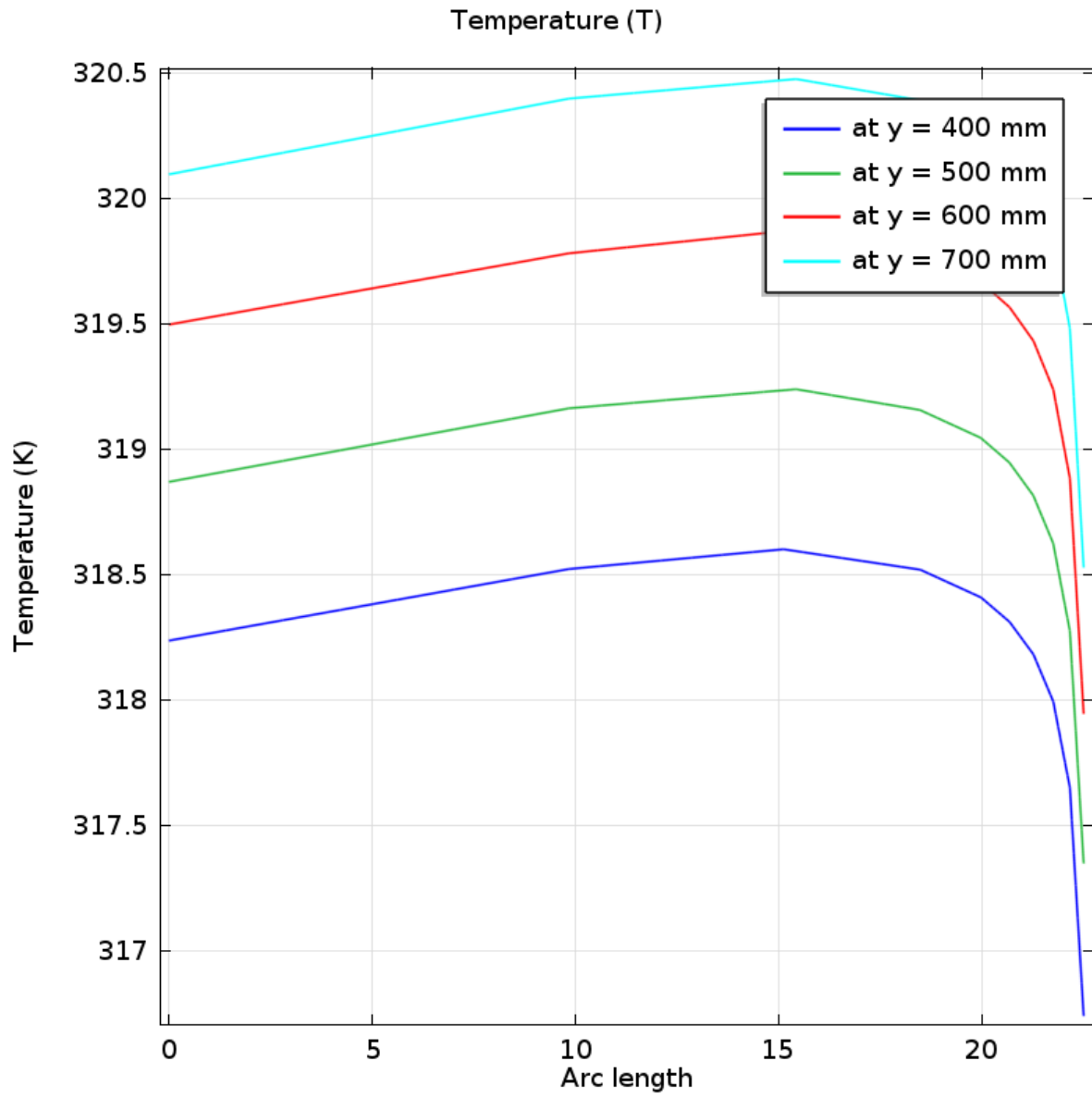


Figure 3.11(b): Temperature at y = 400, 500, 600 and 700 mm using $v_{in} = -0.5$ m/s

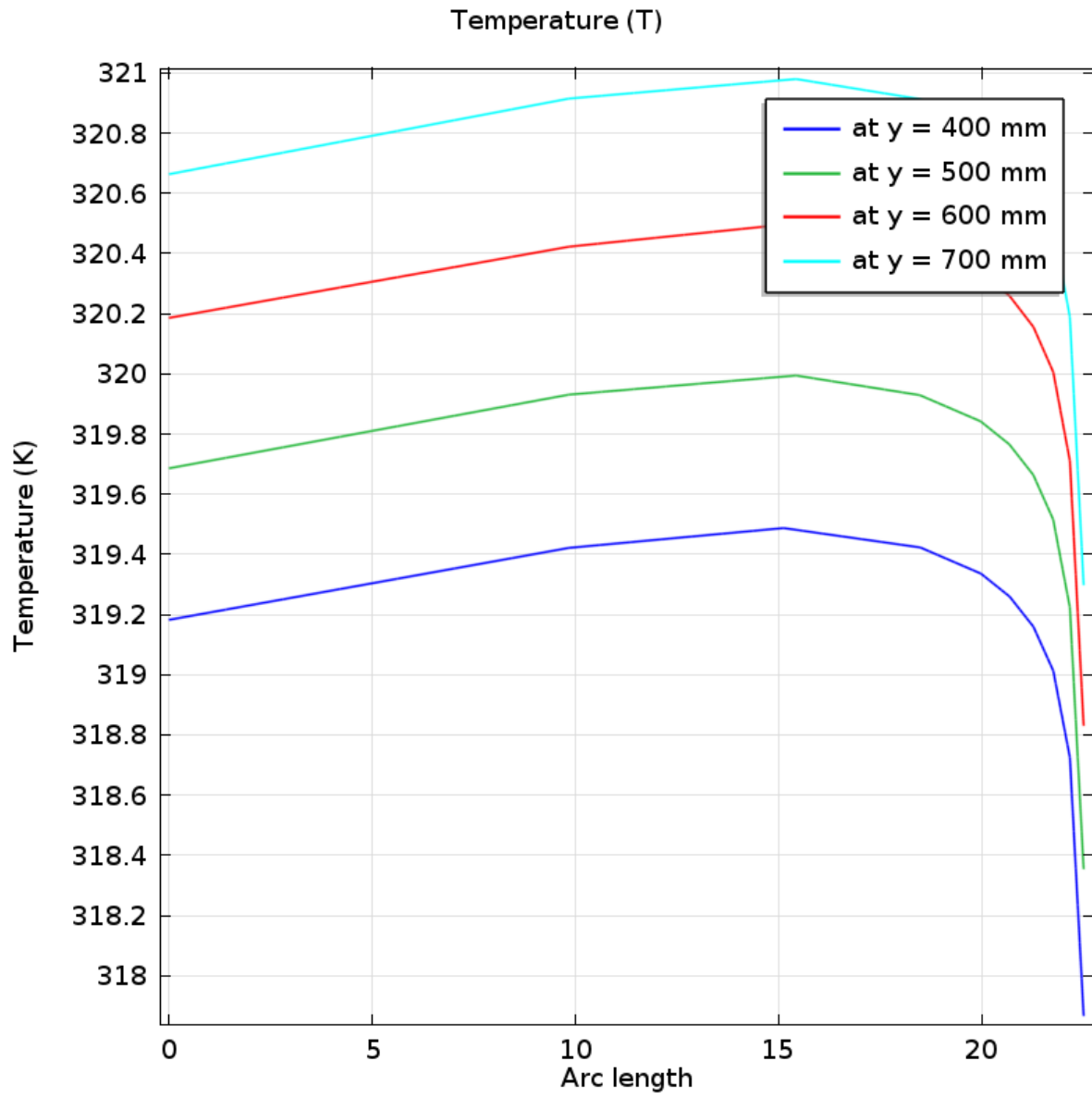


Figure 3.11(c): Temperature at y = 400, 500, 600 and 700 mm using $v_{in} = -1$ m/s

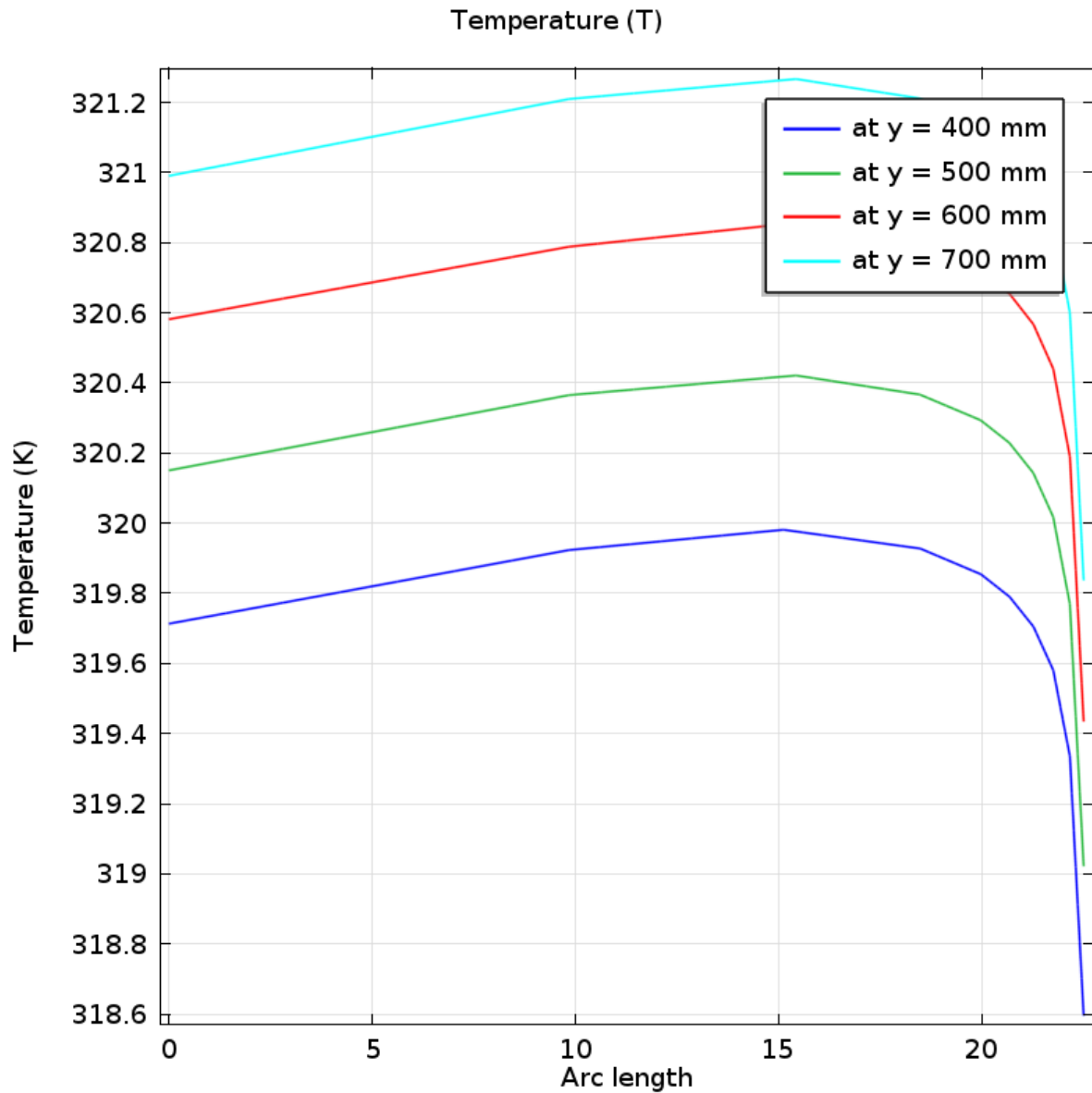


Figure 3.11(d): Temperature at y = 400, 500, 600 and 700 mm using $v_{in} = -1.5$ m/s

Figures 3.11(a-d) represent the temperature distribution at y = 400, 500, 600 and 700 mm for inflow velocities - 0.1, - 0.5, - 1 and - 1.5 m/s respectively of 1% concentrated water-MWCNT nanofluid. From the figures, it is observed that temperatures at y = 700 are 318.6, 320.1, 320.7 (approximate), and 321 K for inflow velocities - 0.1, - 0.5, - 1 and - 1.5 m/s respectively. That means temperature increases at a certain point with rising values of inflow velocities of water-MWCNT nanofluid.

3.4 Effect of temperature

To identify the effect of temperature on water-MWCNT nanofluid, four inlet temperatures such as 323 K, 318 K, 313 K and 308 K are considered for 1% concentrated water-MWCNT nanofluid. Fixed values of inflow velocity and mass flow rate of water-MWCNT nanofluid have been chosen as - 1.5 m/s and 2.91 kg/s respectively. It is checked the difference in streamlines and temperature contours. The significant changes are noticed in velocity, pressure and temperature at $y = 400, 500, 600$ and 700 mm of arc length.

Figure 3.12(a-d) shows the streamlines of 1% concentrated water-MWCNT nanofluid at different temperatures which are 323, 318, 313 and 308 K. The figures 3.12(a) and 3.12(d) are similar for 323 and 308 K inlet temperatures. The velocity at the highest corner of the exterior region of circular pipe is the lowest in figure 3.12(a) for 323 K inlet temperature.

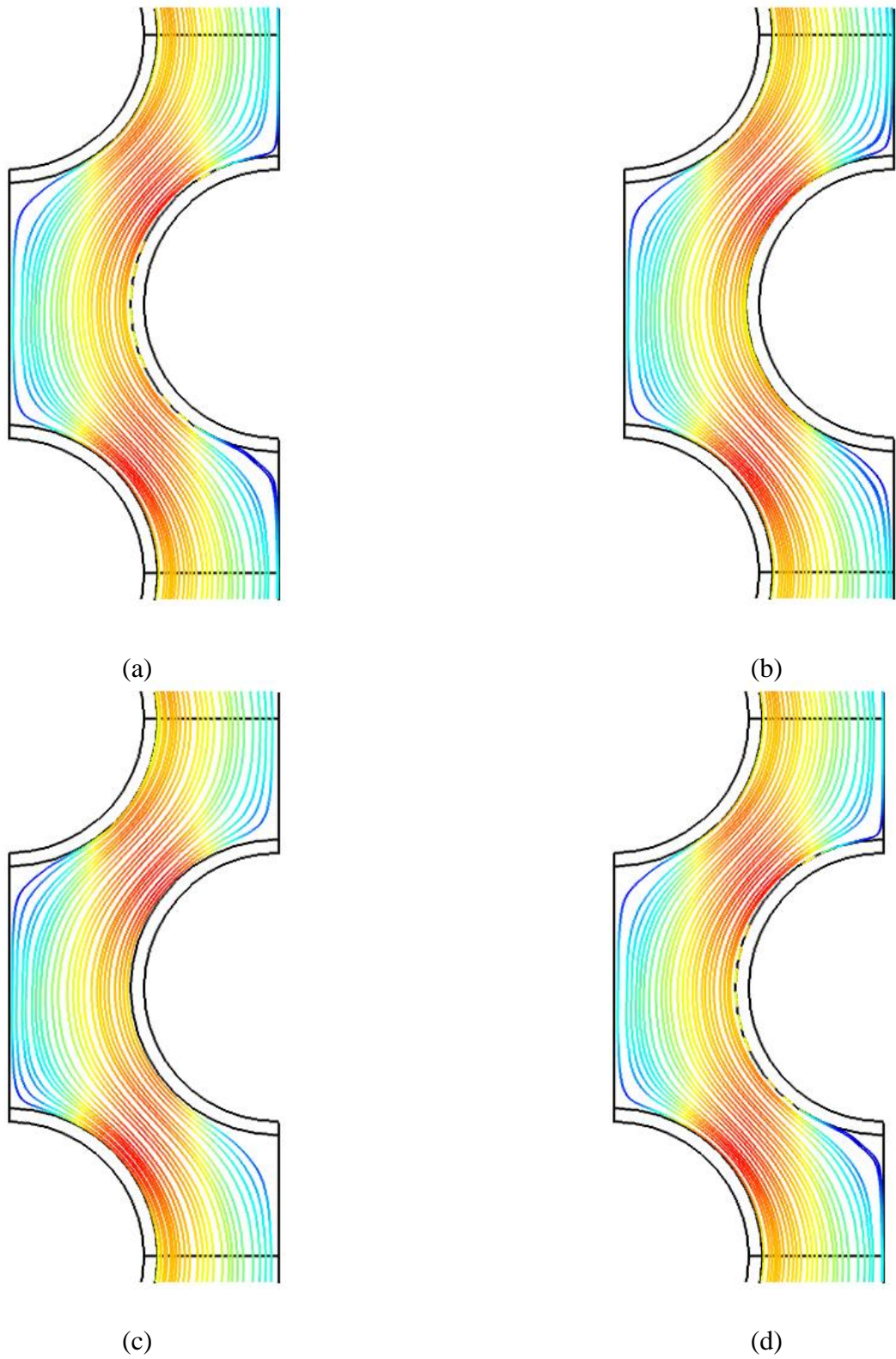


Figure 3.12: Velocity contours using T_{in} (a) 323, (b) 318, (c) 313 and (d) 308 K

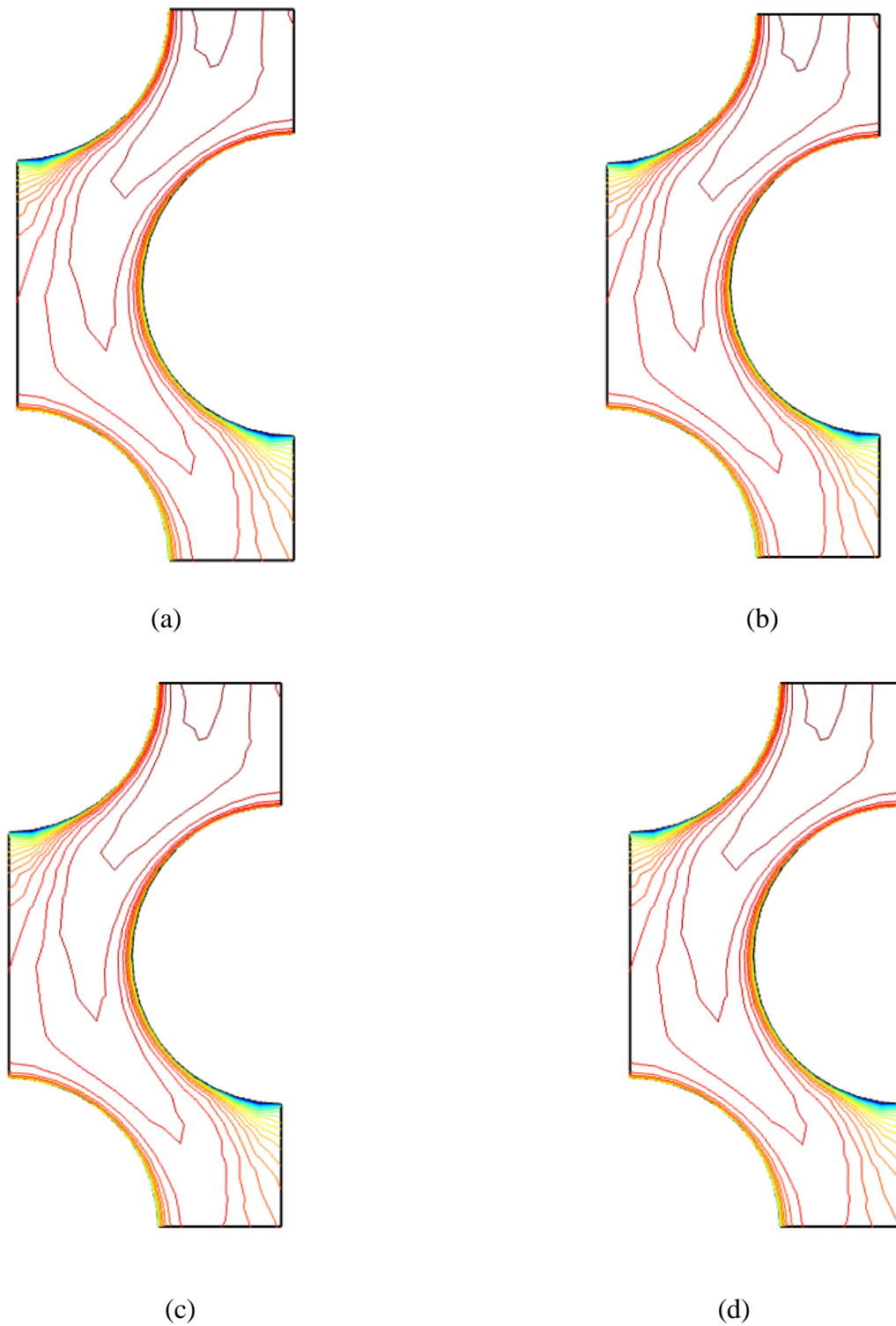


Figure 3.13: Temperature contours using T_{in} (a) 323, (b) 318, (c) 313 and (d) 308 K

Temperature contours of 1% concentrated water-MWCNT nanofluid at inlet temperatures 323, 318, 313 and 308 K are represented in figures 3.13(a-d). The figures are same for all

considered inlet temperatures and temperature is the lowest at the lower portions of the circular pipes in the exterior region.

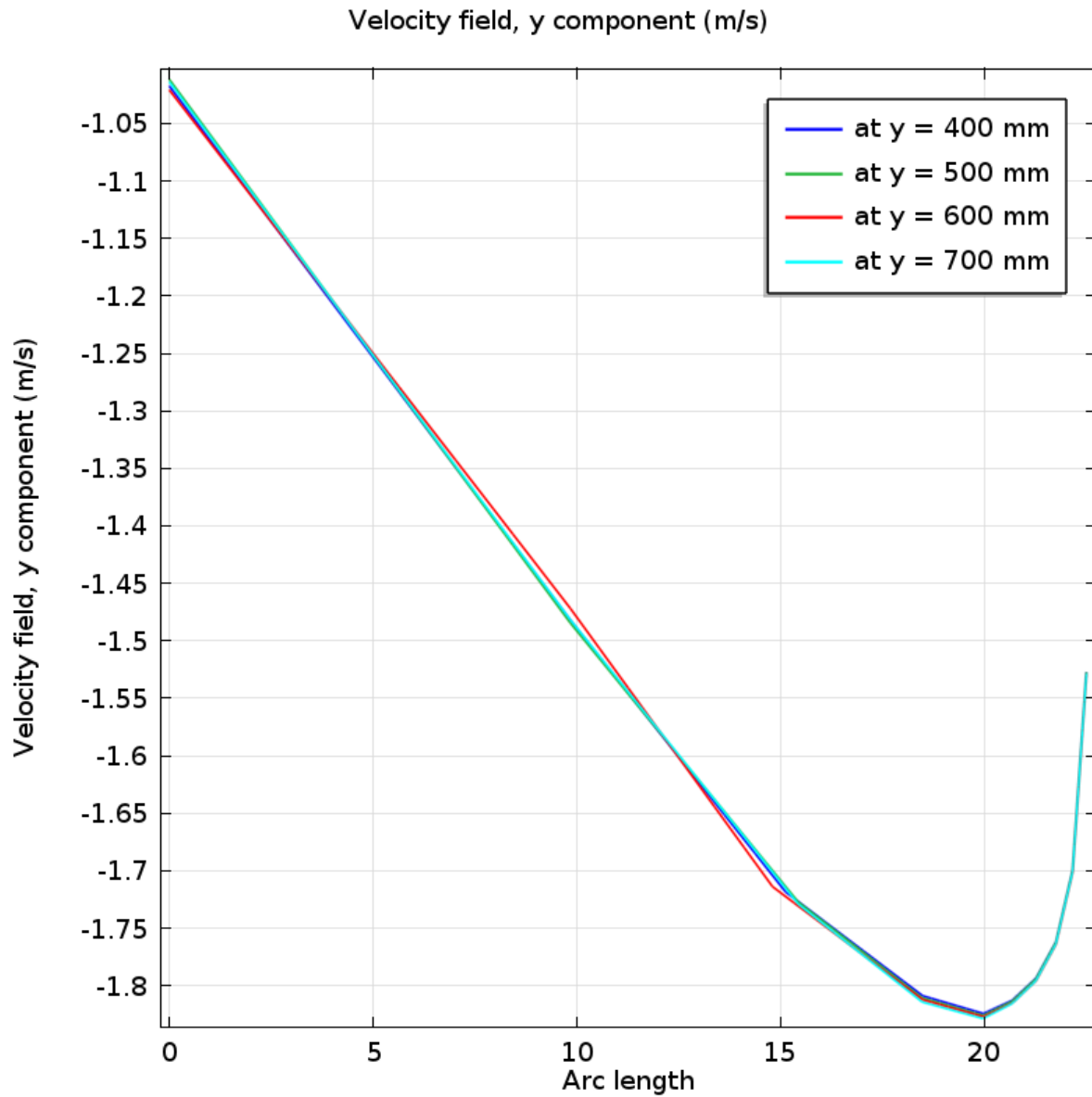


Figure 3.14(a): Velocity of y-component at y = 400, 500, 600 and 700 mm using $T_{in} = 323$ K

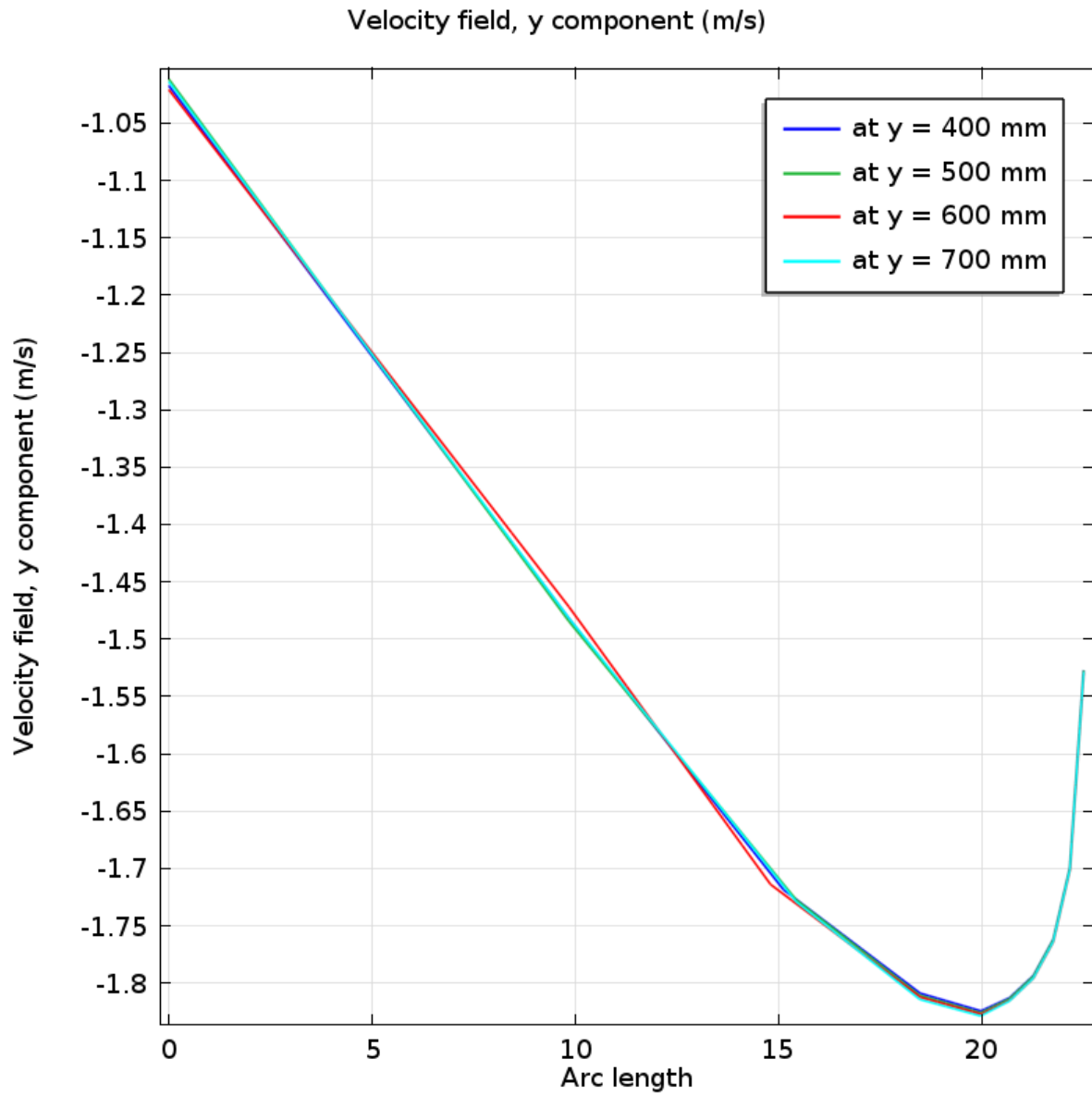


Figure 3.14(b): Velocity of y-component at y = 400, 500, 600 and 700 mm using $T_{in} = 318$ K

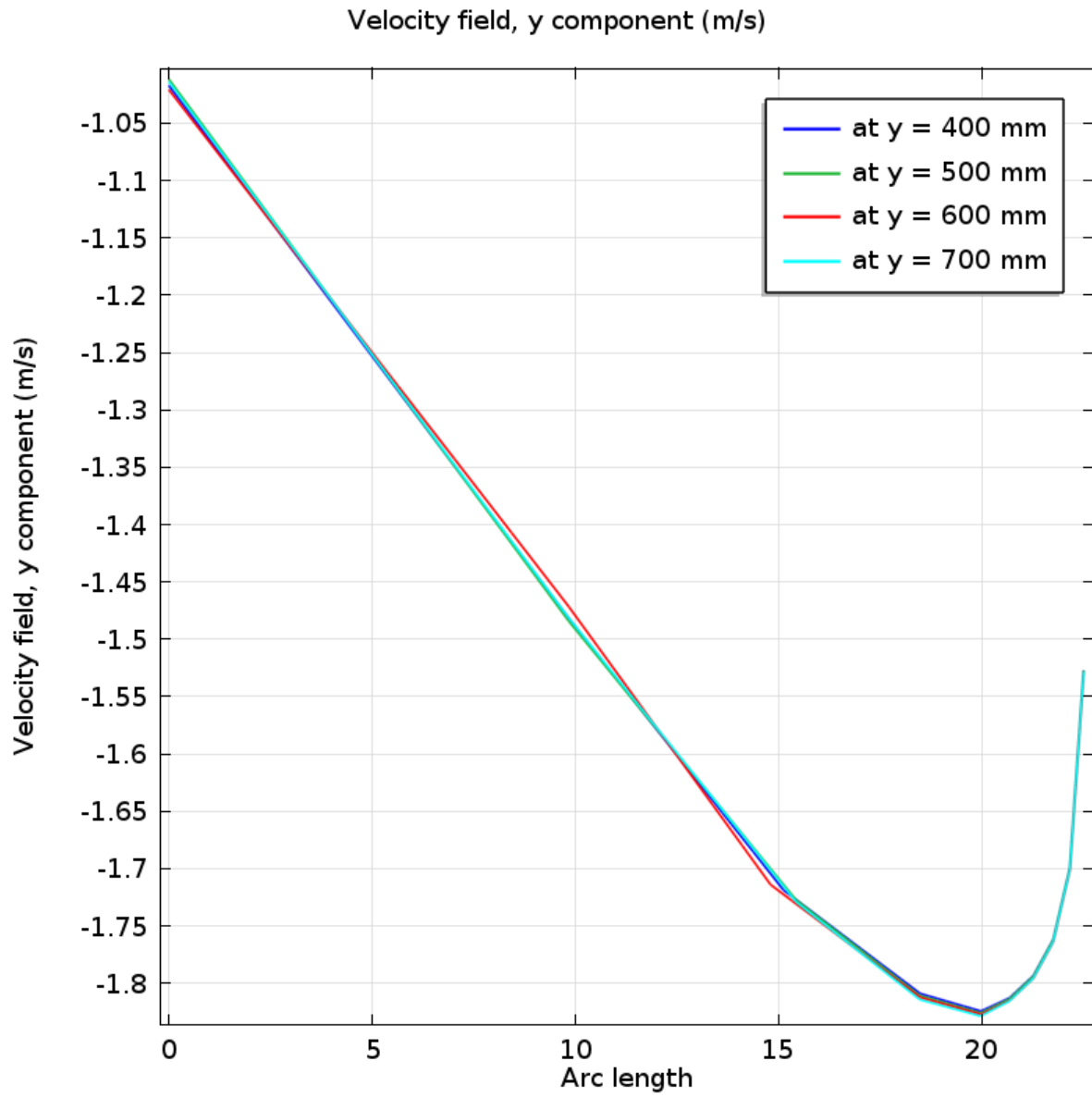


Figure 3.14(c): Velocity of y-component at y = 400, 500, 600 and 700 mm using $T_{in} = 313\text{ K}$

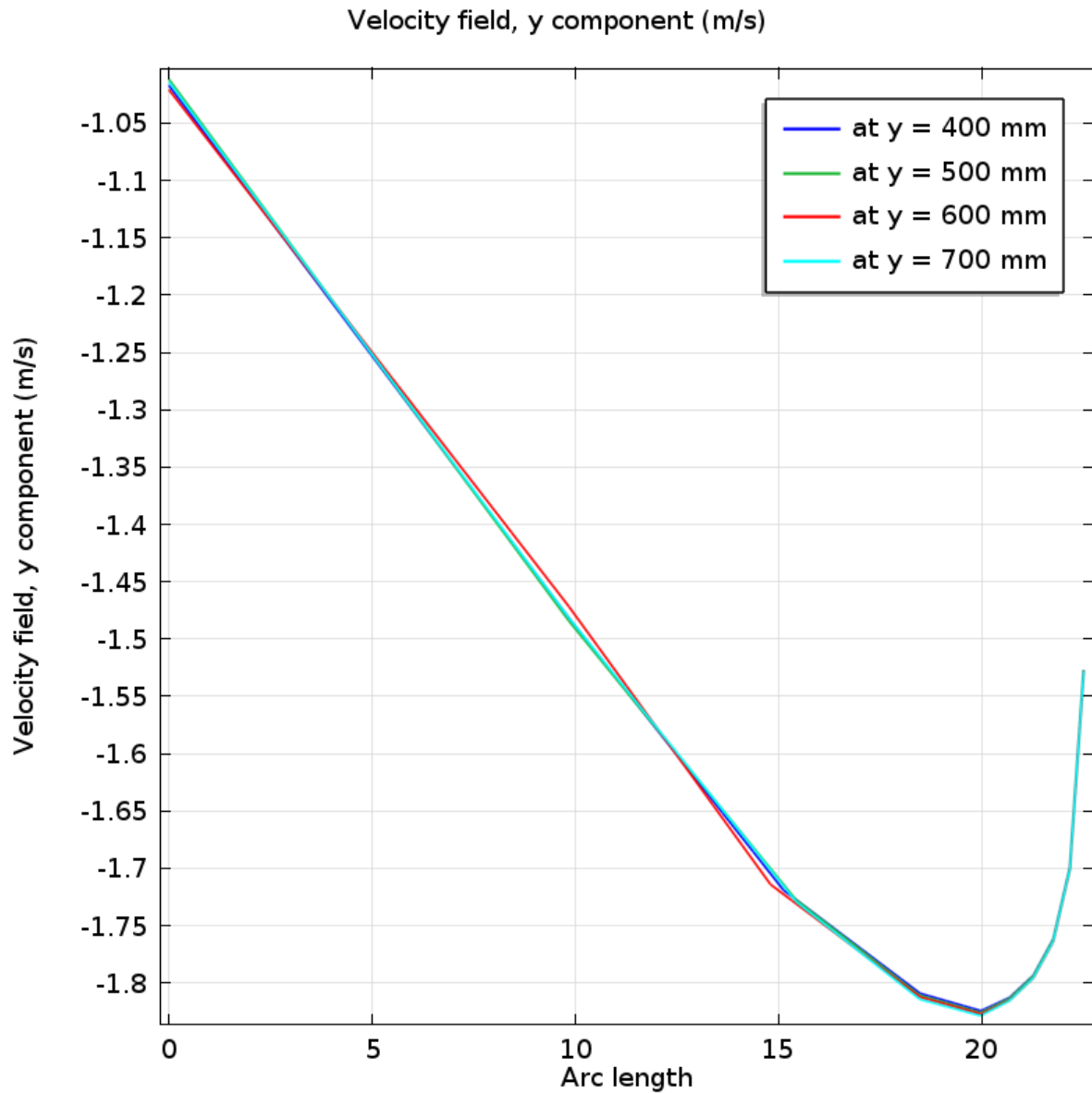


Figure 3.14(d): Velocity of y-component at y = 400, 500, 600 and 700 mm using $T_{in} = 308$ K

Figures 3.14(a-d) represent the velocity of y component at y = 400, 500, 600 and 700 mm for inlet temperatures 323, 318, 313 and 308 K respectively of 1% concentrated water-MWCNT nanofluid. The figures are similar for all considered inlet temperatures and they are showing that the maximum velocity is 1 m/s.

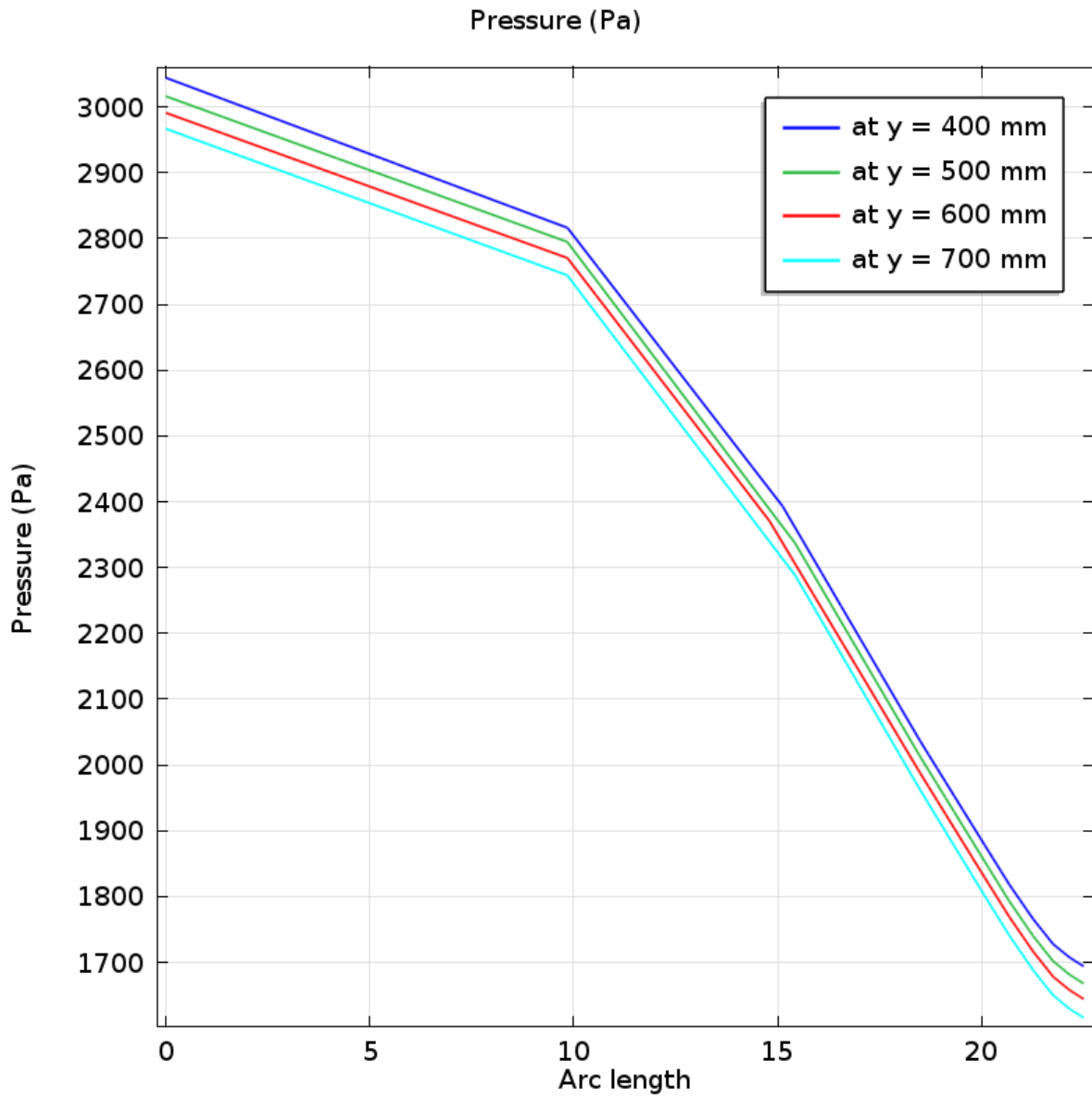


Figure 3.15(a): Pressure at y = 400, 500, 600 and 700 mm using $T_{in} = 323$ K

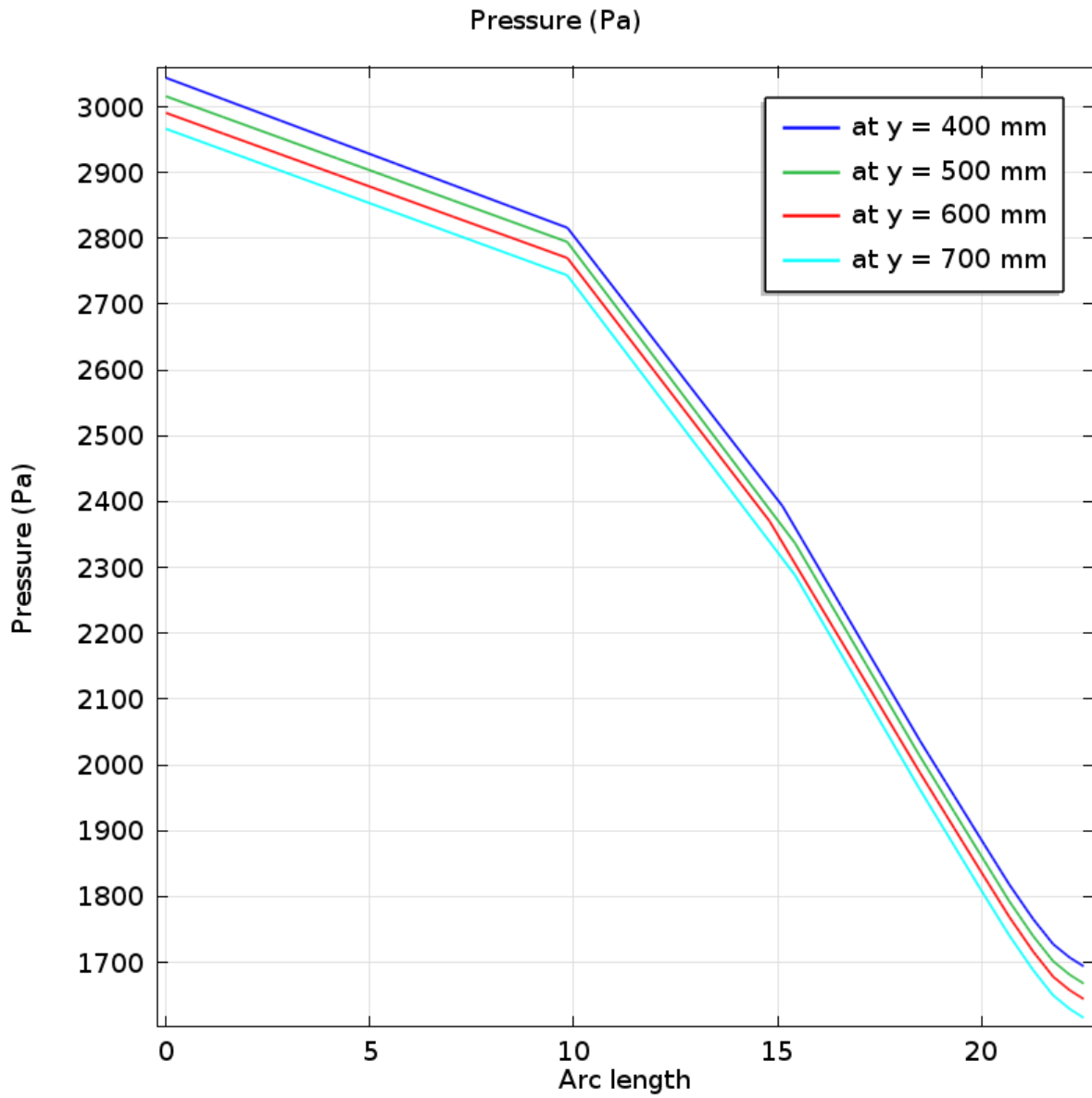


Figure 3.15(b): Pressure at $y = 400, 500, 600$ and 700 mm using $T_{in} = 318$ K

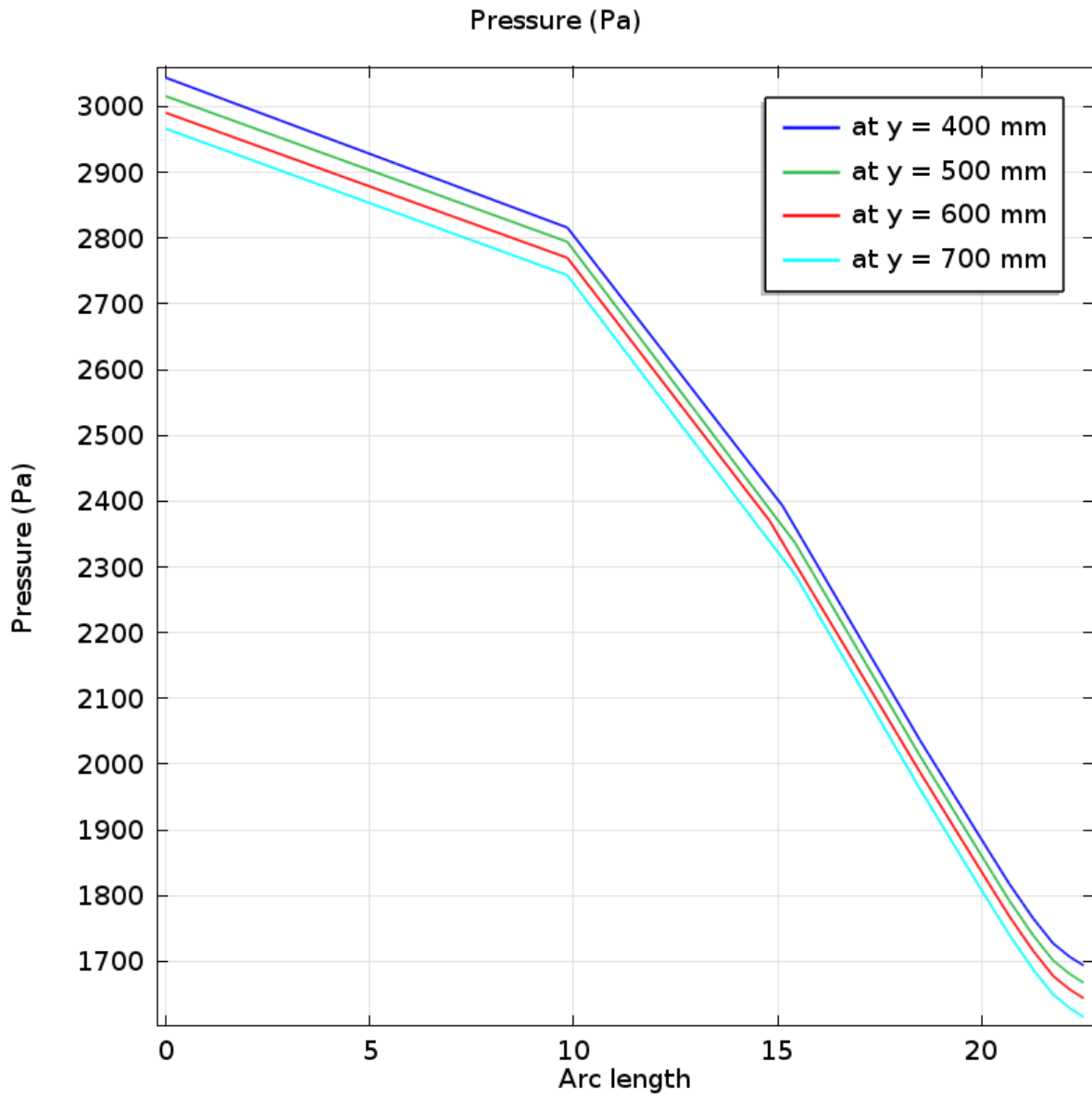


Figure 3.15(c): Pressure at y = 400, 500, 600 and 700 mm using $T_{in} = 313$ K

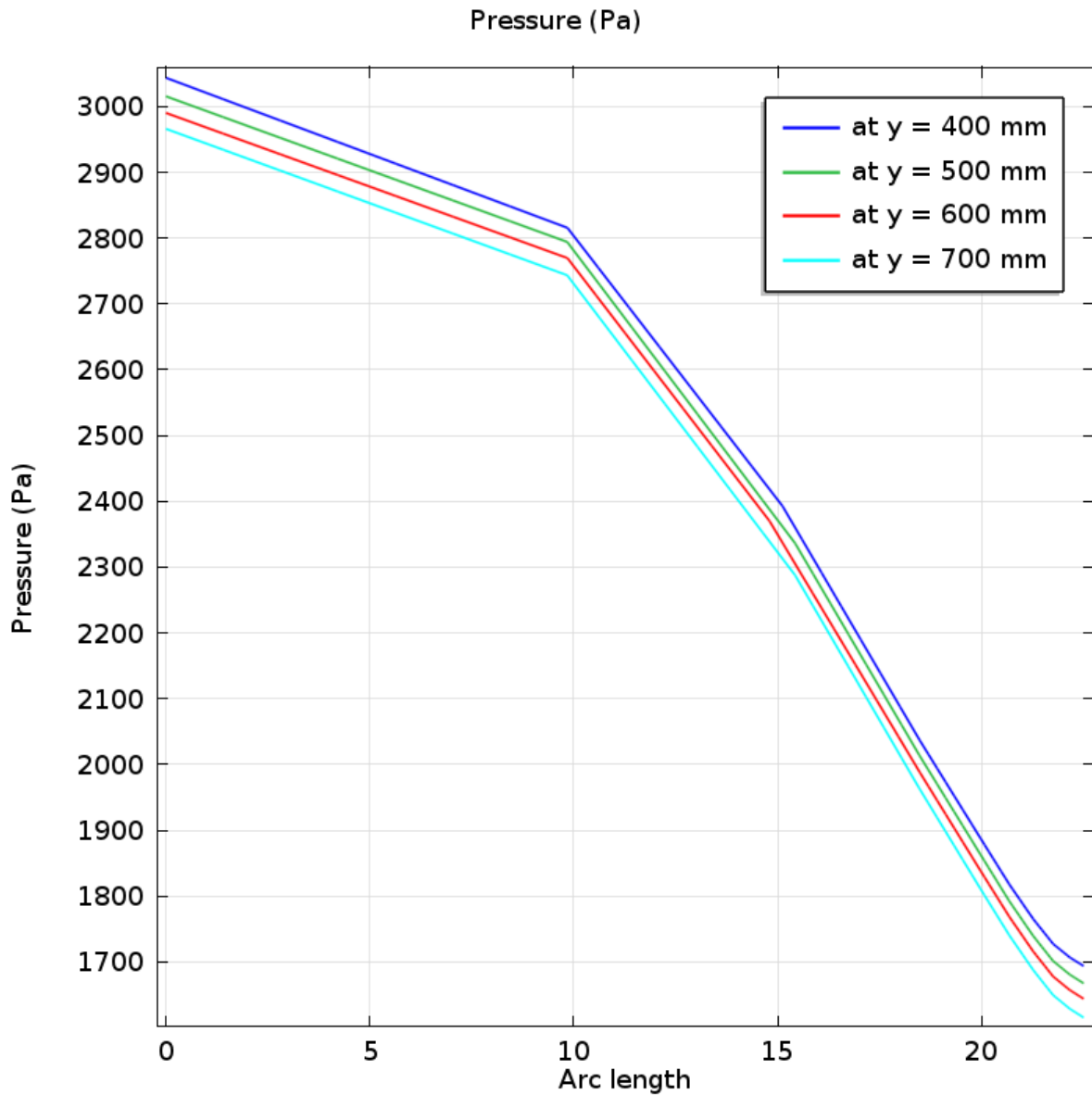


Figure 3.15(d): Pressure at $y = 400, 500, 600$ and 700 mm using inlet $T_{in} = 308$ K

Figures 3.15(a-d) represent the pressure at $y = 400, 500, 600$ and 700 mm for inlet temperatures 323, 318, 313 and 308 K respectively of 1% concentrated water-MWCNT nanofluid. The figures are similar for all considered inlet temperatures and the maximum pressure at $y = 600$ mm is 3000 Pa.

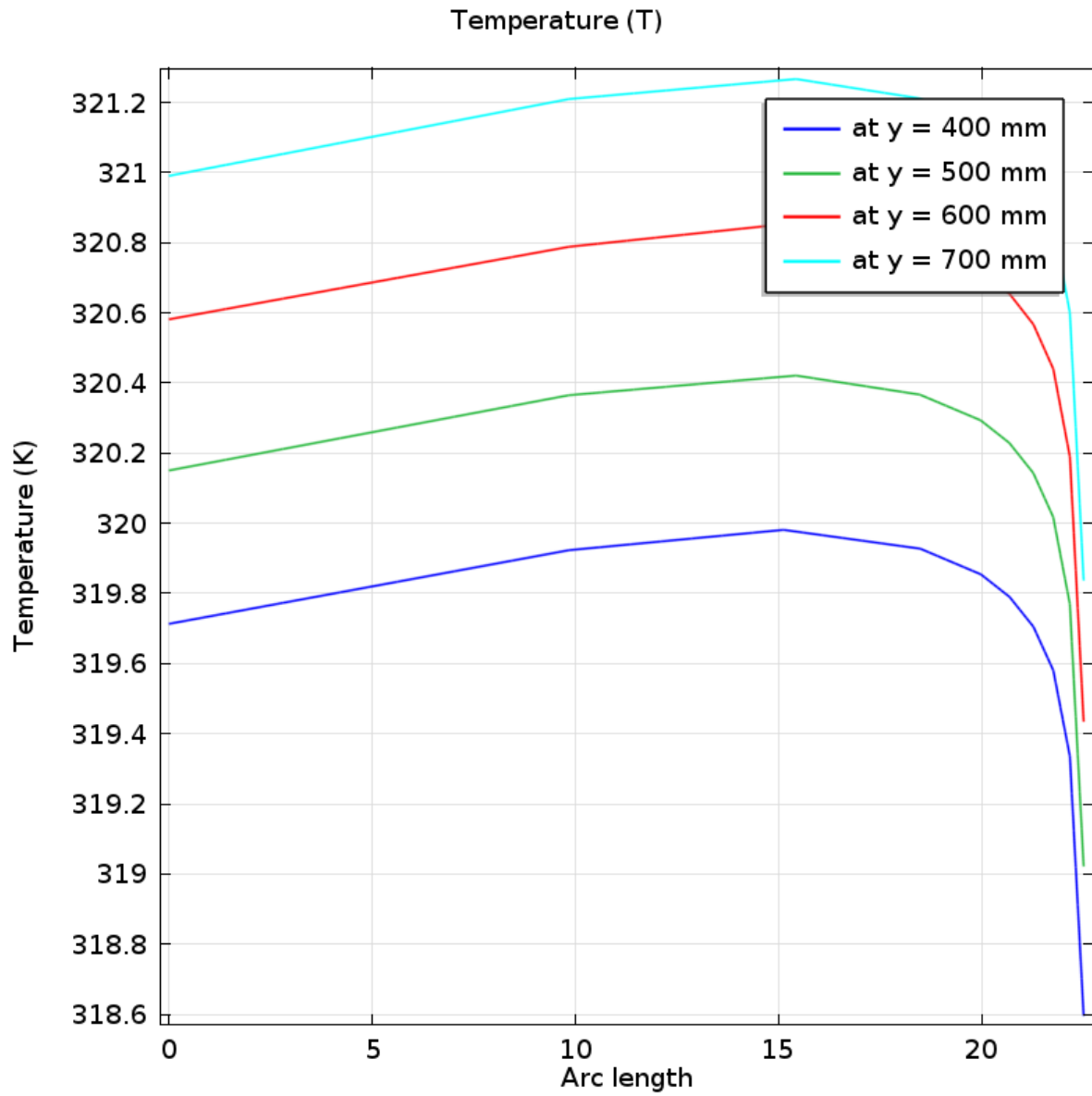


Figure 3.16(a): Temperature at y = 400, 500, 600 and 700 mm using $T_{in} = 323$ K

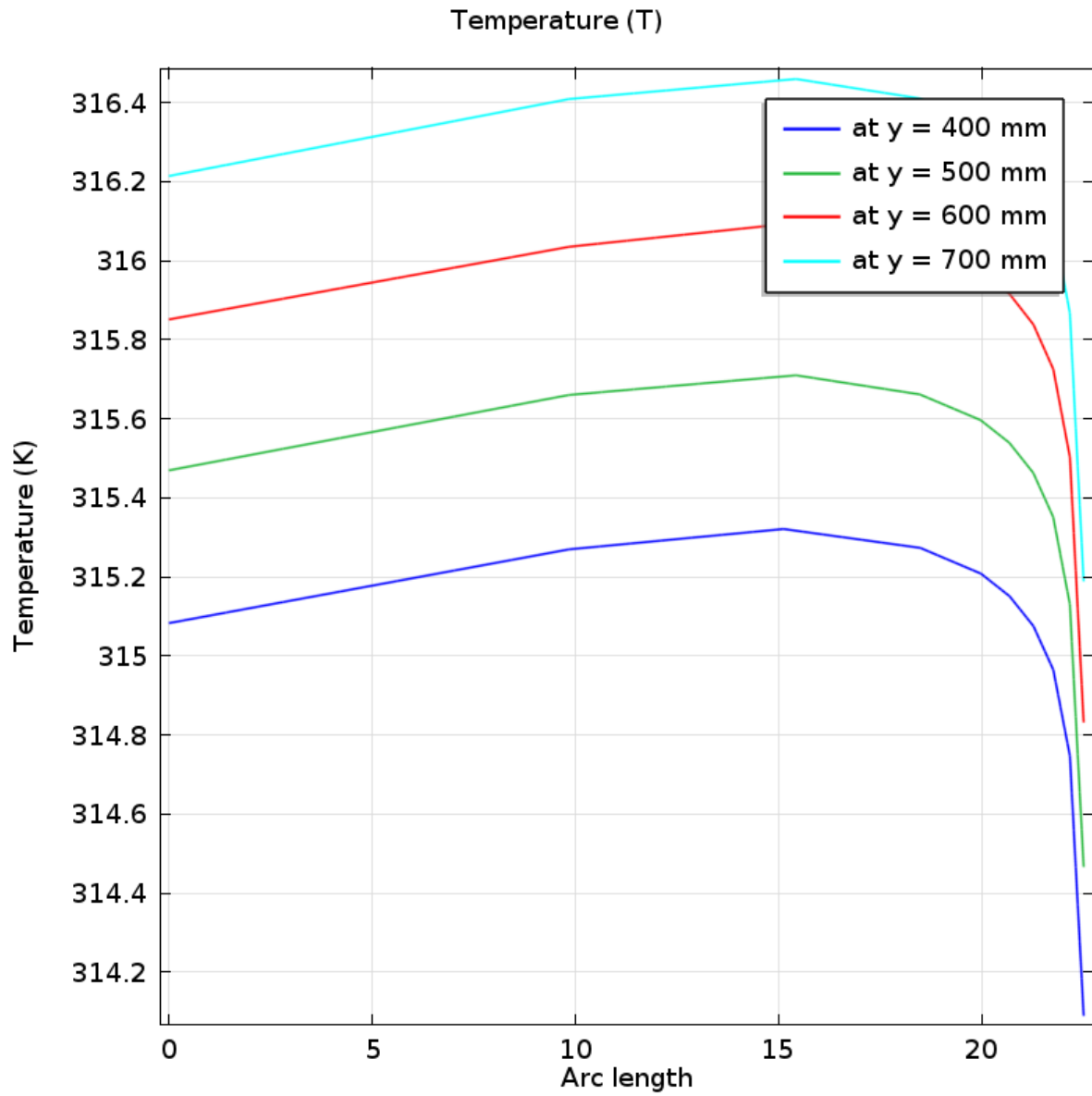


Figure 3.16(b): Temperature at y = 400, 500, 600 and 700 mm using $T_{in} = 318$ K

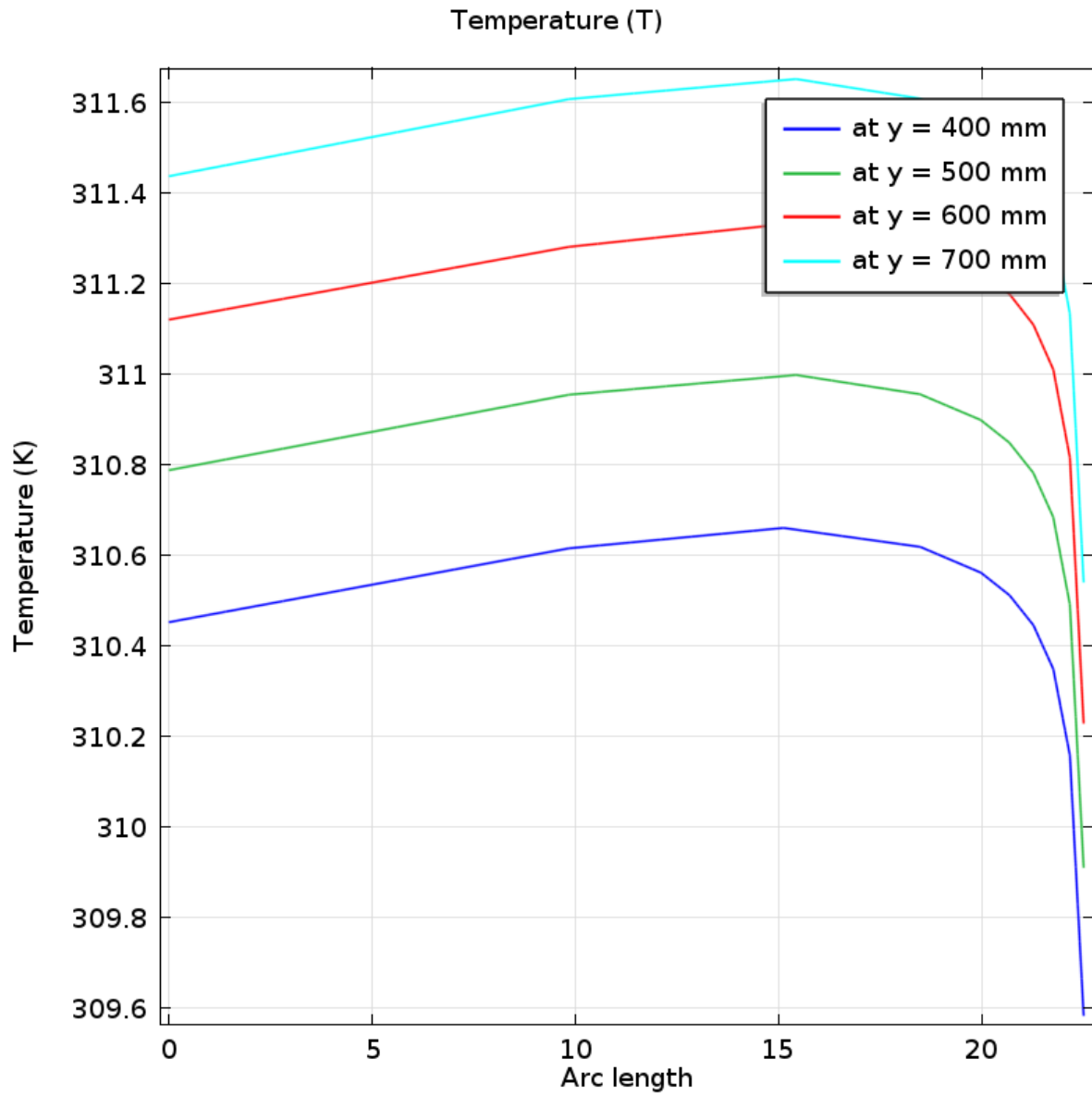


Figure 3.16(c): Temperature at y = 400, 500, 600 and 700 mm using $T_{in} = 313$ K

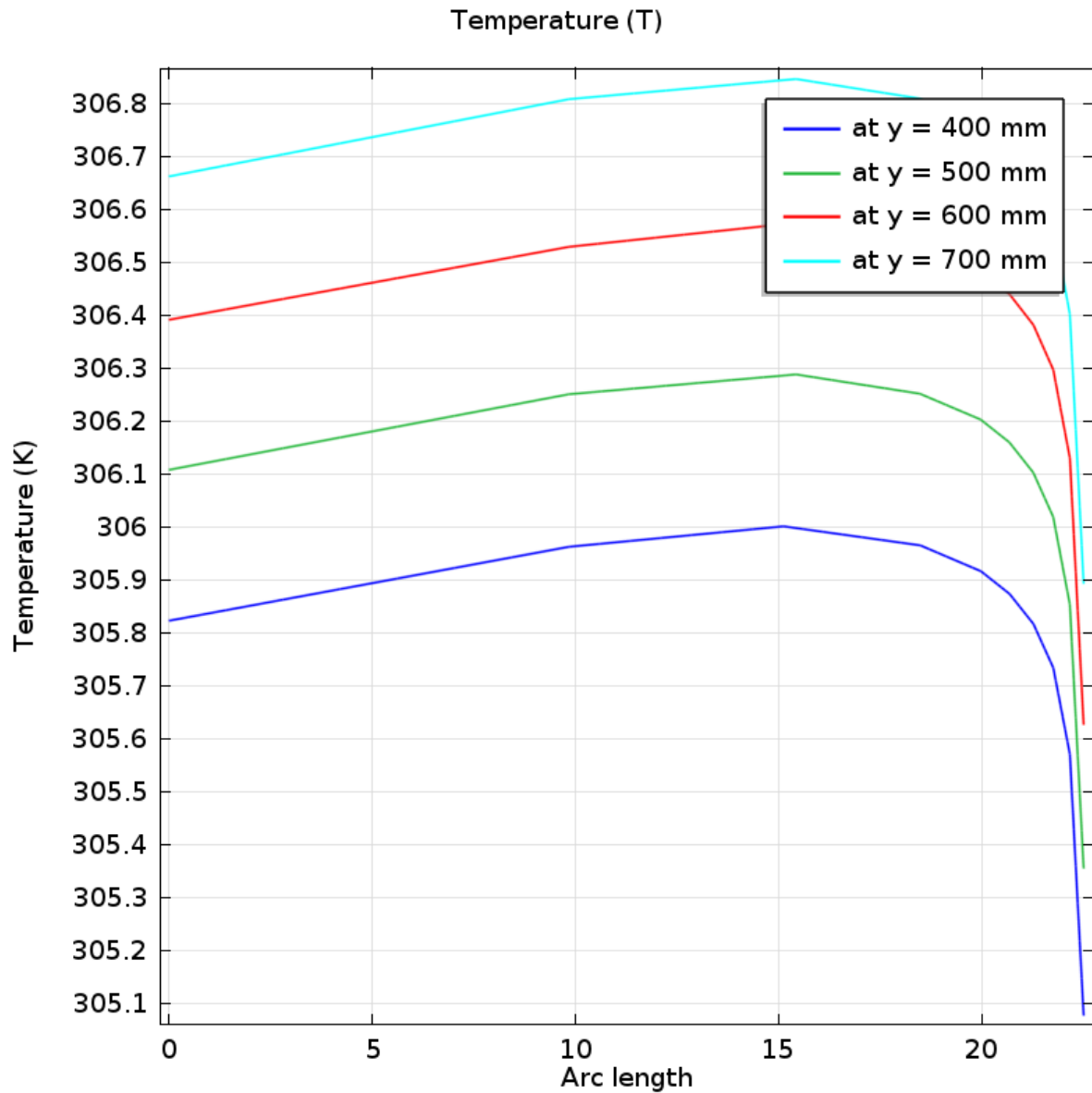


Figure 3.16(d): Temperature at y = 400, 500, 600 and 700 mm using $T_{in} = 308$ K

Figures 3.16(a-d) represent the temperature at y = 400, 500, 600 and 700 mm for inlet temperatures 323, 318, 313 and 308 K respectively of 1% concentrated water-MWCNT nanofluid. The figures are similar for all considered inlet temperatures and the temperatures at y = 500 mm are approximately 320.1, 315.5, 310.8 and 306.1 K for inlet temperatures 323, 318, 313 and 308 K respectively.

3.5 Heat Transfer Rate

In this section, heat transfer rate will be calculated. Figure 3.17 represents the average Nusselt number for various solid volume fraction of water- MWCNT nanofluid with fixed value of inflow velocity, temperature and mass flow rate - 1.5 m/s, 323 K and 2.91 kg/s respectively.

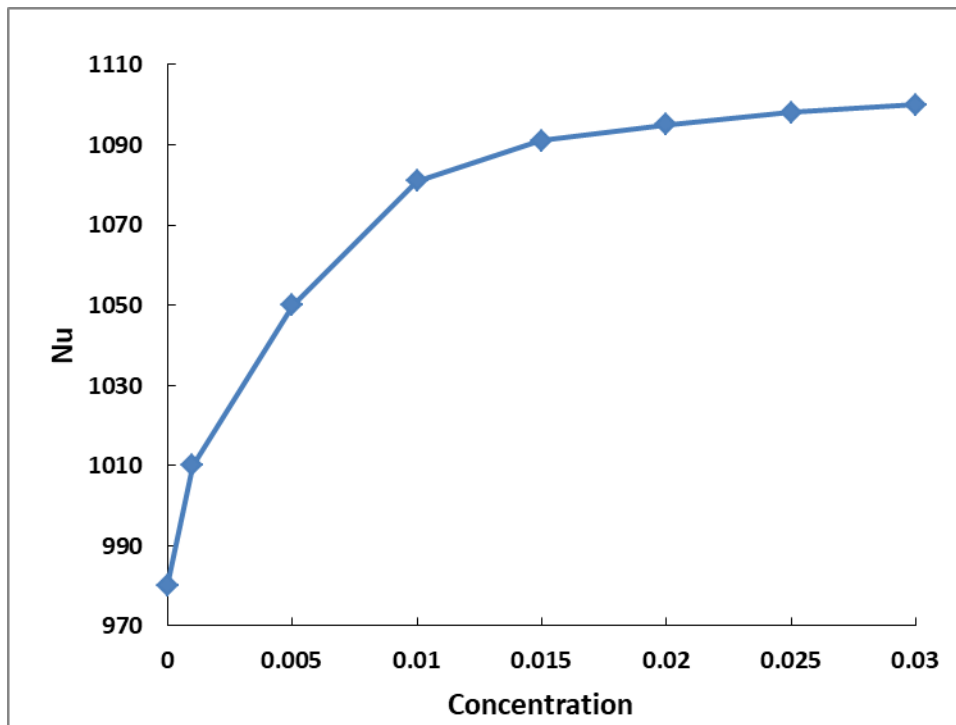


Figure 3.17: Average Nusselt number against solid concentration of water-MWCNT nanofluid

Table 3.1 is showing the values of heat transfer rate for water (base fluid) and different concentrated water-MWCNT nanofluids as well as the percentage of increasing of Nu from base fluid to water-MWCNT nanofluid. The value of volume fraction has been taken 0, 0.1, 1, 2, and 3%. The values of average Nusselt number against volume fraction 0, 0.001, 0.01, 0.02, 0.03 of water-MWCNT nanofluid are 980, 1035, 1088, 1095 and 1100, respectively. The heat transfer rate of volume fraction from 0 to 1 is greater than that of other volume fraction. The heat transfer rate is also increasing for other volume fraction (for 2 and 3%) but increasing rate is a little bit downcast. The rate of heat transfer is obtained 12.24% for increasing values of solid volume fraction from 0 to 3%. Thus, using water-MWCNT

nanofluid is more beneficial to obtain expected rate of heat transfer for shell and tube heat exchanger than plain/normal water.

Table 3.1: Heat Transfer rate at different concentration of water-MWCNT nanofluid

Concentration	Nu	Water	Percentage of increasing
0	980	980	0
0.001	1010	980	3.06122449
0.005	1050	980	7.142857143
0.01	1081	980	10.30612245
0.015	1091	980	11.32653061
0.02	1095	980	11.73469388
0.025	1098	980	12.04081633
0.03	1100	980	12.24489796

3.6 Comparison

The obtained numerical results of the mean Nusselt number for various volume fractions of water-MWCNT nanofluid in the present study have been compared with that of Yang and Liu [44]. Figure 3.18 depicts the comparative study of mean Nusselt number (Nu) for the variation of Reynolds number (Re) using water as heat transfer medium. The values from the research of Yang and Liu [44] and the present research have been shown also in the Table 3.2. Here percentage of error between these two studies has also been included. This table also contains the percentage of error of the values between these two researches. The minimum percentage of error in this case is 3.35 (approximate) for Reynolds number (Re) 9000. The maximum percentage of error (approximately 5.33%) occurs due to Reynolds number (Re) 7000 for which obtained values of Nusselt number (Nu) are 150 and 158 from the research of Yang and Liu [44] and the present research respectively. A nice agreement is shown in this comparison of results.

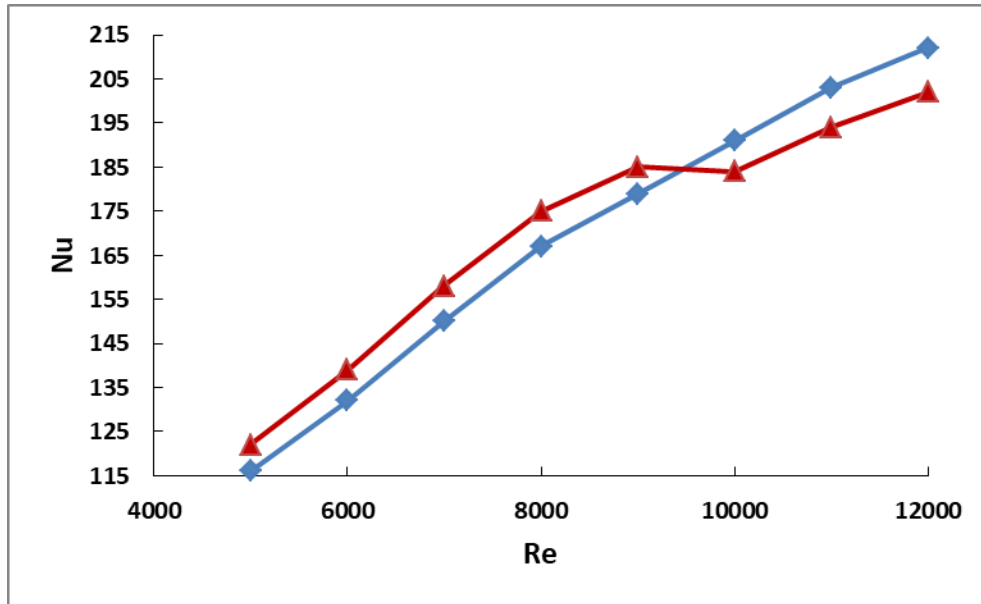


Figure 3.18: Comparison for Nu between Yang and Liu [44](blue color) and present research (red color)

Table 3.2: Comparison of Nusselt number between present numerical research and research of Yang and Liu against Reynolds number

Re	Yang and Liu	Present result	Percentage of error
5000	116	122	5.172413793
6000	132	139	5.303030303
7000	150	158	5.333333333
8000	167	175	4.790419162
9000	179	185	3.351955307
10000	191	184	3.664921466
11000	203	194	4.433497537
12000	212	202	4.716981132

Chapter 4

Conclusions and Recommendations

A numerical analysis of turbulent flow through a shell and tube heat exchanger using Galerkin weighted residual finite element technique has been conducted. The Reynolds-averaged Navier-Stokes (RANS) equations and a $\kappa - \epsilon$ turbulence model in the water-MWCNT domain as well as Keys-Crawford heat transport turbulence model in the water-MWCNT and the solid (steel) tube walls have been implemented. To find the effects of velocity, temperature and solid concentration on fluid flow and heat transfer phenomena, we have considered different inlet velocities, temperatures and volume fraction of working nanofluid. The y-component of velocity field, pressure and temperature against arc length at $y = 400, 500, 600$ and 700 mm of the exterior region of circular pipes for the variation of above mentioned physical parameters have also been presented to explain the numerical results in the previous chapter. The rate of heat transfer for different solid concentration of water-MWCNT nanofluid has been calculated. Varying the volume fraction, inflow velocity, inlet temperature we have led to the following conclusions:

4.1 Conclusions

- Velocity and temperature contours are appreciably changes due to the variation of solid volume fraction from 0 to 3% of water-MWCNT nanofluid. The velocity, temperature and pressure in the inlet of several segments of the computational domain are observed to be more significant using 3% concentrated nanofluid than base fluid.
- The heat transfer is strongly influenced by the details of the velocity field. The flow field is observed to be periodic in the y- direction with the constant pressure drop about 1600 Pa for inflow fluid velocity - 1.5 m/s.
- The y-component of velocity field is found to be more distorted for inlet temperature 323 K. At this stage the highest value of fluid pressure is noticed about 3040 Pa. The lowest temperature is calculated as 318.6 K at the position of arc length 25 mm and $y = 400$ mm.
- Approximately 12.24% higher heat transfer rate is found for water-MWCNT nanofluid with 3% solid volume fraction than clear water.

4.2 Recommendations

Since using nanofluids can improve the heat transfer performance and therefore the efficiency of shell and tube heat exchangers, there is a lot of scope for research in this area in future. Different size, shape, material and volume fraction of dispersed nanoparticles act in different way and can play very important roles in the absorption of heat. In consideration of the present research, the recommendations for future works are as follows:

- ◆ The present numerical study can also be done for 3-dimensional model.
- ◆ The present investigation can be performed using different size, shape and volume fraction of others dispersed nanoparticles to check the efficiency of shell and tube heat exchanges.
- ◆ The present numerical analysis can also be computed to compare heat transfer performance of different nanofluids.
- ◆ Using hybrid nanofluids, this present research can be performed in future.

References

- [1] Z. Said, S.M.A. Rahman, M.E.H. Assad, A.H. Alami, "Heat transfer enhancement and life cycle analysis of a shell and tube heat exchanger using stable CuO/water nanofluid", *Sustainable Energy Technologies and Assessments*, vol. 31, pp. 306-317, 2019.
- [2] B. Farajollahi, S.Gh. Etemad, M. Hozzat, "Heat transfer of nanofluids in a shell and tube heat exchanger", *International Journal of Heat and Mass Transfer*, vol. 53, pp. 12-17, 2010.
- [3] J. Sunil, R. Maheshwaran, A.G. Vincy, "Enhancement of thermal conductivity using nanofluids", 1st edition, Lambert Academic Publications, Germany, 2018.
- [4] S. Jana, A. Salehi-Khojin, W.H. Jong, "Enhancement of fluid thermal conductivity by the addition of single and hybrid nano-additives", *Thermochemica Acta*, vol. 462, pp. 45-55, 2007.
- [5] S.M. Shahril, G.A. Quadir, N.A.M. Amin, I.A. Bodruddin, "Numerical investigation on the thermohydraulic performance of a shell and double concentric tube and heat exchanger using nanofluid under the turbulent flow regime", *Numerical Heat Transfer*, vol. 71, pp. 215-231, 2017.
- [6] A.M. Hussein, K.V. Sharma, R.A. Bakar and K. Kadirgama, "Heat transfer enhancement with nanofluids – A review", *Journal of Mechanical Engineering and Sciences*, vol. 4, pp. 452-461, 2013.
- [7] A M. Hussein, K. V. Sharma, R. A. Bakar, K. Kadirgama, "The effect of nanofluid volume concentration on heat transfer and friction factor inside a horizontal tube", *Journal of Nanomaterials*, vol. 2013, pp. 1-12, 2013.
- [8] M.S. Baba, A.V.S.R. Raju, M.B. Rao, "Heat transfer enhancement and pressure drop of Fe₃O₄-water nanofluid in a double tube counter flow heat exchanger with internal longitudinal fins", *Case Studies in Thermal Engineering*, vol. 12, pp. 600-607, 2018
- [9] S.S. Kamthe, S.B. Brave, "Effect of different nanofluids on performance of shell and tube heat exchanger: A review", *International Journal of Research in Engineering and Technology*, vol. 6, pp. 8-41, 2017.

References

- [10] Ms.S. Shankar, P. Immanuel, M. Eswaran, "Heat transfer analysis of shell and tube heat exchanger using Al_2O_3 nanofluids", International Journal of Mechanical Engineering and Technology, vol. 9, Issue 11, pp. 980-989, 2018.
- [11] M.H. Aghabozorg, A. Rashidi, S. Mohammidi, "Experimental investigation of heat transfer enhancement of $\text{Fe}_2\text{O}_3 - \text{C}/\text{water}$ magnetic nanofluids under laminar, transient and turbulent flow inside a horizontal shell and tube heat exchanger", Experimental Thermal and Fluid Science, vol. 72, pp. 182-189, 2016.
- [12] N. Krishnan M.C., B.S. Kumar, "Review on shell and tube heat exchanger using nanofluids", International Journal of Engineering Science and Technology, vol. 6, pp. 236-239, 2017.
- [13] S. Anitha, S. Sathyapriya, "Tubeside flow analysis for shell and tube heat exchanger using CFD", International Journal of Pure and Applied Mathematics, vol. 119, pp. 2077-2087, 2018.
- [14] W.H. Emerson, "Shell side pressure drop and heat transfer with turbulent flow in segmentally baffled shell and tube heat exchangers", International Journal of Heat and Mass Transfer, vol. 6, pp. 649-668, 1993.
- [15] R. Beigzadeh, A. Parvareh, M. Rahim, "Experimental and CFD study of the tube configuration effect on the shell side thermal performance in shell and helically coiled tube heat exchanger", Iranian Journal of Chemical Engineering, vol. 12, pp. 13-25, 2015.
- [16] K. Mohammadi, W. Heidmann and H.M. Steinhagen, "Numerical investigation of the edge of baffle orientation on heat transfer and pressure drop in a shell and tube heat exchanger with leakage flows", Heat Transfer Engineering, vol. 30, pp. 1123-1135, 2009.
- [17] F. Khoddamrezaee, R.Motallebzadeh and D.J. Vahid, "Simulation of $(\text{EG} + \text{Al}_2\text{O}_3)$ nanofluid through the shell and tube heat exchanger with rectangular arrangement of tubes and constant heat flux", Journal of Applied Sciences, vol. 6, pp. 500-505, 2010.
- [18] M. Hasanuzzaman, R. Saidur and N.A. Rahim, "Effectiveness enhancement of heat exchanger by using nanofluids", IEEE First Conference on Clean Energy and Technology, pp. 98-10, 2011.
- [19] D. Guerrieri, F. Viana, S.C. Fragoso, M.M. Aeliano, "Shell and tube heat exchangers using nanofluids", 14th Bazilian Congress of thermal Science and Engineering, 2012.

References

- [20] J. Cox, A. Kanjirakat, R. Sadr, “Applications of nanofluids in a shell and tube heat exchanger”, Proceeding of the ASME 2013, 11th International Conference on Nanochannels, Microchannels and Minichannels, 2013.
- [21] J. Albadr, S. Tayal, M. Alasadi, “Heat transfer through heat exchanger using Al₂O₃ nanofluid at different concentrations”, Case Studies in Thermal Engineering”, Issue 1, vol. 1, pp. 38-44, 2013.
- [22] R. Barzegarian, A. Aloueyan, T. Yousefi, “Thermal performance augmentation using water based Al₂O₃-gamma nanofluid in a horizontal shell and tube heat exchanger under forced convection”, International Communications in Heat and Mass Transfer, vol. 86, pp. 52-59, 2017.
- [23] M.R. Ullah, T.M. Ishtiaq, M.A.H. Mamun, “Heat transfer enhancement in shell and tube heat exchanger by using Al₂O₃/water and TiO₂-water nanofluid”, AIP Conference Proceedings, 2121, 070018, 2019.
- [24] H.S. Majdi, H.A. Aabdly, M.F. Hamad, B.O. Hasan, M.M. Hathal, “Enhancement of heat transfer using Aluminium Oxide nanofluid on smooth and finned surfaces with COMSOL multiphysics simulation in turbulent flow”, Al-Nahrain Journal of Engineering Sciences, vol. 22, pp. 44-54, 2019.
- [25] M.R. Saffarian, P. Pazelpour, M. Sham, “Numerical study of shell and tube heat exchanger with different cross-section tubes and combined tubes”, International Journal of Energy and Environmental Engineering, vol. 10, pp. 33-46, 2019.
- [26] M.S.E. Rao, D. Sreeramulu and D.A. Naidu, “Experimental investigation of heat transfer rate of nanofluids using a shell and tube heat exchanger”, IOP Conf. Series: Materials Science and Engineering 149 (2016) 012204.
- [27] J. Albadr, “Thermal performance of shell and tube heat exchanger using PG/water and Al₂O₃ nanofluid”, Advances in Heat Exchangers, Laura Castro Gómez and Víctor Manuel Velázquez Flores, IntechOpen, 2018.
- [28] D. Mansoury, F.I. Doshmanziari, A. Kiani, A.J. Chamkha, M. Sharifpur, “Heat transfer and flow characteristics of Al₂O₃/water nanofluid in various heat exchangers: experiments on counter flow”, Heat Transfer Engineering, issue 3, vol. 41, pp. 220-234, 2020.
- [29] S. Etaig, G. Hshem, R. Hasan, N. Perera, “Investigation of the heat performance for hyper nanofluid in a co-current shell and tube heat exchanger”, International Journal of Engineering Research & Technology, vol. 08, Issue 12, pp. 187-194, 2019.

References

- [30] G.A. Abdali, H.M. Maghrabie, M. Attalla, "Investigation of heat transfer and friction factor of Al₂O₃ nanofluid inside shell and tube heat exchanger", *Journal of Scientific and Engineering Research*, vol. 5, pp. 549-556, 2018.
- [31] R.G. Gontigo, "The numerical modeling of thermal boundary wall flows with the classical Kays-Crawford model", *Journal of Brazilian Society of Mechanical Science and Engineering*, vol. 33, pp. 419-428, 2011.
- [32] B. Weig and M.E. Crawford, "An extended Kays and Crawford turbulent Prandtl number model", *International Journal of Heat and Mass Transfer*, vol. 40, pp. 4191-4196, 1997.
- [33] J.R. Welty, C.E. Wicks and R.E. Wilson, *Fundamentals of momentum, Heat and Mass Transfer*, 3rd ed, John Wiley & Sons, Inc., 1984.
- [34] B.E. Launder and D.B. Spalding, "The Numerical Computation of Turbulent Flows", *Computer Methods in Applied Mechanics*, vol. 3, pp. 269-289, 1974.
- [35] D.C. Wilcox, *Turbulence Modeling for CFD*, 2nd ed, DCW Industries, 2000.
- [36] H.K. Versteeg and W. Malalasekera, *An Introduction to Computational Fluid Dynamics*, Prentice Hall, 1995.
- [37] H.C. Brinkman, "The viscosity of concentrated suspensions and solution", *Journal of Chemical Physics*, vol. 20, pp. 571-581, 1952.
- [38] J.C.M. Garnett, "Colours in metal glasses and in metallic films", *Royal Society*, vol. 203, pp. 385-420, 1904.
- [39] R. Nasrin, M. Hasanuzzaman and N.A. Rahim, "Effect of nanofluids on heat transfer and cooling system of the photovoltaic/thermal performance", *International Journal of Numerical Methods for Heat Transfer and Fluid Flow*, vol. 29, no. 6, pp. 1920-1946, 2019.
- [40] R. Nasrin, N.A. Rahim, H. Fayaz and M. Hasanuzzaman, "Water/MWCNT nanofluid based cooling system of PVT: Experimental and numerical research", *Renewable Energy*, vol. 121, pp. 286-300, 2018.
- [41] R. Nasrin, Saddam Hossain, I. Zahan, K.F.U. Ahmed and H. Fayaz, "Performance analysis of hybrid nanofluid on enhancement of fluid thermal conductivity in lid-driven undulated cavity", *Heat Transfer Journal*, vol. 49, issue 8, pp. 4204-4225, 2020.
- [42] P. Dechaumphai, "Finite Element Method in Engineering", 2nd edition, Chulalongkorn University Press, Bangkok, 1999.

References

- [43] C. Taylor, P. Hood, "A numerical solution of the Navier-Stokes equations using finite element technique", *Computer and Fluids*, vol. 1, pp. 73–89, 1973.
- [44] J. Yang, W. Liu, "Numerical investigation on a novel shell-and-tube heat exchanger with plate baffles and experimental validation", *Energy Conversion and Management*, vol. 101, pp. 689–696, 2015.